ISSN 0252-1075
ESSO/IITM/SERP/SR/02(2015)/185

A Research Report on the 2015 Southwest Monsoon

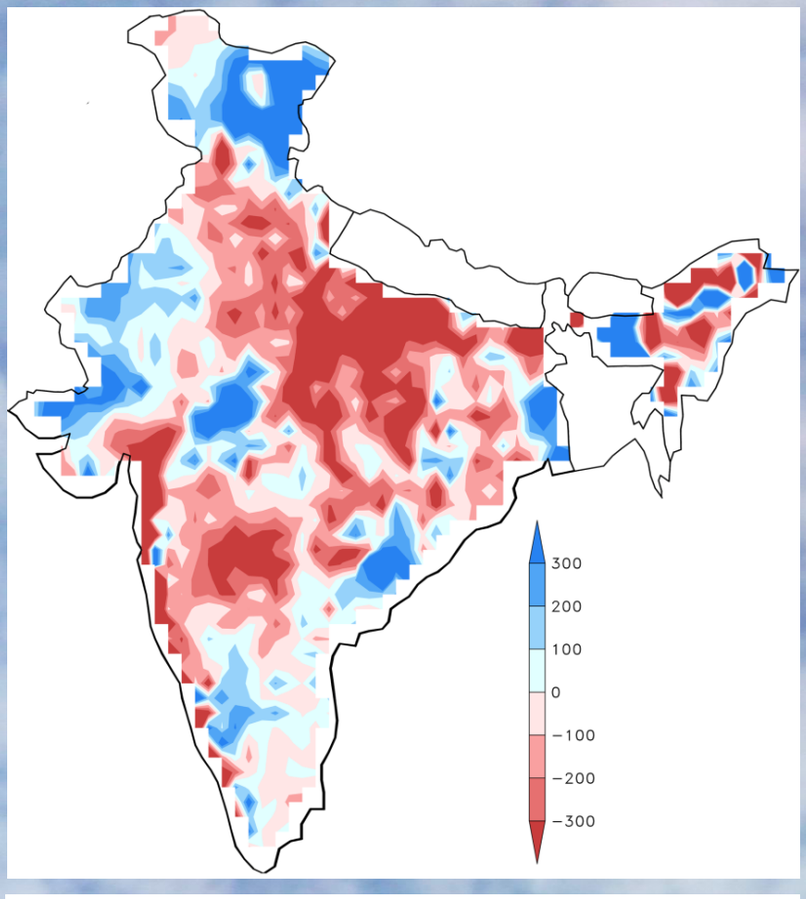

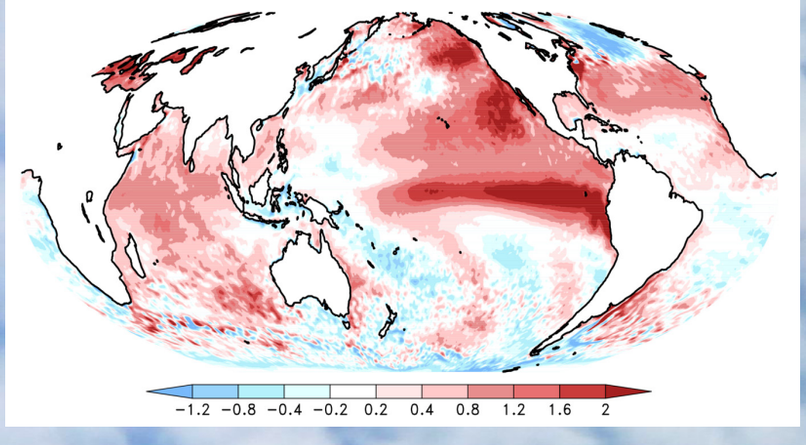

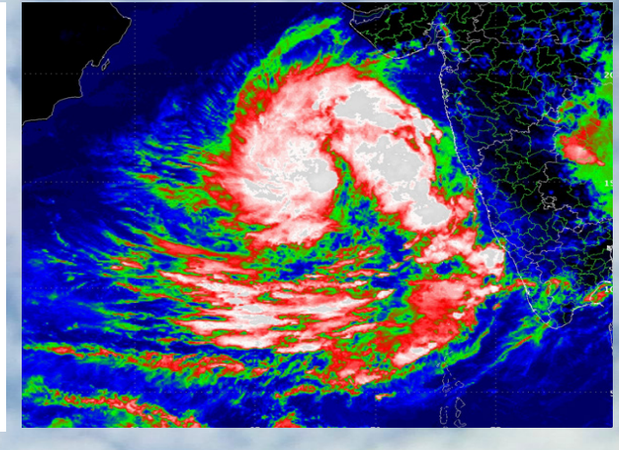

Edited by
Milind Mujumdar, C. Gnanaseelan and M. Rajeevan

Indian Institute of Tropical Meteorology (IITM)
Earth System Science Organisation (ESSO)
Ministry of Earth Sciences (MoES)
Pune, INDIA
http:/www.tropmet.res.in/

Seasonal rainfall anomaly (mm)

Drought conditions in Marathawada

August 2015 heavy down pour, leading to extreme rainfall event near Khandwa

Courtersy : Mr. Jai Nagda

SST anomalies (ºC) depicting 2015 El Nino

INSAT 3D picture of Cyclone ASHOBAA

ISSN 0252-1075

ESSO/IITM/SR/02(2015)/185

A Research Report on the 2015 Southwest Monsoon

Edited by

Milind Mujumdar, C. Gnanaseelan and M. Rajeevan

Indian Institute of Tropical Meteorology, Pune, India

*** Corresponding Author Address:**
Dr. M. Rajeevan
Director, Indian Institute of Tropical Meteorology,
Dr. Homi Bhabha Road, Pashan,
Pune-411008, INDIA
Email: rajeevan@tropmet.res.in
Ph: +91-20-25904200
Fax: +91-20-25865142

Indian Institute of Tropical Meteorology (IITM)
Earth System Science Organisation (ESSO)
Ministry of Earth Sciences (MoES)
Pune, INDIA
http:/www.tropmet.res.in/

DOCUMENT CONTROL SHEET

Earth System Science Organisation (ESSO)
Ministry of Earth Sciences (MoES)
Indian Institute of Tropical Meteorology (IITM)

ESSO Document Number
ESSO/IITM/SR/02(2015)/185

Title of the report
A Research Report on the 2015 Southwest Monsoon

Edited by
Milind Mujumdar, C. Gnanaseelan and M. Rajeevan

Type of Document
Scientific Report (Research Report)

Number of pages and figures
78, 72

Number of references
56

Keywords
Southwest Monsoon, ENSO, El Niño, IOD, Walker Circulation

Security classification
Open

Distribution
Unrestricted

Date of Publication
17 November 2015

Abstract

The present report is a collection of research results presented, by IITM scientists and other experts at the IITM Monsoon Discussion Forums (IMDF) during conspicuous boreal summer of 2015. The evolution of the consecutive deficit Indian summer monsoon, with developing El Niño phenomenon over the Pacific, turned out to be the fourth intriguing episode of last century. This report highlights the challenging regional and global research as well as prediction aspects of the complex atmosphere-ocean-coupled Asian monsoon system, which was dominated by faster mode of rainfall variability. The prominent elements of this system are evolution of the canonical El Niño, ENSO induced anomalous Walker circulation, weakening of Southwest monsoon flow, recurvature of west-Pacific tropical cyclones, isolated extreme rainfall events and recurrent dry spells over South-Asia during 2015.

A Research Report on the 2015 Southwest Monsoon

Edited by
Milind Mujumdar, C. Gnanaseelan and M. Rajeevan

CONTENTS

Introduction

After the persistent hot weather and dryness during the pre-monsoon months, the Southwest monsoon (SWM) rains arrive over the Indian subcontinent with amazing regularity. The SWM is a unique component of the boreal summer monsoon. The long-term stability of Indian summer monsoon, an integral part of SWM, is unique in itself; however, every year it throws manifold surprises and challenges to the operational and research community. The Pacific ENSO and Indian summer monsoon teleconnection was found to be one of the key factors in understanding of year-to-year monsoon variability (Walker 1910, 1914, 1923, Sikka, 1980; Pant and Parthsarthy 1981; Rasmusson and Carpentor, 1983, Shukla and Paolino, 1983). The evolution of the 2015 Indian summer monsoon with developing El Niño over the Pacific was very intriguing. In early June, India Meteorological Department (IMD) had issued the seasonal forecast for the 2015 SWM suggesting that it would be a deficient one. It is worth highlighting that this forecast was for the year succeeding a deficient monsoon year (seasonal rainfall deficit of 2014 is 12%). However, above normal rainfall distribution during the month of June 2015 raised doubt over the influence of the developing El Niño, paving the way for discussions on the robustness of El Niño teleconnections and the reliability of IMD's operational forecasts of a deficient 2015 monsoon. However, by the second half of July, the well marked regional and remote impacts of the canonical El Niño, such as the anomalous east-west Walker circulation, weakening of SWM flow, the recurvature of tropical cyclones in the west-Pacific, etc. were observed. Moreover, isolated extreme flood events, prolonged dry spells spreading across the country and the peculiar evolution of synoptic events over the northern Arabian Sea and the Bay of Bengal (BoB) are some of the key features of 2015 monsoon season.

The present report is a collection of research results presented at the IITM Monsoon Discussion Forums (IMDF) during boreal summer of 2015 (see Appendix I). The main objective of IMDF was to motivate students and researchers in understanding and exploring the challenges of current Southwest Monsoon. The IITM scientists have participated in the lively discussions on various aspects of the southwest monsoon like synoptic and large scale atmospheric and oceanic features, observational aspects, extended range and seasonal forecasts. The valuable inputs and association from other organizations like India Meteorological Department (IMD), INCOIS, NCMRWF and experts like, Prof. (Mrs.) Sulochana Gadgil, Prof. Raghu Murtugudde, Dr. D. S. Pai and others, widened the scope of discussions. The present report includes the major research findings made by the IITM scientists during the Monsoon Discussion Forums. The large-scale features of SWM are covered in Chapter-1. Chapter-2 covers the intriguing oceanic features. The highlights of important synoptic scale systems are presented in Chapter-3. The relevant observational evidences and facts are outlined in Chapter-4. The various aspects of the Extended Range Prediction System (ERPS) and Long Range Seasonal Forecast are covered in Chapter-5 and Chapter-6, respectively. The challenges and intriguing features of the boreal summer monsoon 2015 are summarized at the end.

Chapter 1

Chapter 1 - Large Scale Features of Southwest Monsoon During 2015

Hamza Varikoden, Bhupendra Bahadur Singh, K.P. Sooraj, Manish K. Joshi, B. Preethi, Milind Mujumdar and M. Rajeevan

1.1 Rainfall features

During 2015, the southwest monsoon (SWM) rainfall over the country remained deficient with seasonal rainfall of about 86% of the long period average (Table 1.1). Last year, the seasonal rainfall deficiency over the country as a whole was 12% (www.imd.gov.in). Thus, this is a fourth episode of two consecutive years, with deficient monsoon, similar to 1904-05, 1965-66 and 1986-87 (www.imd.gov.in).

However, the analysis at a monthly scale reveals the intrinsic and pronounced spatial variability of the 2015 monsoon. For June 2015, rainfall over the country as a whole was 16% above the long period average (Figures 1.1a-c and Table 1.1). During this month, the rainfall activity was above normal over Central India, with a deluge of rainfall extending to eastern and southern Peninsular India. But, the monthly rainfall remained subdued over the northeastern part of India. This was in contrast to the rainfall during June 2014 (figure not shown), which received only 58% of the long period average. During July 2015 (Figures 1.1d-f), the rainfall across the country was deficient by 16% (Table 1.1). The monthly rainfall was above normal only over central to northwest India, with the rest of the country registering below normal rainfall activity during July 2015. Note that the daily cumulative rainfall over India as a whole, until 31st July (www.imd.gov.in), showed a percentage departure of only -4% from the long period cumulative mean. In contrast, the 2014 SWM registered a dauntingly enormous percentage deficit of 22% by 31 July 2014 (figure not shown). During August 2015 (Figures 1.1g-i), the country as a whole witnessed subdued rainfall activity, with the rainfall deficit deteriorating further to 24%. However, there was isolated rainfall activity over the eastern Peninsular region, particularly confined to Tamil Nadu and erstwhile Andhra Pradesh. During September 2015 (Figures 1.1j-l), the rainfall activity further reduced, with the whole country receiving only 76% of the long period average rainfall. Rainfall activity was confined to Orissa and its neighboring regions. In particular, the region extending from central to northeast India registered an acute rainfall deficit. The seasonal rainfall (Figures 1.1m-o) for the entire country was 86.4% of the long period average, thus amounting the rainfall deficit to 14%. Over the four homogenous rainfall zones (defined by IMD, www.imd.gov.in), the seasonal cumulative rainfall showed a percentage of departure -17, -8.4, -16.4 and -15.4%, respectively over the northwest, east-northeast, central and south Peninsular India. Moreover, the standardized daily rainfall anomalies over the core monsoon zone (Rajeevan et al., 2010) recorded a significant amount of break monsoon days (accumulating to 36) during the entire season (Figure 1.2), with prolonged below normal rainfall activity during August to September 2015, further corroborating the seasonal rainfall deficit across the country (Rajeevan et al., 2010). There were only isolated above normal rainfall activities (during 13-26 June and 15-23 September). The subdued rainfall activity across the country is further manifested in the weekly rainfall departure, as shown in Figure 3.3.

1.2 Mean and anomalies of wind at lower and upper levels

During the southwest monsoon season, the winds at lower levels from the southern hemisphere cross the equator off the Somali coast and turn towards the Indian Peninsula with an average speed of

around 15 ms-1 and this wind is called the Low Level Jetstream (LLJ, Joseph and Raman, 1966). The strength of the LLJ increases from June to August and thereafter it decreases. During 2015, the LLJ was weaker compared to the climatological value (Figure 1.3). The weaker LLJ is due to a weaker Mascarene High and associated weaker outflow and cross equatorial flow along the Somali coast. The strong easterly anomalies over the Arabian Sea and BoB, indicate the weaker LLJ. Over the Indian region, anomalous anticyclonic flow is observed suggesting a weaker monsoon circulation. In July and August 2015, the Arabian Sea and south Bay of Bengal branches of the LLJ were considerably weaker. During September 2015, the low level winds over the Arabian Sea slightly intensified; however the BoB branch remained weak. For the season as a whole, the wind at 850 hPa did not pick up enough strength over the entire north Indian Ocean, showing easterly anomalies over the north Indian Ocean and weaker cross equatorial flow across the Somali coast (Figures 1.3e,j). The weaker cross equatorial flow was due to a weaker Mascarene High in the southern hemisphere and associated outflow (figure not shown). Over the equatorial Pacific, westerly anomalies were observed at 850 hPa suggesting El Niño conditions as documented in section 1.3 (Figure 1.5).

Similar to the LLJ evolution during the SWM season, the evolution of the Tropical Easterly Jet Stream (TEJ) is also a characteristic feature of the SWM (Koteswaram, 1958). It evolves over the north off-equatorial regions with slight northward movement and its core is situated at an altitude of about 150 hPa. During June 2015, the TEJ evolved around the central equatorial Indian Ocean (Figure 1.4a), however, an anomalous westerly component, over the northern Indian Ocean, indicates a weaker TEJ (Figure 1.4f). Interestingly, the Tibetan anticyclone depicted weaker to moderate monthly variation (Figures 1.4f-i), however on the seasonal scale this structure is weak (Figure 1.4j). The slight northward movement of upper level tropical easterlies (part of the TEJ) and subtropical westerlies during the month of July 2015 seems to be conducive for moderate monsoonal activity (Figure 1.4b and g). During September, TEJ was weak and located over the equator. The Subtropical Westerly Jet stream was shifted southward with westerly anomalies over the northern parts of the country. However, the large-scale anomalous circulation over Asia-Pacific region clearly indicates weaker monsoon flow. Over the equatorial Pacific Ocean, the 200 hPa wind anomalies were easterlies as seen during canonical El Niño conditions (Rasmusson and Carpenter 1983) indicating weaker/reversed Walker Circulation. In general, the weaker SWM circulation patterns are consistent with the deficient rainfall activity over India as evident from Figure 1.1.

1.3 Sea Surface Temperature (SST) anomalies

During the month of June, the Indo-Pacific SST anomalies were mostly positive, with excessive warming over the equatorial Indian Ocean and the eastern Pacific Ocean. The westward extension of warming beyond the dateline, over the equatorial Pacific Ocean (Figure 1.5a), is suggestive of emerging canonical El Niño conditions (Rassmussen and Carpenter, 1983). The warm anomalies are prominent over the northeast Pacific Ocean as well. The BoB and the Arabian Sea also experienced positive SST anomalies during the month of June. Meanwhile, the amplitude of the anomalous warming over the Indian Ocean reduced during the following summer monsoon months and resulted in a negative north-south anomalous SST gradient (Shankar et al., 2007), particularly over the Bay of Bengal (Figure 1.5b). This feature is somewhat surprising. Moreover, the El Niño signal became prominent during the month of July. The detailed description of El Niño related Oceanic features is given in Chapter 2. This anomalous Indo-Pacific SST pattern is consistent with the reduction in July rainfall (Figure 1.1f) and the associated weakened low level monsoon circulation (Figure 1.3g). During the

month of August, the Indian Ocean witnessed a signature of moderate positive IOD (Saji et al., 1999), with anomalously warm SSTs over the western equatorial Indian Ocean and moderately cooler-than-normal SSTs over the eastern equatorial Indian Ocean (Figure 1.5c). However, the signature weakened during September due to the weakening of negative anomalies over the eastern Indian Ocean (Figure 1.5d). On the other hand, the anomalous warming over the western Indian Ocean strengthened and extended northward over the Arabian Sea. The Indian Ocean warming and Indian Ocean Dipole are dealt with details in Section 2.4 of Chapter 2.

It is interesting to note that the abnormal warming of the northeast Pacific Ocean has prevailed throughout the season (Figure 1.5a-d), strengthening and extending westward, especially from June to September. Over the tropical Pacific, the maximum SST anomalies were located along the Niño1+2 region during the beginning of the monsoon season (in June). As the season progressed, the maximum SST anomalies moved to the Niño 3 and Niño 3.4 regions (Figures 1.5b-d). The El Niño related equatorial Pacific SST gradient also strengthened with the progression of the seasons and the maximum amplitude was observed during the month of September (Figure 1.5d). Concisely, the most prominent signal for the season as a whole is the eastern Pacific El Niño pattern extending to the date line and the anomalous warming over the northeast Pacific Ocean (Figure 1.5e), which made the El Niño condition of 2015 distinct from previous El Niño years. On the other hand, the most interesting feature of the Indian Ocean is the existence of a negative north-south gradient in SST anomalies, especially in the Bay of Bengal (Shankar et al., 2007) with more anomalous warming over the western Indian Ocean as compared to that of its eastern counterpart (Figure 1.5e).

1.4 Mean and anomalous Outgoing Longwave Radiation (OLR) patterns

Figure 1.6 shows that during June, high convective activity with OLR less than 200 Wm^{-2} (Gruber and Krueger, 1984; Lau et al., 1997) is mainly observed over the equatorial western Pacific, BoB and Arabian Sea. However, the anomaly pattern indicates enhanced convection over the Arabian Sea, but with suppressed convection over the equatorial western Pacific and BoB. This contrasting convective pattern over the Arabian Sea and the BoB is intriguing. The July mean pattern shows enhanced convection over the head BoB, but with reduced convection over the equatorial western Pacific as compared to that of June. The anomaly pattern during July shows suppressed convection over the equatorial western Pacific and most of the north Indian Ocean. A clear east-west gradient of OLR anomalies is seen in the equatorial Pacific during July. This is also consistent with the July lower level wind pattern (Figure 1.3) where a westerly anomaly is seen over the equatorial Pacific.

During August the mean convection over the BoB has weakened as compared to July and the corresponding anomaly pattern reveals suppressed convection over most of the equatorial western Pacific and north Indian Ocean. The east-west gradient in the anomalous pattern over the equatorial Pacific has strengthen (Figure 1.6h). These features are consistent with the anomalous upper level wind circulation as discussed earlier (Figure 1.4). During September, convection weakens over the BoB, while strengthening of convection over the central and eastern Pacific is evident. The anomaly pattern shows a stronger east-west gradient in the equatorial Pacific depicting a strong El Niño signal (Figure 1.5). It is also interesting to note the enhanced convection over the southern Indian Peninsula (Figure 1.6i). The extension of suppressed convection from the warm pool region to the central Indian Ocean seems to be associated with the weakening of negative SST anomalies over the eastern Indian Ocean (Figure 1.5d). The seasonal mean OLR (Figure 1.6e) shows intense convection over the BoB and the equatorial eastern Pacific, associated with the El Niño event. The seasonal anomaly clearly reflects the Pacific El Niño conditions with suppressed convection over the equatorial

western Pacific, BoB and over the Indian subcontinent, while enhanced convection over the equatorial central Pacific extends up to the equatorial eastern Pacific. It is worth noting that the suppressed convection over the west Pacific warm pool region extends westwards up to the central equatorial Indian Ocean (Figure 1.6j).

1.5 Velocity Potential anomalies at lower and upper levels

Figure 1.7 shows the velocity potential anomalies at 850 hPa and 200 hPa for the months of June, July, August, and September as well as for the entire monsoon season. The low-level convergence (rising branch)/ divergence (sinking branch) at 850 hPa is generally manifested as the upper level divergence/convergence at 200 hPa, which strongly indicates the large-scale zonal overturning circulations (Krishnamurti, 1971; Palmer et al., 1992). The climatology of velocity potential at 850 hPa (figure not shown) shows a rising branch of the Walker circulation over the western Pacific and Maritime Continent, coinciding with strong convection over the region, and a descending branch over the eastern Pacific. These ascending and descending branches are connected with low-level easterlies and upper level westerlies over the central and eastern Pacific. During June, the anomalous east-west overturning circulation over the Indo-Pacific region is not very clear. In contrast to June, the anomalies for the months of July to September as well as for the entire monsoon season depict a weakening of the zonal overturning circulation. This is consistent with the eastern Pacific warming signal (Figure 1.5), and indicates an El Niño related anomalous Walker cell, i.e., showing divergence (convergence) over the western end of Pacific extending to the Indian subcontinent and convergence (divergence) over the eastern to central Pacific at 850 hPa (200 hPa). This anomalous circulation weakens easterly (westerly) winds across the eastern Pacific in the lower (upper) atmosphere, which is clearly seen in the wind anomalies as depicted in Figure 1.3 (Figure 1.4). These anomalous circulation features clearly reflect anomalous Walker circulation related to the canonical El Niño episode (Webster et al., 1998).

1.6 Monsoon convection propagation characteristics

The summer monsoon 2015 is associated with two prominent northward propagating bands of anomalous convection from the equatorial Indian Ocean to the Indian subcontinent, one during the month of June and another during the end of July to the beginning of August (Figure 1.8a,d). The time-latitude section of daily OLR averaged over the Indian subcontinent clearly depicts the anomalous south to north propagation of convection, extending mainly from 5o S to 25o N (Figure 1.8a,d). Furthermore, the northward movement of convection is anomalously suppressed during the month of July and from the second week of August through September (Figure 1.8d), consistent with the anomalous reduction in rainfall during these months (Figure 1.1f,i,l). It is to be noted that the northward propagating convective cloud bands were less over the Arabian Sea compared to the BoB (Figure 1.8b,c). Intriguingly, the Arabian Sea witnessed strong northward propagation of anomalous convection during the month of June, and weakened propagation by the end of July (Figure 1.8b,e). On the other hand, strong northward propagation is observed over the BoB during the first half of June and August, with a weak propagation during the first half of July (Figure 1.8c,f). The comparison between the northward propagation of convection over the Indian subcontinent (Figure 1.8a,d), the Arabian Sea (Figure 1.8b,e) and the BoB (Figure 1.8c,f) suggest that the convection over the Indian subcontinent has a significant contribution from the BoB branch throughout the season, whereas the Arabian Sea contribution was mainly during the month of June.

The propagation of convection to the core monsoon region from the east is mainly associated with the westward propagation of synoptic scale convective systems that originate over the warm waters of the

BoB and also from the remnants of the west Pacific typhoons (Sikka and Gadgil, 1980; Rajeevan, 1993). These propagation characteristics have been examined by averaging daily OLR over the latitudinal belt of 15-25o N (Figure 1.9). Clear westward propagation can be observed during the month of June, second half of July, first half of August and also during the end of September (Figure 1.9a,b), supporting the prominent contribution of synoptic scale disturbances to the rainfall during these periods (as described in Section 3.1 see Figure 3.1). The modelling and simulation aspects of meridional and zonal propagation of convection on intra-seasonal scale are mostly dealt in Section 5.2 of Chapter 5. Consistently, rainfall averaged over the core monsoon zone (Rajeevan et al., 2010) is also anomalously high during the month of June, the second half of July and the last two weeks of September (Figure 1.2). Spectral analysis of rainfall over the core monsoon region clearly depicts that the oscillations with approximately 8 day and 16 day periodicities are significantly dominant during the monsoon season (Figure 1.10a). The maximum variance in the oscillation with 8 days periodicity occurs during the second half of June to the first half of August (Figure 1.10b), when a considerable amount of rainfall occurs over the region (Figure 1.2). This therefore suggests that the significant contribution of rainfall is from the seven intense low pressure systems formed during the three month period (Figure 3.1). On the other hand, the anomalous rainfall during the second half of September (Figure 1.2) appears to be mainly associated with the 10-20 day periodicity (Figure 1.10b). This is supported by the occurrence of a depression over the BoB during the third week of September (Figure 3.1), manifested as the westward propagation of anomalous convection (Figure 1.9) and by the absence of northward propagation (Figure 1.8a,d). A slower 30 day mode was also present during early June to mid-July and towards the end of September, but was statistically insignificant. It is known that the westward propagating synoptic scale systems are the manifestation of oscillations with 10-20 day (faster mode) periodicity, whereas the northward propagation of convection from the equatorial Indian Ocean is the manifestation of 30–60 day (slower mode) oscillations (Sikka and Gadgil, 1980). Thus it is intriguing to note that the rainfall activity during the deficient monsoon season of 2015 is dominated by the faster mode of variability. However, this is in contrast to the previous deficient years, which are mainly dominated by the slower 30-60 day mode of variability, whereas the faster 10–20 day mode is generally dominant during normal years of Indian summer monsoon rainfall (Kripalani et al., 2004).

Table 1.1 Area weighted rainfall (mm) for the country as a whole during the summer monsoon season of 2015. Courtesy: IMD

Months	Actual (mm)	Normal (mm)	% of long period mean
June	189.5	163.6	115.8
July	241.9	289.2	83.7
August	204.2	261.3	78.1
September	131.4	173.4	76.0
June to September	767.0	887.5	86.4

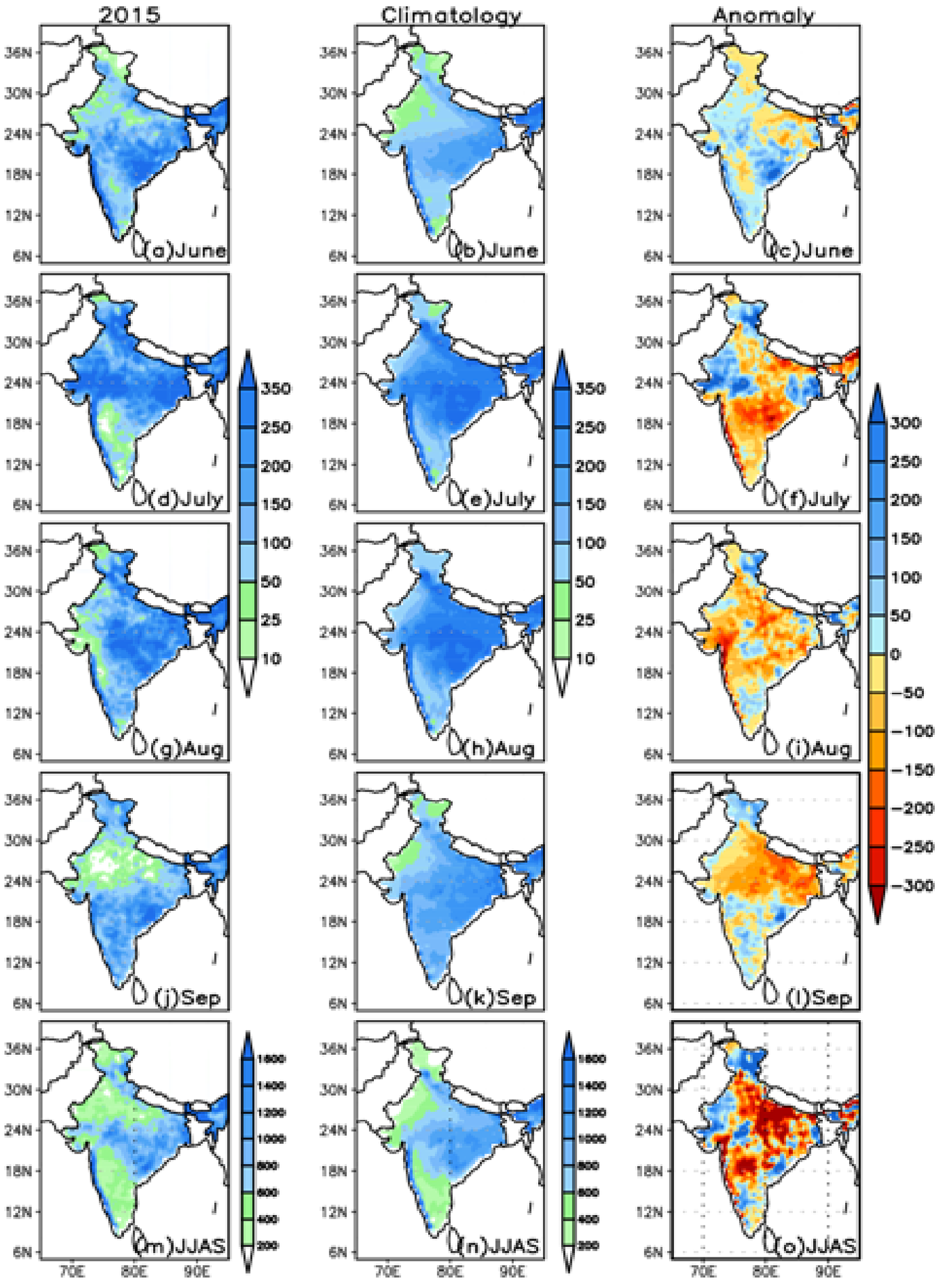

Figure 1.1 Cumulative rainfall (mm) maps for the 2015 southwest monsoon. (a) Actual, (b) Climatology and (c) Anomalous rainfall for the month of June. (d)-(f) are the same, but for July. Similarly, (g)-(i) for August, (j)-(l) for September and (m)-(o) for June to September (JJAS) season. Gridded data are from www.imd.gov.in. The base period for climatology is 1980-2010, for all figures of this chapter.

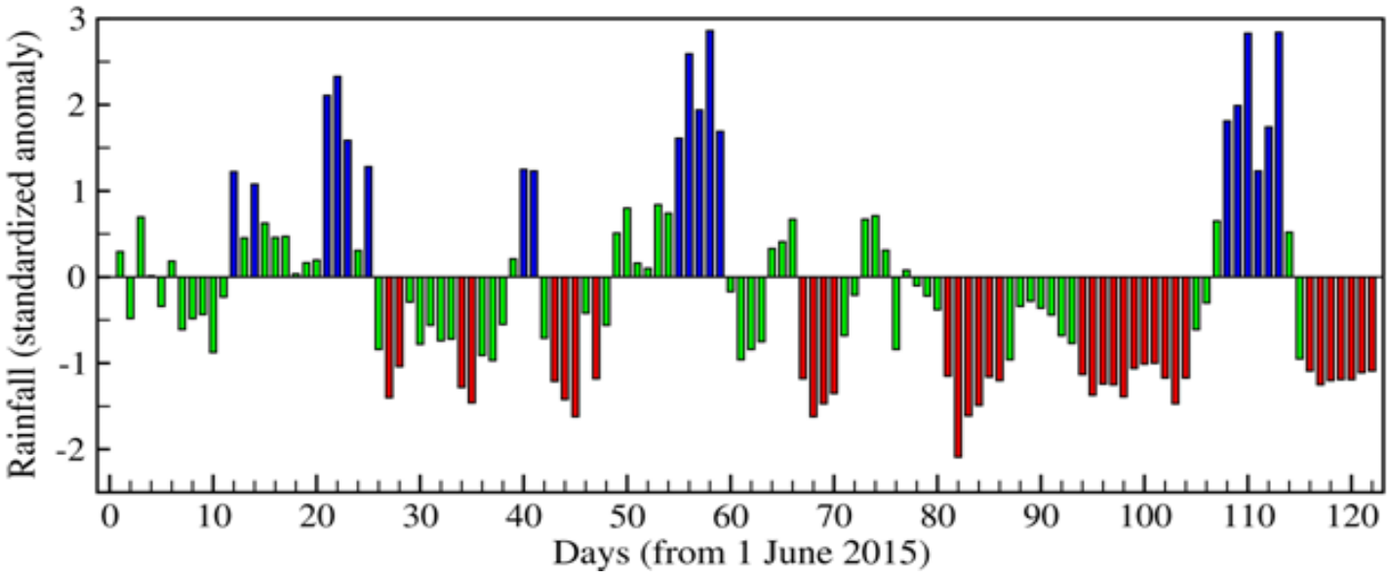

Figure 1.2 Standardized daily rainfall anomaly over the core monsoon zone, for the summer monsoon 2015. Days with rainfall anomalies in red color indicates break monsoon days (Standardized anomaly less than -1.0) and blue colour indicates active monsoon days (Standardized anomaly more than +1.0).

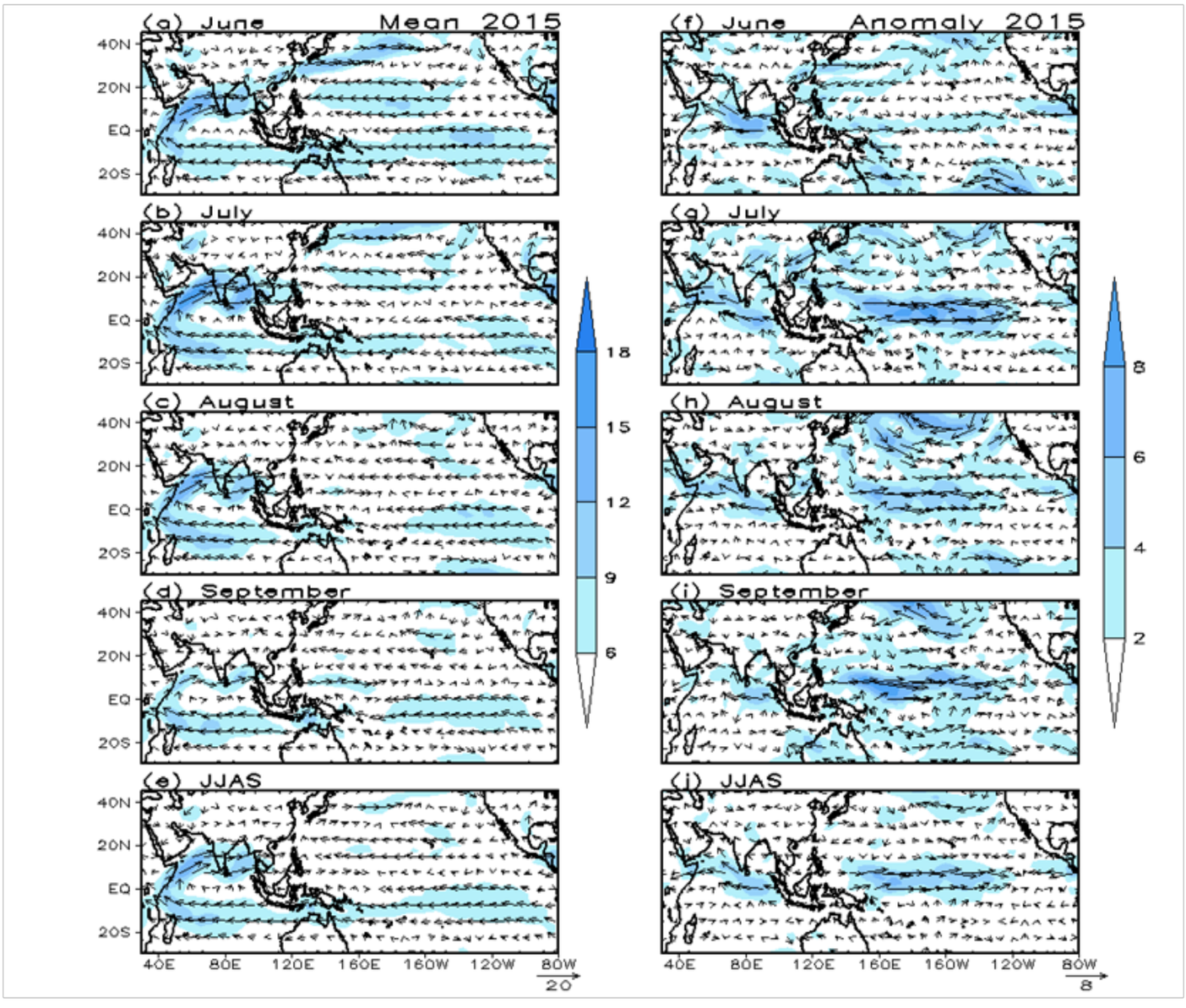

Figure 1.3 (a-e) mean and (f-j) anomalies of winds (ms-1) at 850 hPa for (a,f) June, (b,g) July, (c,h) August, (d,i) September and (e,j) JJAS season during 2015. Data source: NCEP/NCAR reanalysis.

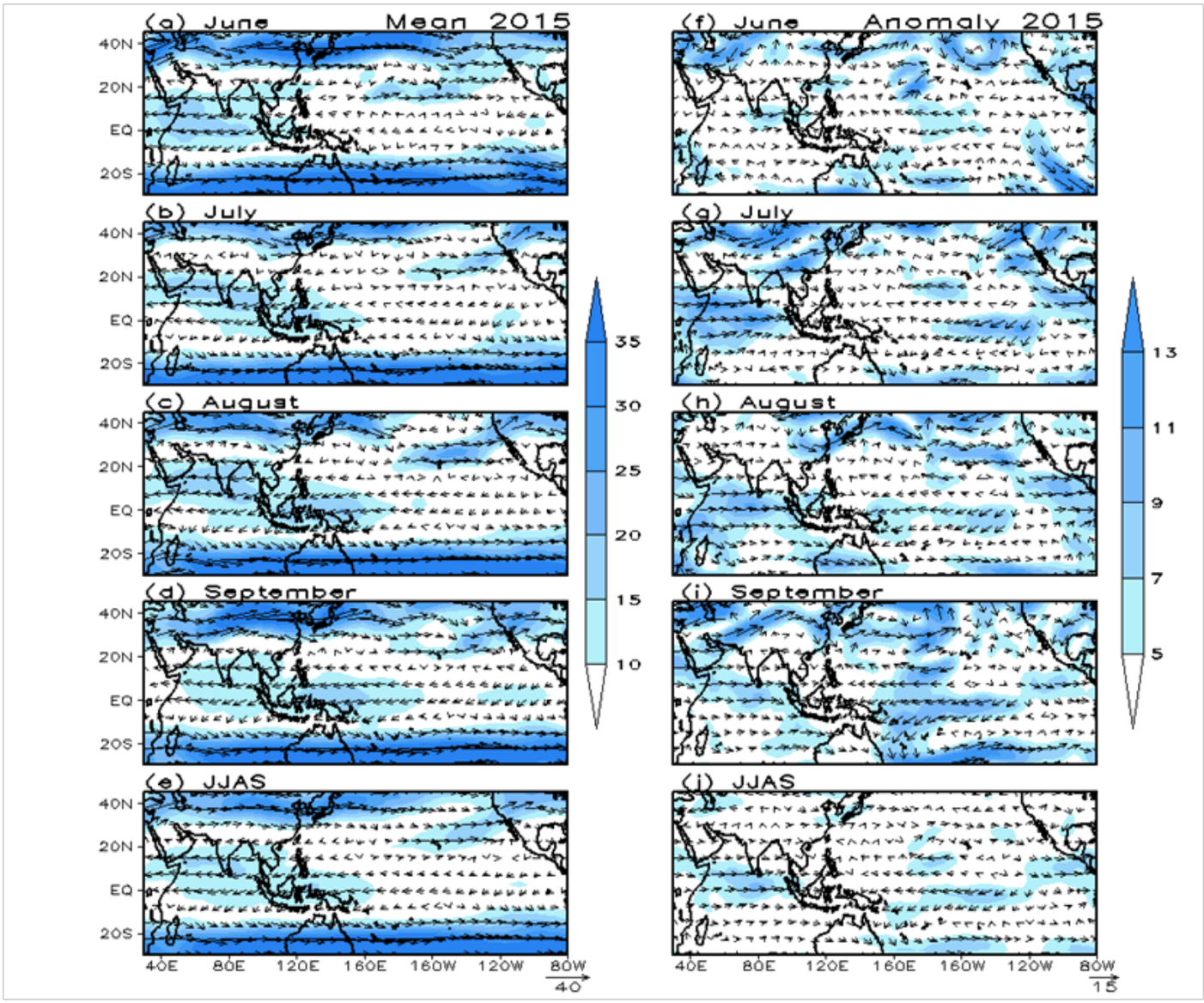

Figure 1.4 Similar to Figure 1.2, except for 200 hPa.

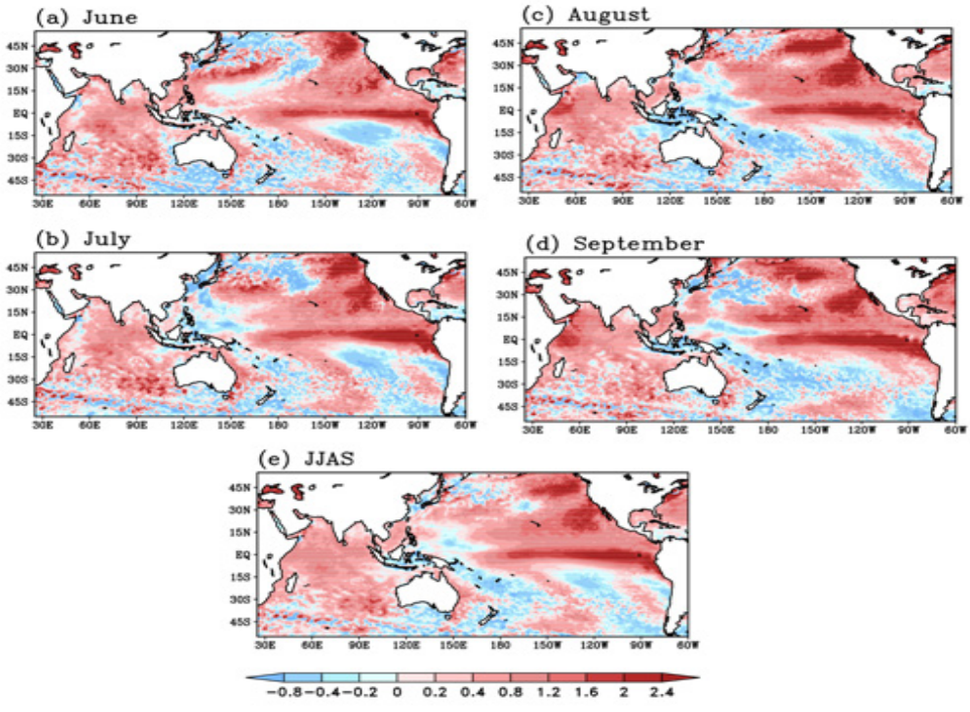

Figure 1.5 Sea surface temperature anomalies (°C) for (a) June, (b) July, (c) August, (d) September and (e) JJAS season during 2015. Data source: Reynolds SST.

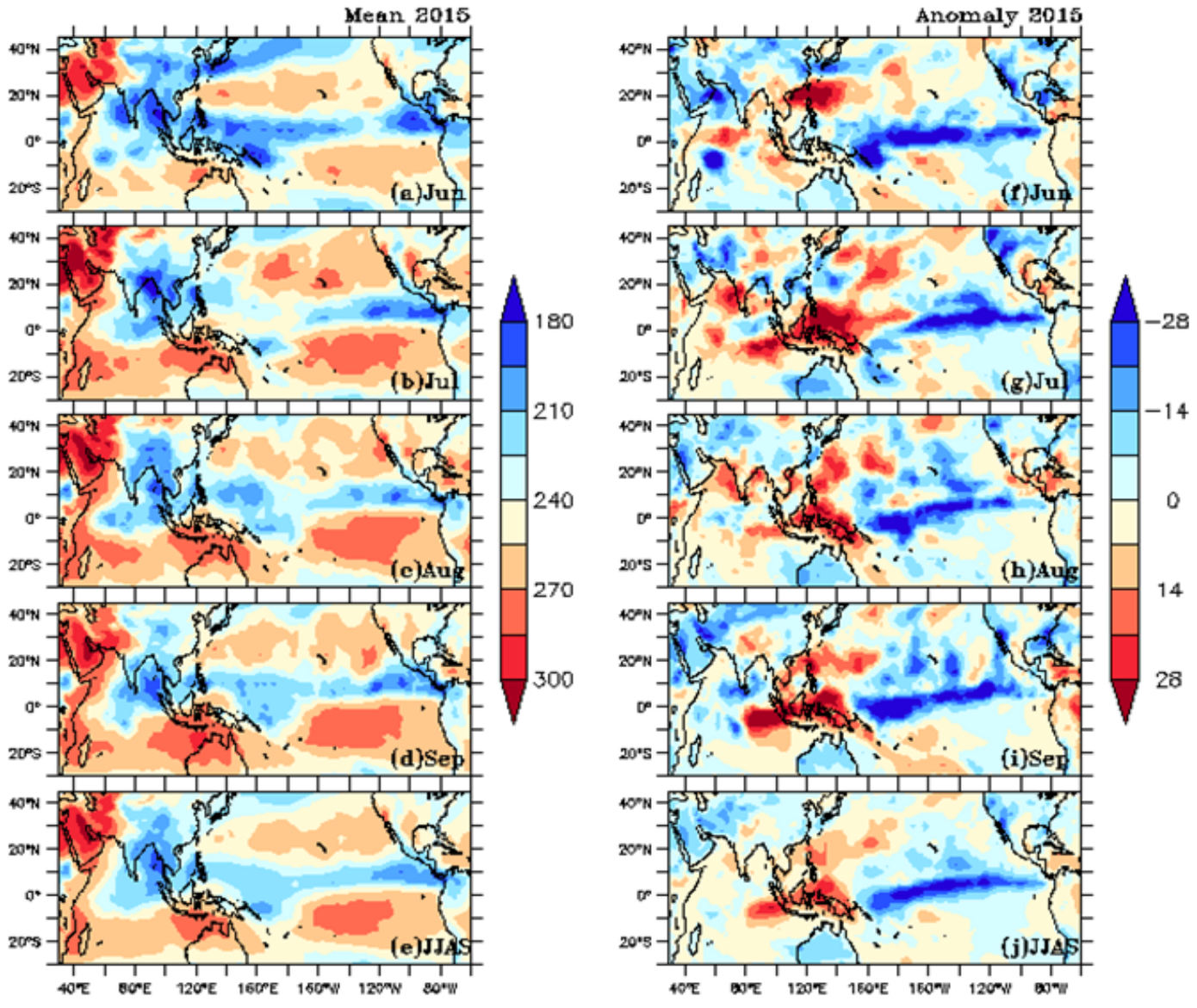

Figure 1.6 Monthly mean (left panel) and anomalies (right panel) of OLR (Wm^{-2}) during 2015. Deep convection in the tropics is characterized by low cloud-top temperatures and small OLR values; while high OLR values indicate scarcity or absence of cloud cover. The spatial distributions of monthly mean OLR during the months of June to September are shown in (a) to (d), respectively. (e) Illustrates the JJAS seasonal mean of OLR. Right panel is similar to that of left panel, except for OLR anomalies. Low (high) / negative (positive) OLR values are blue (red) shaded. Data source: NOAA (http://www.cdc.noaa.gov).

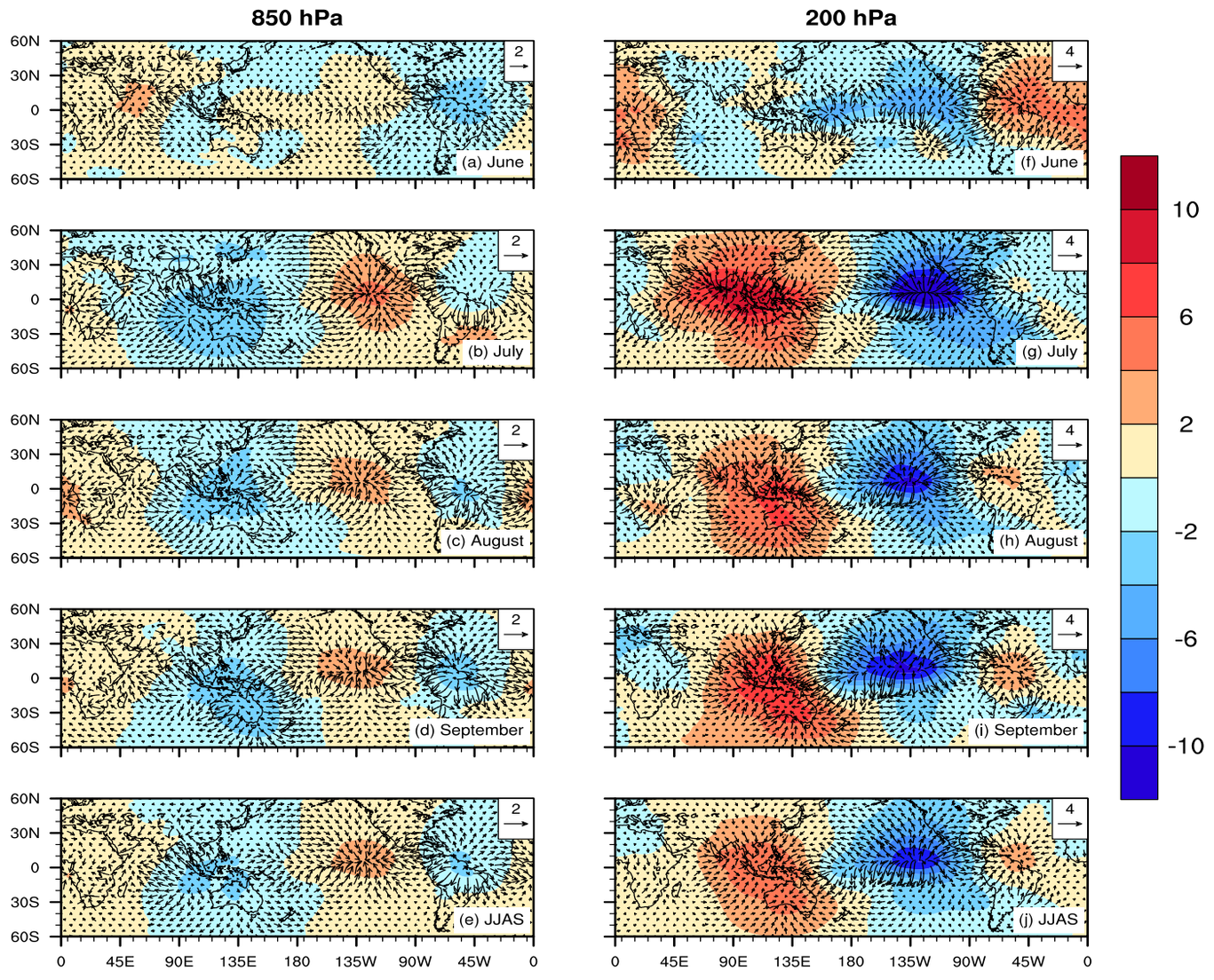

Figure 1.7 Velocity Potential anomalies (10^6 m^2/s) at (a-e) 850 hPa and (f-j) 200 hPa for the months of June, July, August, September and for the JJAS season. Data source: NCEP/NCAR reanalysis

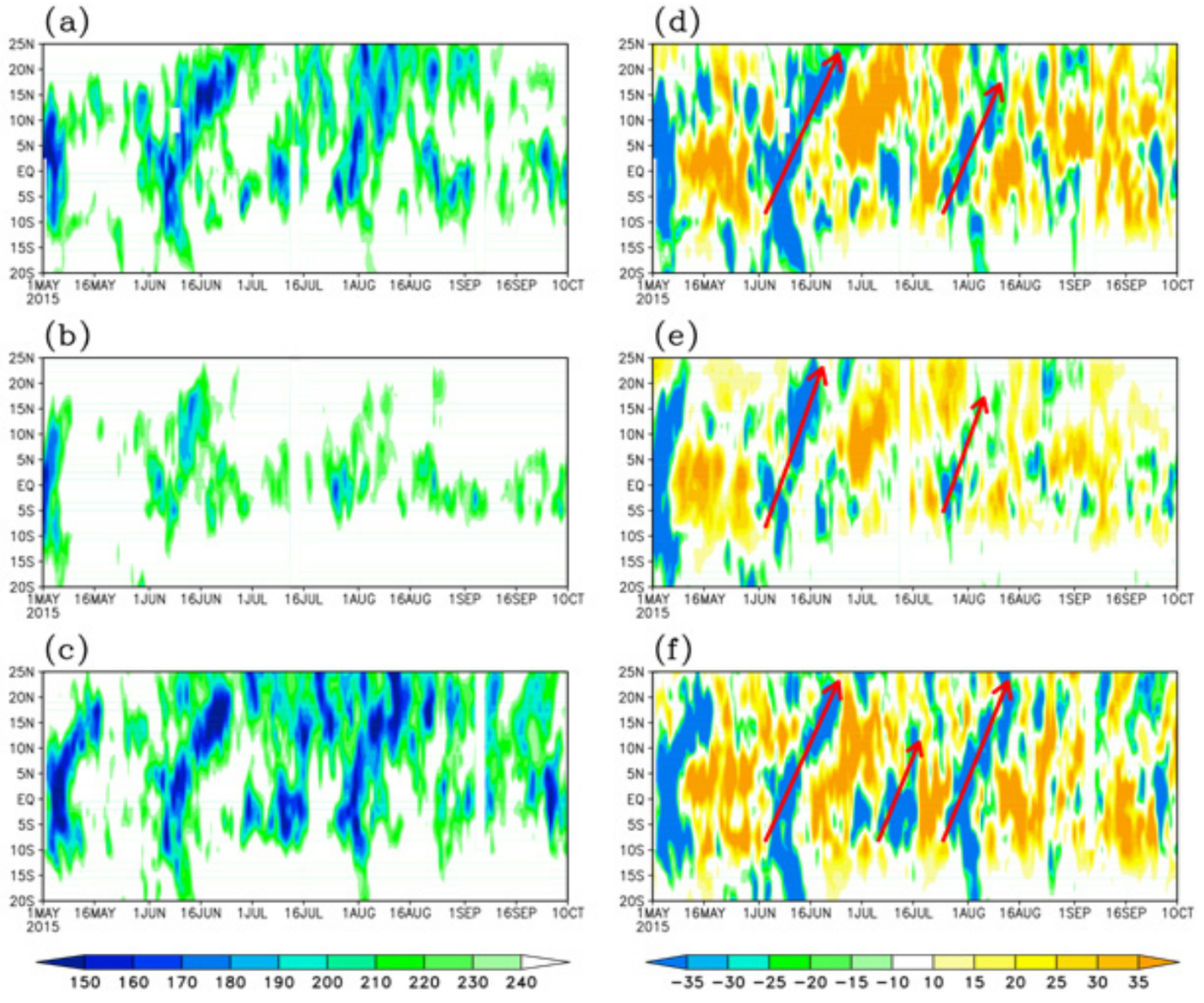

Figure 1.8 Time-Latitude sections of (a-c) mean and (d-f) anomalies in daily OLR (Wm^{-2}) for the summer monsoon 2015. Panels (a and d) for the Indian subcontinent (averaged over the longitude belt of 70-85°E), (b and e) for the Arabian Sea (averaged over the longitude belt of 50-75°E) and (c and f) for the Bay of Bengal (averaged over the longitude belt of 80-95°E). Red arrows denote dominant northward propagating bands of anomalous convection. Data source: NOAA.

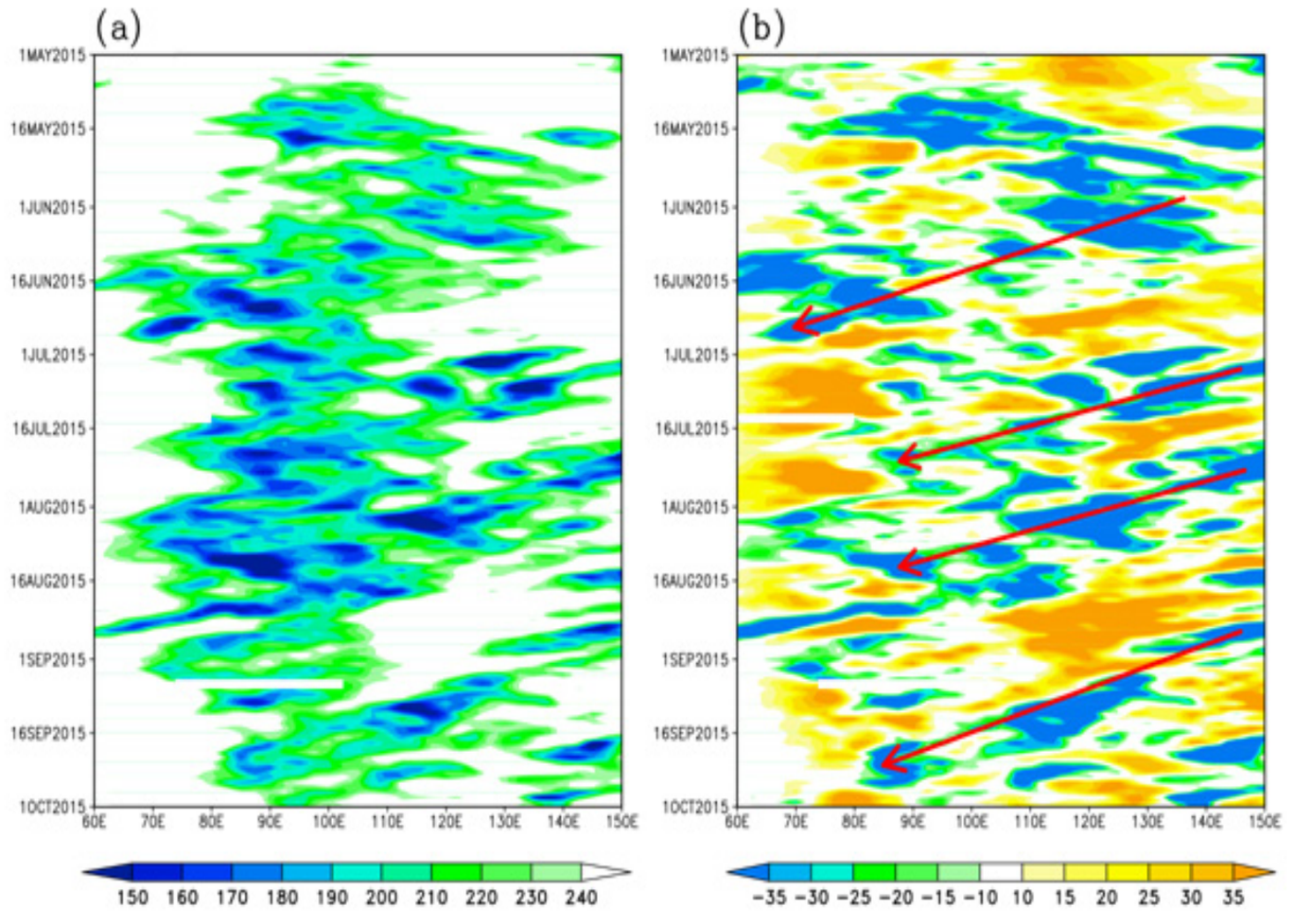

Figure 1.9 Time-Longitude sections of (a) mean and (b) anomalies in daily OLR (Wm^{-2}) for the summer monsoon 2015, averaged over the latitude belt of 15-25°E. Red arrows denote dominant westward propagating bands of anomalous convection. Data source: NOAA

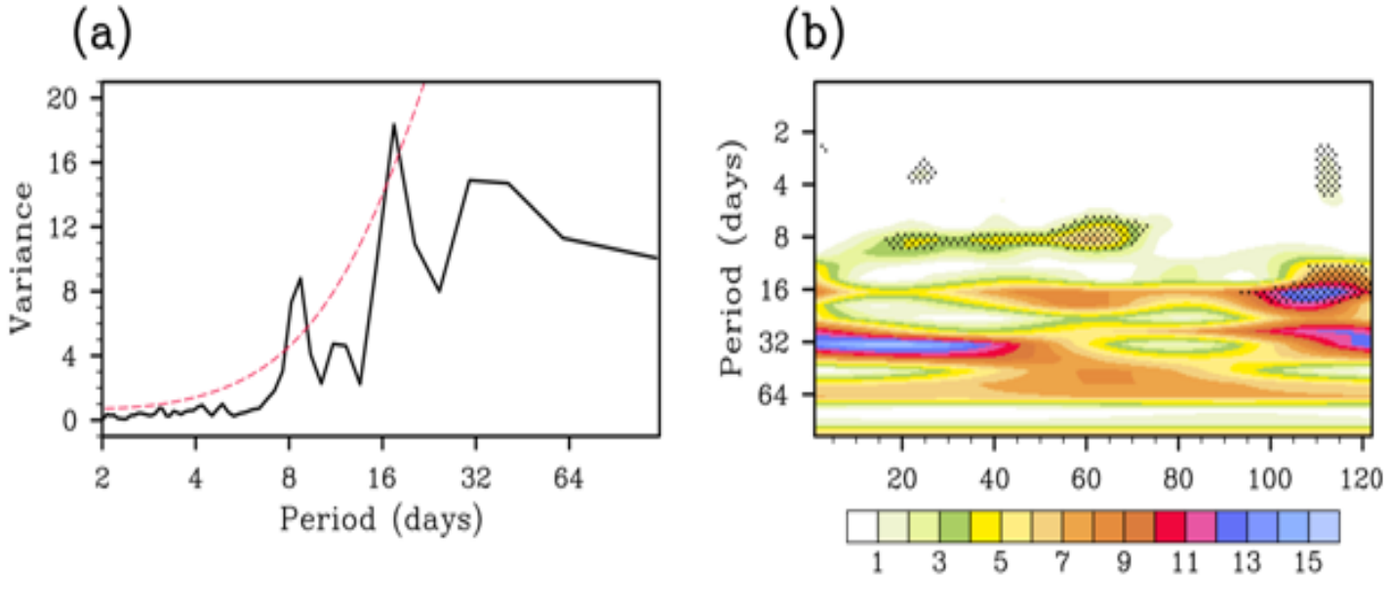

Figure 1.10 (a) Spectral and (b) wavelet analysis of rainfall over the core monsoon zone, for the summer monsoon 2015. Red dash line in (b) and black dots in (c) denote statistical significance at 95% confidence level. Data source: IMD.

Chapter 2

Oceanic Features in the Indo-Pacific Region During the Southwest Monsoon 2015

Rashmi Khandekar, C. Gnanaseelan, P. Swapna, Anant Parekh, P. Sreenivas, G. Srinivas, J. S. Chowdary and J. S. Deepa

2.1 Evolution of sea surface temperature anomalies during summer 2015

The evolution of global SST anomalies (^oC) and the tendency from previous month during summer 2015 (June to September) is shown in Figure 2.1. A peculiar feature is the warming in the east and central equatorial Pacific with warm SST anomalies extending west of the date line. Positive SST anomalies exceed 2^oC in the eastern Pacific, indicating the evolution of El Niño conditions. Anomalous warming can also be seen in the northeast Pacific off California coast, which may be associated with a positive phase of Pacific Decadal Oscillation or could be a precursor to a strong El Niño as shown by Vimont et al. (2003). The warming in the Niño 3 region has enhanced with the advancement of the season. However the positive SST anomalies over the Niño 1+2 regions fade away from July to August. Another important feature is the basin wide warming of the Indian Ocean with significant warming in the central equatorial Indian Ocean and southern Indian Ocean which can be seen throughout the summer season 2015. The SST tendency clearly indicates that the enhancement of warm anomalies from May to June in the eastern equatorial Pacific (Figure 2.1b), whereas the warming tendency moves westward with the progression of the season. The Indian Ocean warming tendency is mostly over the central basin until July and spreads to the western basin from August onwards.

Figure 2.2 displays the evolution of SST anomalies and SST tendency in IITM-GODAS (Sreenivas et al. 2015). This version of the assimilation system is slightly different from the one discussed in Chapter 5, where surface salinity in IITM-GODAS is restored to climatology. No such restoration is done in this version. It is important to note that the global SST evolution in IITM-GODAS is consistent with HadISST. Different El Niño indices are shown in Figure 2.3. All the Niño indices except Niño1+2 were in the positive phase throughout the year, whereas Niño1+2 entered the positive phase in April, peaked in July and thereafter the intensity of warming decreased. Niño3 and Niño3.4 show a steady increase throughout the summer monsoon season. The warming in Niño4 region remained steady during 2015.

2.2 Subsurface conditions in the Pacific associated with El Niño

The positive feedback between ocean and atmosphere through Bjerknes feedback (Bjerknes, 1969) is essential for the growth and persistence of an El Niño. The time evolution of SST, heat content and zonal wind anomalies are shown in Figure 2.4. The positive SST anomalies are seen in the central equatorial Pacific from boreal spring onwards, which persist till the end of the summer season (Figure 2.4a). The propagation of warm SST anomalies is associated with the anomalous westerly winds in the western Pacific during boreal spring. In line with the surface warming of central Pacific the upper ocean temperature shows warming, but which propagates eastward, strongly suggesting the presence of equatorial Kelvin waves. The anomalous westerlies over the western and central equatorial Pacific are known to generate downwelling Kelvin waves (e.g., Yu and Rienecker 1998), which propagate to the eastern Pacific. The downwelling Kelvin wave propagation is evident from the deepening of thermocline as shown by the positive heat content anomalies. The Kelvin waves reach the east Pacific by April and by then the SST anomaly maximum is located in the eastern Pacific.

The SST anomalies start propagating westward from April onwards from the east Pacific as in a typical canonical El Niño year. A deeper than normal eastern Pacific thermocline enhances positive Bjerknes feedback supporting the persistence and strengthening of El Niño. The SST and upper ocean temperature anomalies are well captured by IITM-GODAS and are consistent with Hadley Centre EN4.1.1 (Had-EN4) products. Some of the minor differences could be arising due to the differences in the forcing fields. For example some minor differences between NCEP and NCMRWF winds can be noted in Figures 2.4a,b and IITM-GODAS is forced by NCMRWF winds and fluxes.

The longitude depth plot of subsurface temperature anomalies in the equatorial Pacific during June to September 2015 is shown in Figure 2.5. As discussed before, warm subsurface temperature anomalies in the central to eastern equatorial Pacific and cold anomalies in the west are evident throughout the season. The discharge of warm water towards east and off the equator has resulted in cooling of subsurface water in the western equatorial Pacific Ocean. The western cooling however is restricted to west of the dateline for the entire summer season and the eastward propagation of cold subsurface water is very weak. The eastward propagation is restricted mainly by the coupled ocean atmosphere interaction maintained by Bjerknes feedback. It is important to note that IITM-GODAS is consistent with the observation.

2.3 Surface dynamics

The equatorial dynamics play an important role in the evolution of El Niño. Figure 2.6 displays the surface currents from OSCAR derived from satellite observed sea surface height anomalies, winds and SST. It is evident from the mean surface currents that there is large reduction in the advection of warm water from east-central Pacific to west during 2015. This is evident from the strong eastward surface current anomalies during the summer 2015. These anomalous currents transport warm water to the central and eastern equatorial Pacific. The changes in the currents are closely associated with the anomalous wind pattern over the equatorial Pacific region. Further, currents over the Indian Ocean induced by summer monsoon wind forcing are weak throughout the season (Fig. 2.6, right panel).

2.4 Subsurface conditions in the Indian Ocean and Indian Ocean Dipole

The large scale forcing from El Niño and local air-sea interaction processes over the tropical Indian Ocean are equally important for the SWM rainfall variability. The subsurface temperature anomalies averaged over 10^{o}S to Equator during June to September in the Indian Ocean is shown in Figure 2.7. The upper few meters of Indian Ocean is found to be anomalously warm during the entire summer season except that there is a sign of weak cooling in the east at the subsurface below 80m. However, due to weak thermocline SST coupling (weak Bjerknes feedback, Deshpande et al.2014) the cold anomalies are not evident in eastern equatorial Indian Ocean.. The temporal evolution of SST, upper ocean heat content and zonal wind anomalies are shown in Figure 2.8. The easterly wind anomalies persist in the eastern and central equatorial Indian Ocean right from April 2015 with very significant easterly anomalies during September and October. However there is not much cooling in the eastern equatorial Indian Ocean. This strongly suggests the absence of any air sea coupling or any Bjerknes feedback over this region during summer 2015. The positive heat content anomalies in the eastern equatorial Indian Ocean during boreal spring can act as a precursor for a deficient monsoon rainfall over India (Sreejith et al. 2015). Though the eastern cooling is not present in summer 2015, the western warming was so intense that the dipole mode index (DMI) showed significant positive values during August and September 2015 (Figure 2.9). However, it could not evolve in to a typical strong Indian Ocean Dipole event (Deshpande et al. 2014) during fall and make much impact on SWM rainfall mainly due to the absence of any coupled feedback.

2.5 Summary

As the El Niño progresses, greatest concern is about the extent of associated eastern or central Pacific warming and its persistence because the teleconnections with the monsoon critically depend upon the location of the warm anomalies during an El Niño (Krishna Kumar et al. 2006) event. The evolution of 2015 El Niño is compared with the recent El Niños to understand the possible climatic impact. Figure 2.10 shows the evolution of El Niño during spring and summer of different composites such as strong/weak El Niño's as compared to that of 2015 The cooling in the west and warming in the eastern equatorial Pacific and the spatial pattern during summer 2015 are comparable with previous strong El Niño's of 1982 and 1997 (EL in Fig.2.10). This indicates that the Pacific conditions of 2015 emerged similar to a canonical El Niño event and are similar to the events of 1982/1997.

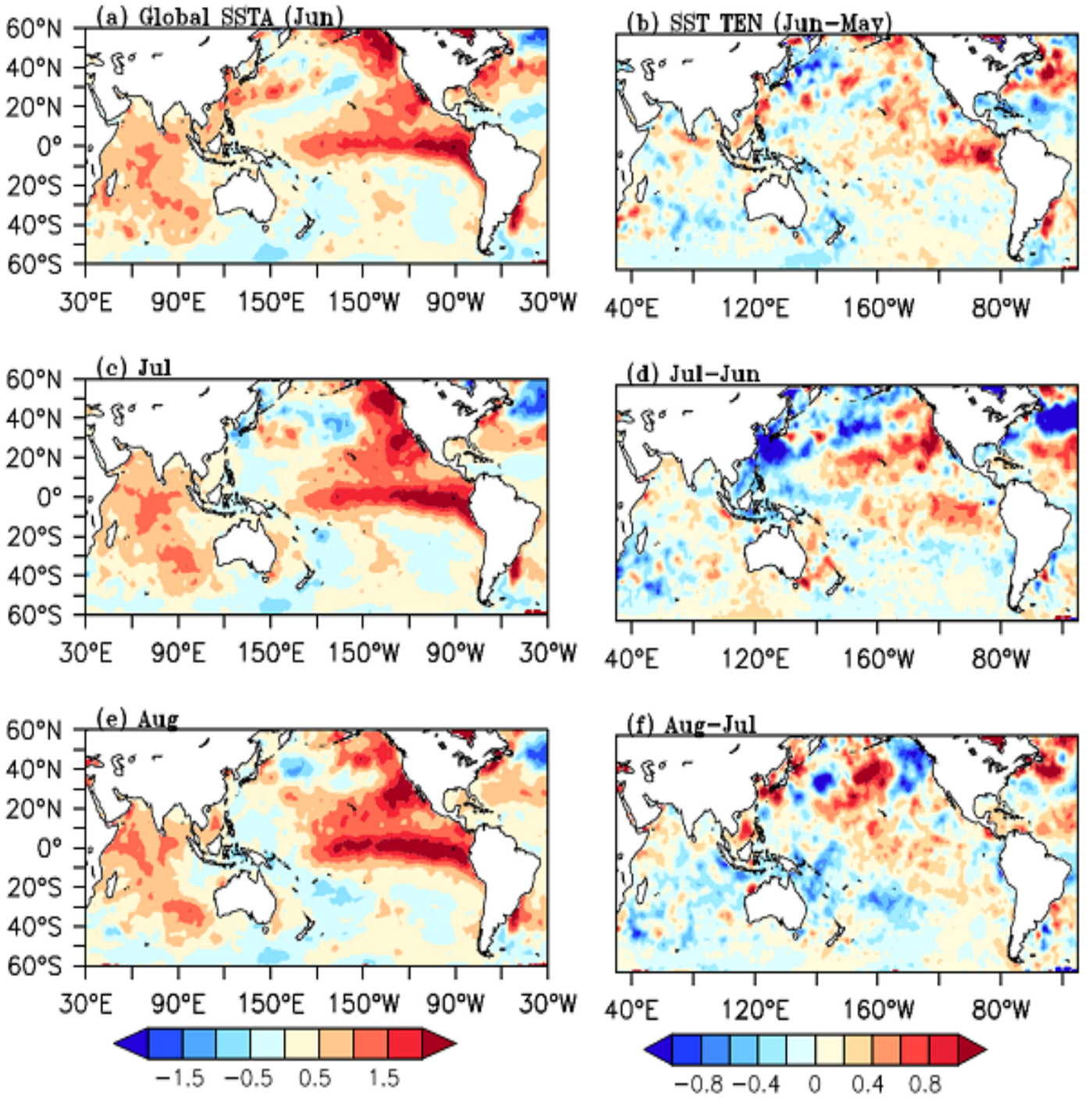

Figure 2.1 a,c,e: Spatial map of HadISST anomalies (°C, left panels) and its tendency (b,d,f) right panels) for June to August/September 2015

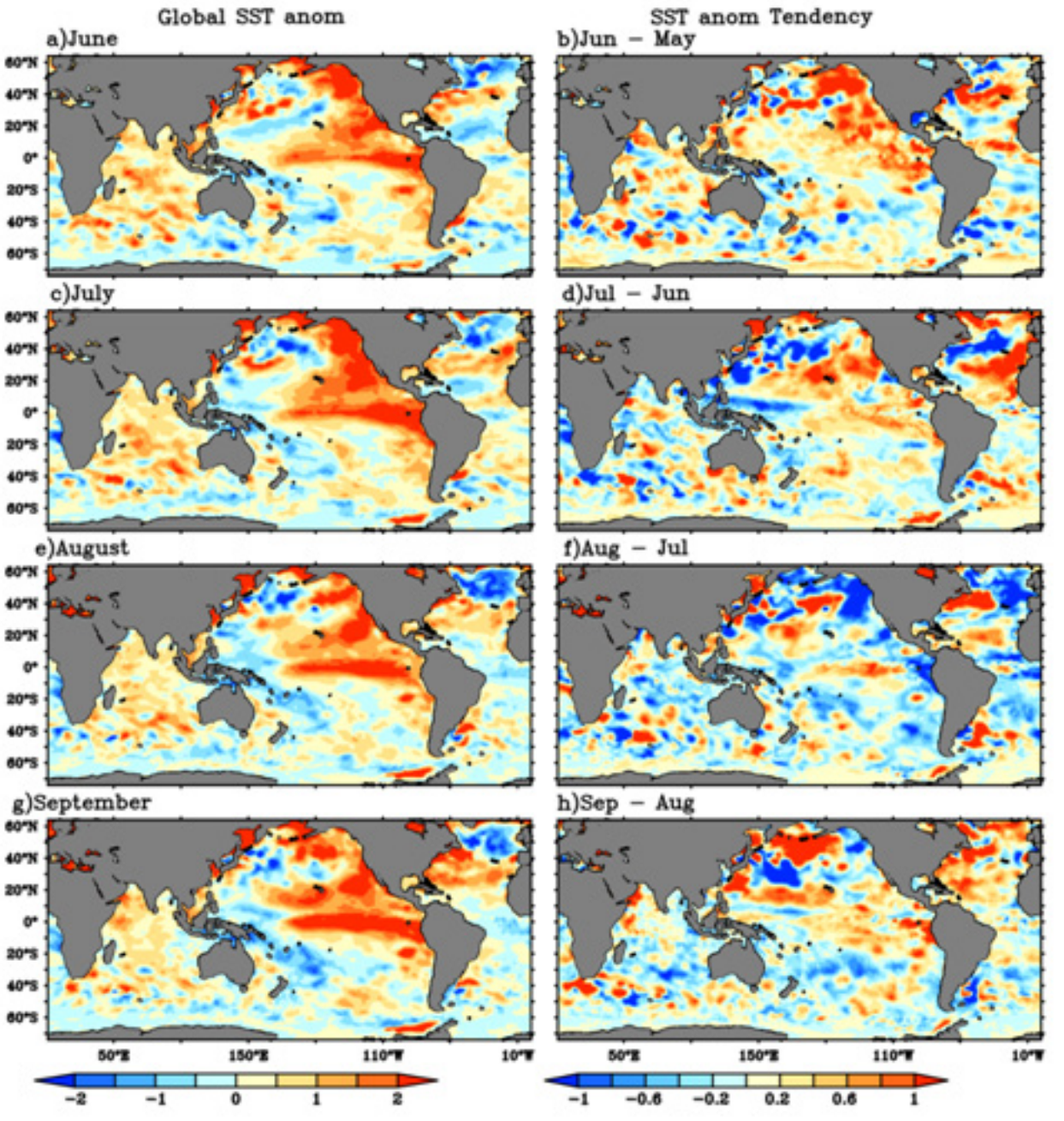

Figure 2.2 Spatial map of SST anomalies (°C) during June to September 2015 from IITM-GODAS (left panels) and its tendency (right panels) for June to September 2015

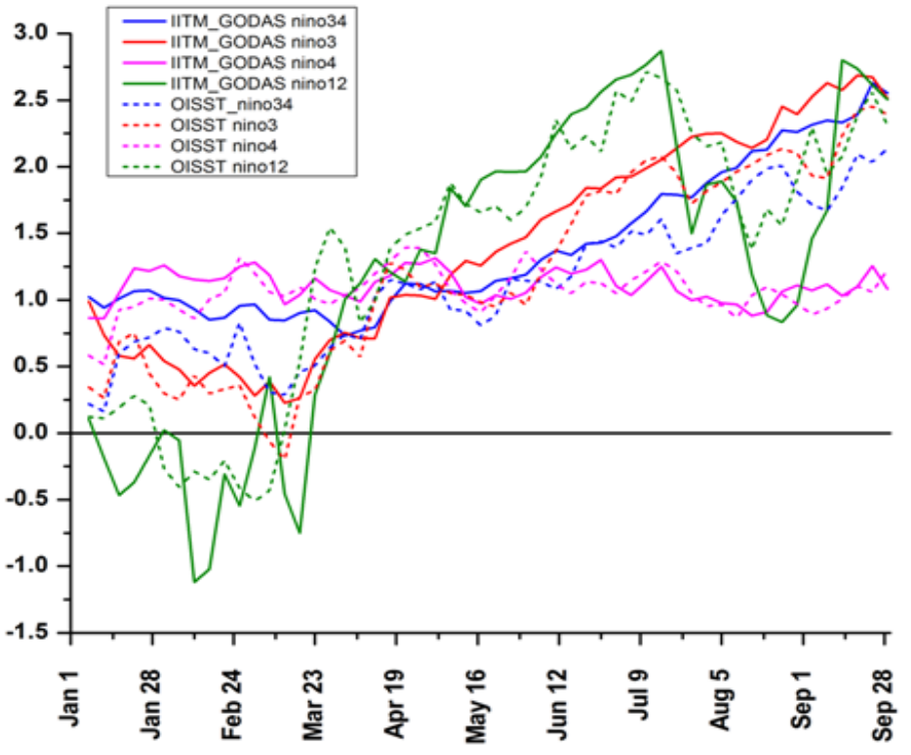

Figure 2.3 El Niño indices based on SST anomalies from IITM-GODAS and OISST

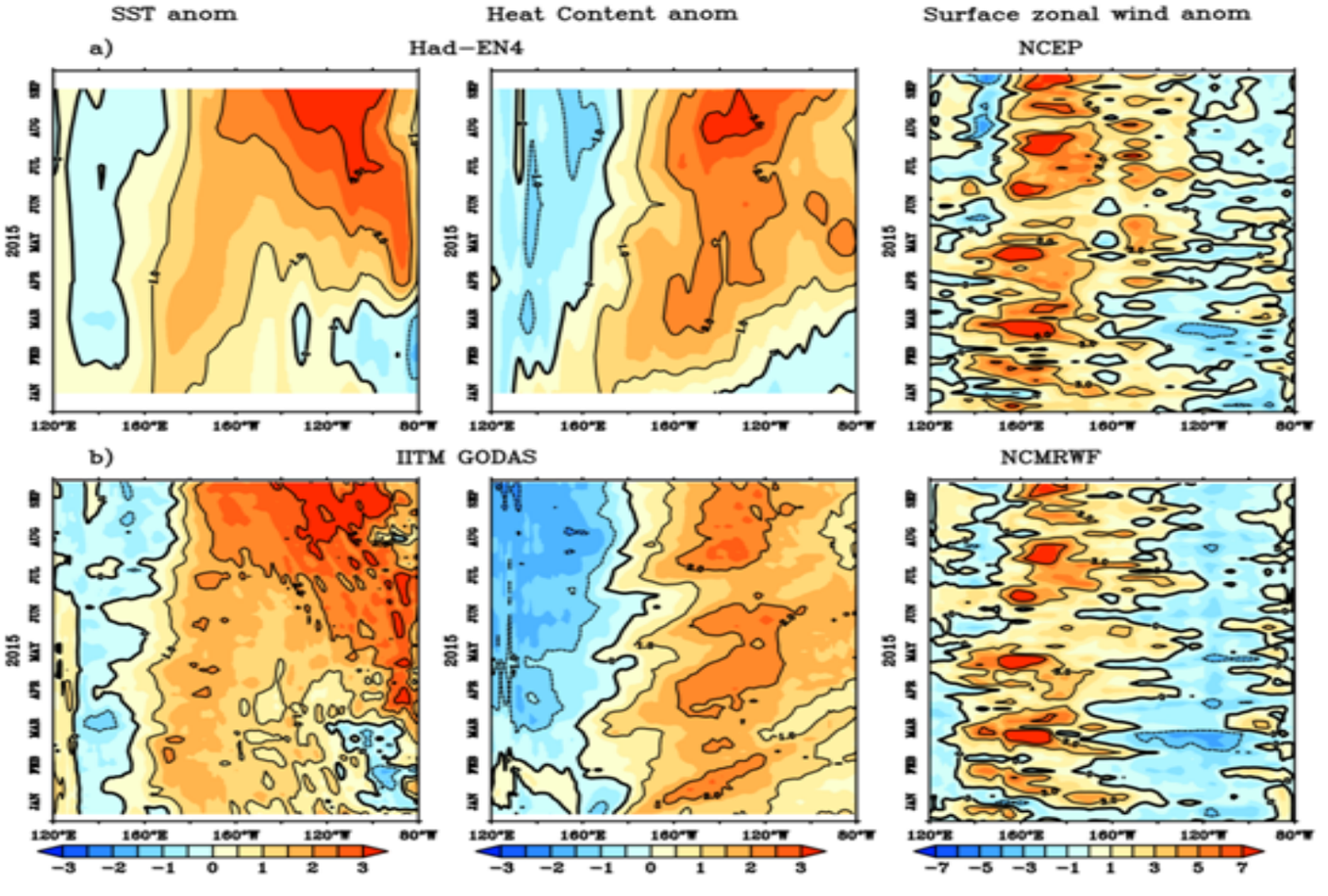

Figure 2.4 Time evolution of anomalous SST (°C), upper ocean (250m) temperature (°C) from Had-EN4, and surface zonal wind (ms-1) from NCEP during January-September 2015 (a) observed and (b) IITM-GODAS.

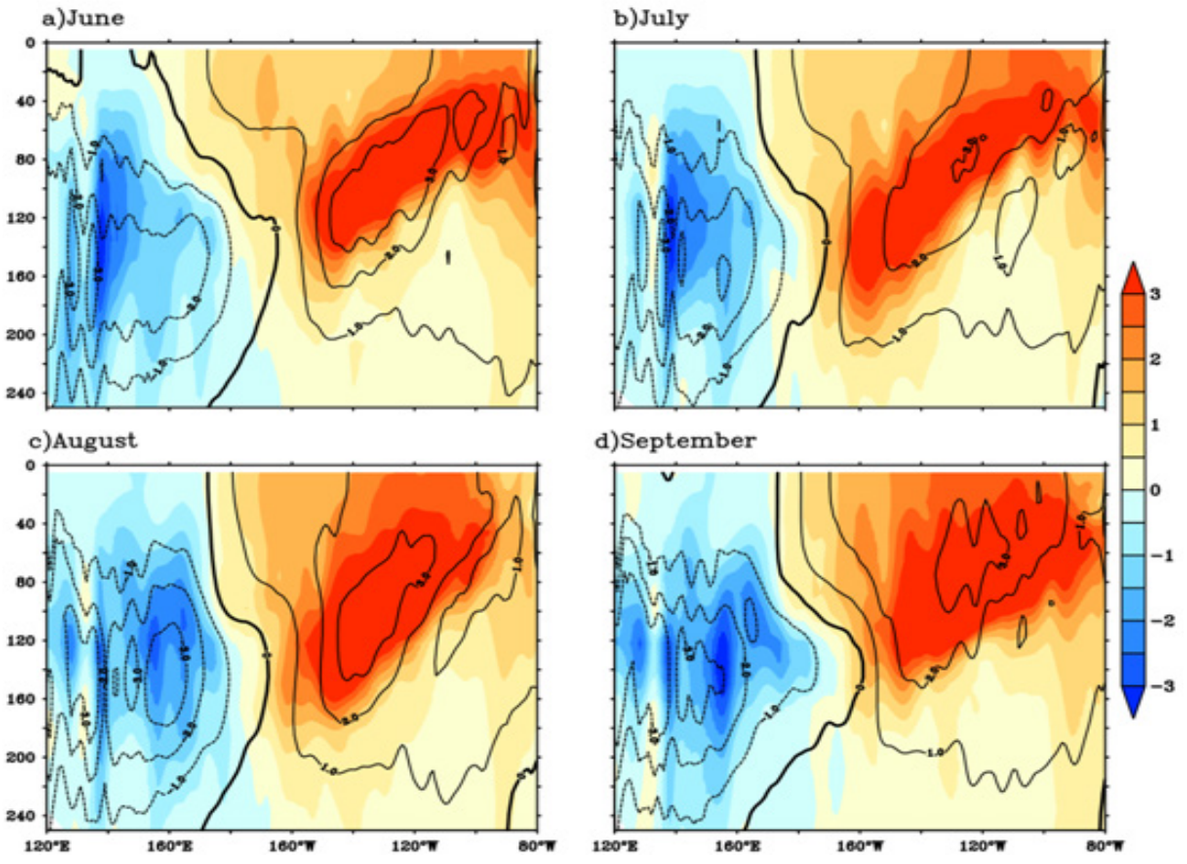

Figure 2.5 Evolution of equatorial Pacific subsurface temperature anomalies in Had-EN4 (shaded) and IITM-GODAS (contour) during June-September 2015.

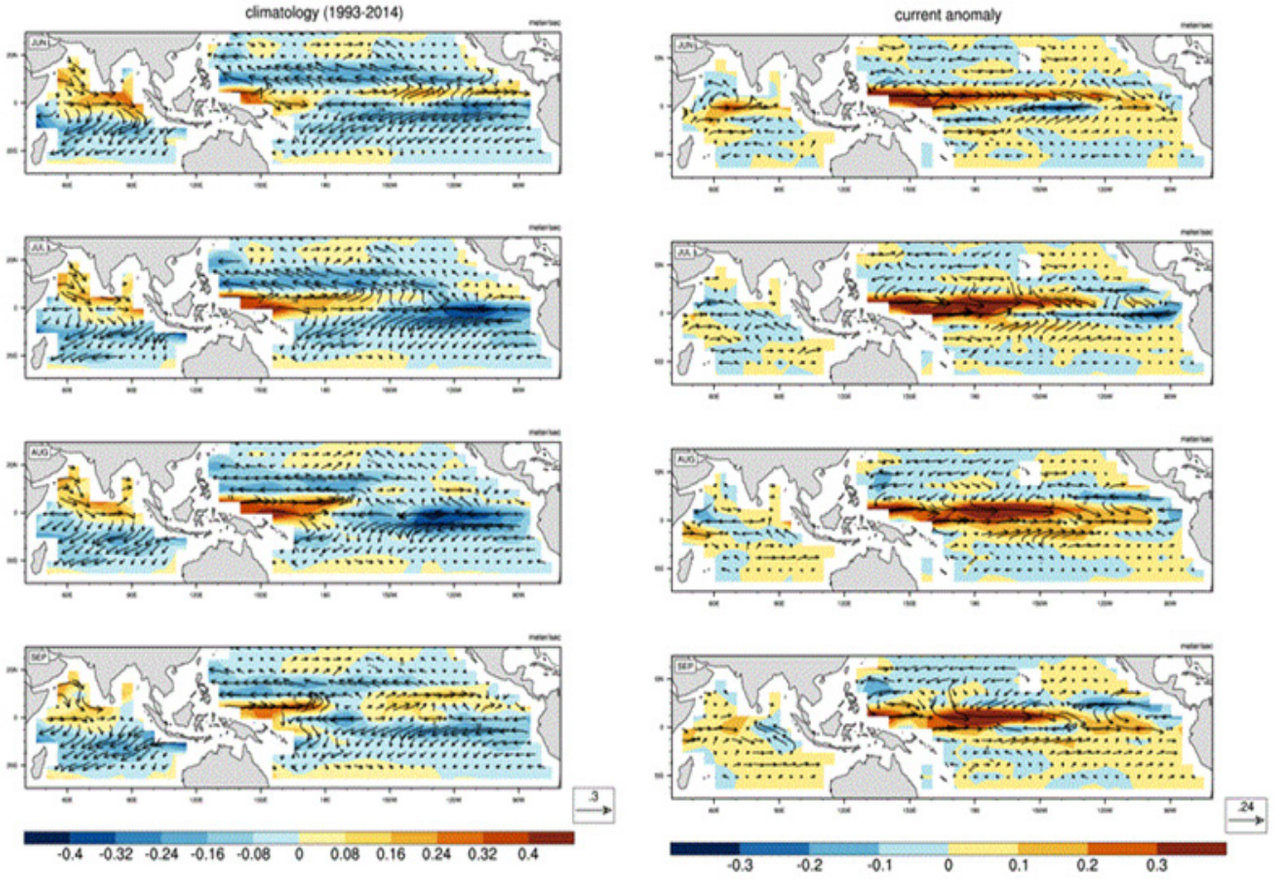

Figure 2.6 OSCAR currents (vectors) during June to September, climatological mean (left panels) and anomalies of 2015 (right panels). The respective zonal currents are shaded.

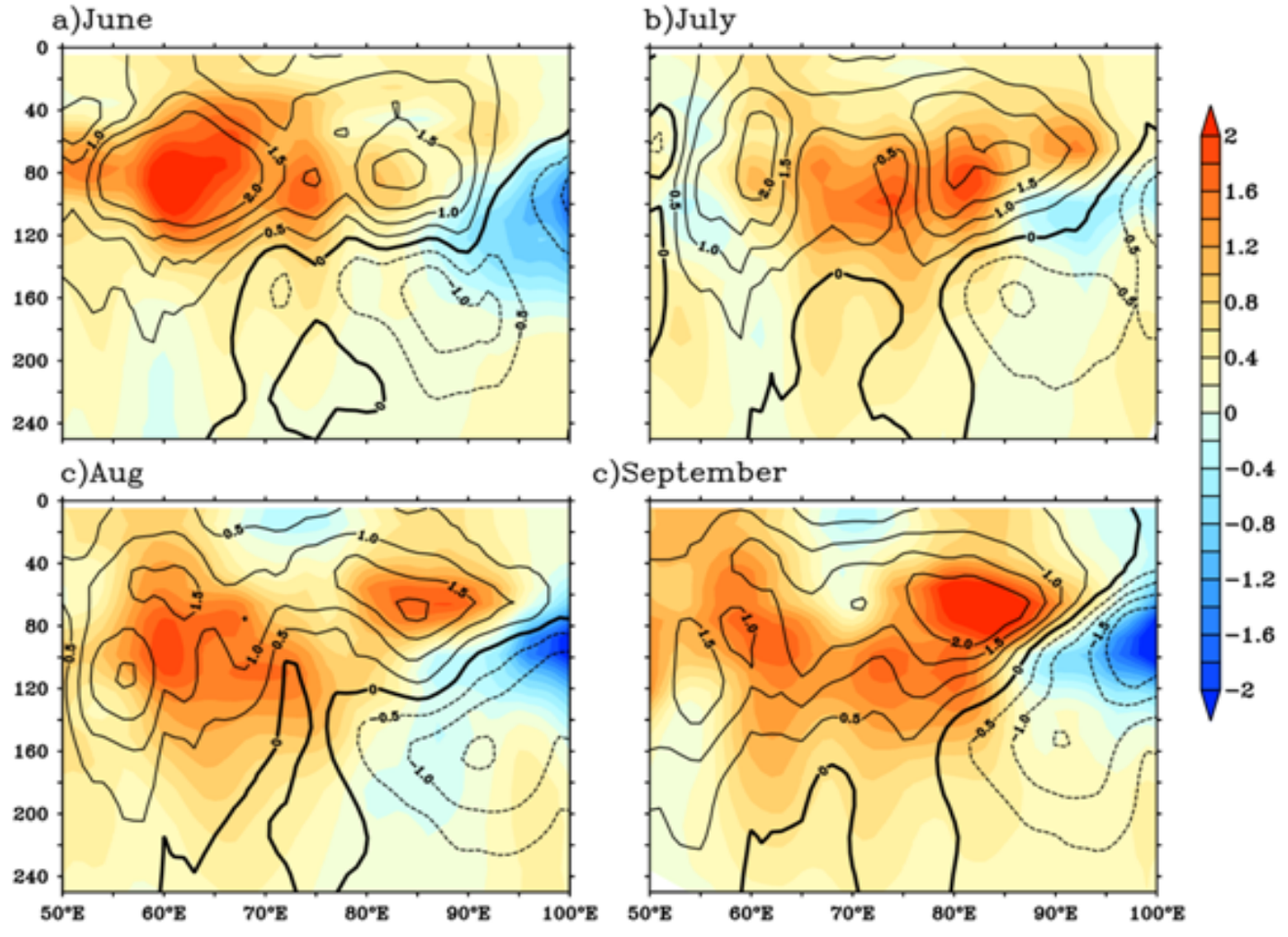

Figure 2.7 Longitude-depth section of temperature anomalies (°C) averaged over 10°S to Equator during June to September from Had-EN4 (shaded) and IITM-GODAS (contour).

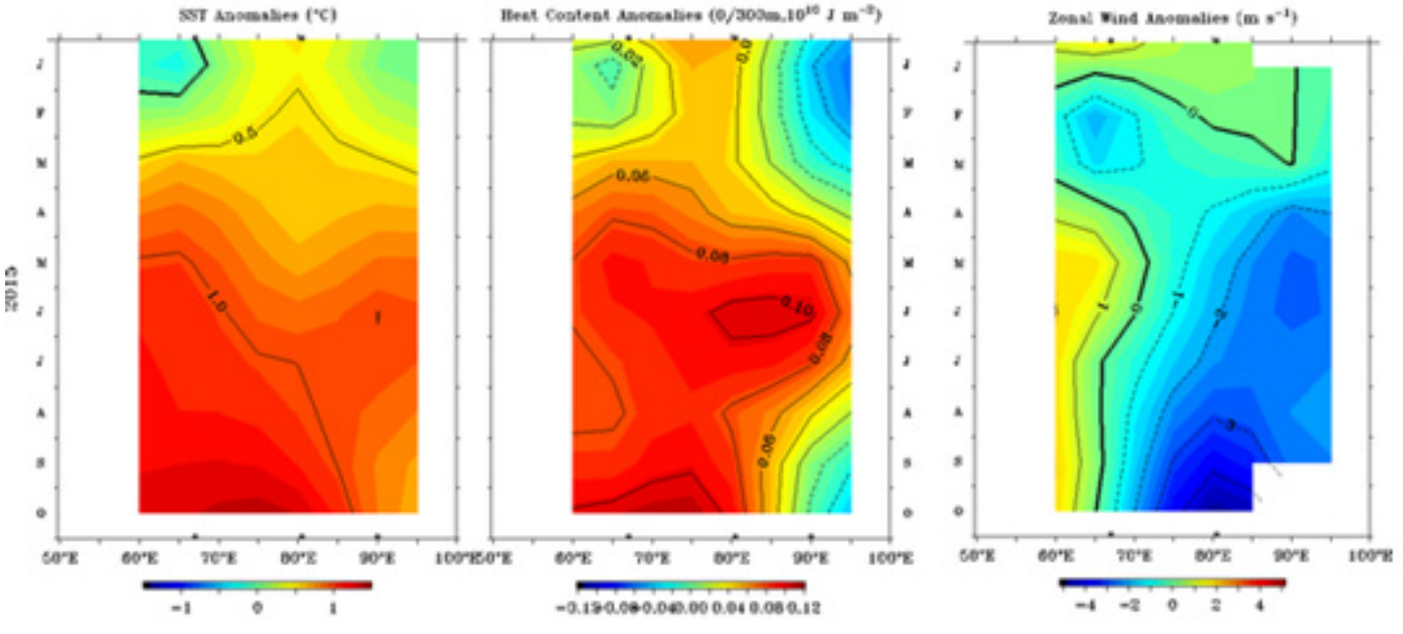

Figure 2.8 Time evolution of anomalies of observed (a) sea surface temperature (°C) (b) heat content (x1010 J m-2) and (c) zonal wind anomalies (m s-1) in the Indian Ocean for 2015 from mooring [Source: CPC, NOAA].

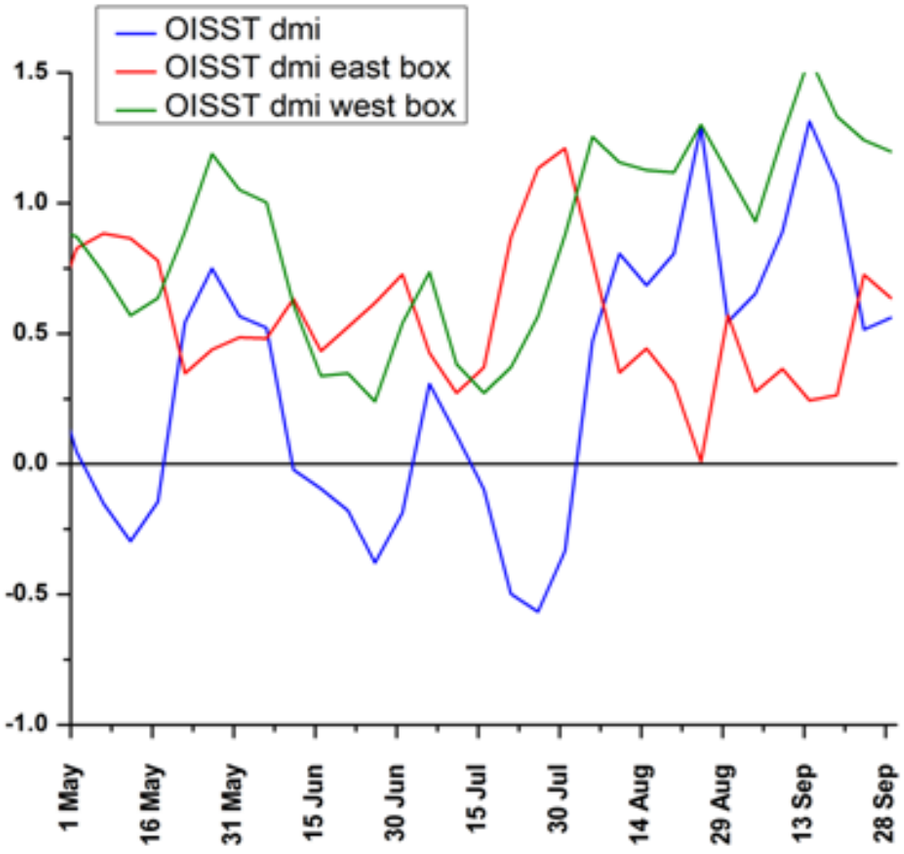

Figure 2.9 Dipole mode index (DMI) and DMI-E (SST anomalies of the eastern IOD box) and DMI-W (SST anomalies of the western IOD box) based on OISST.

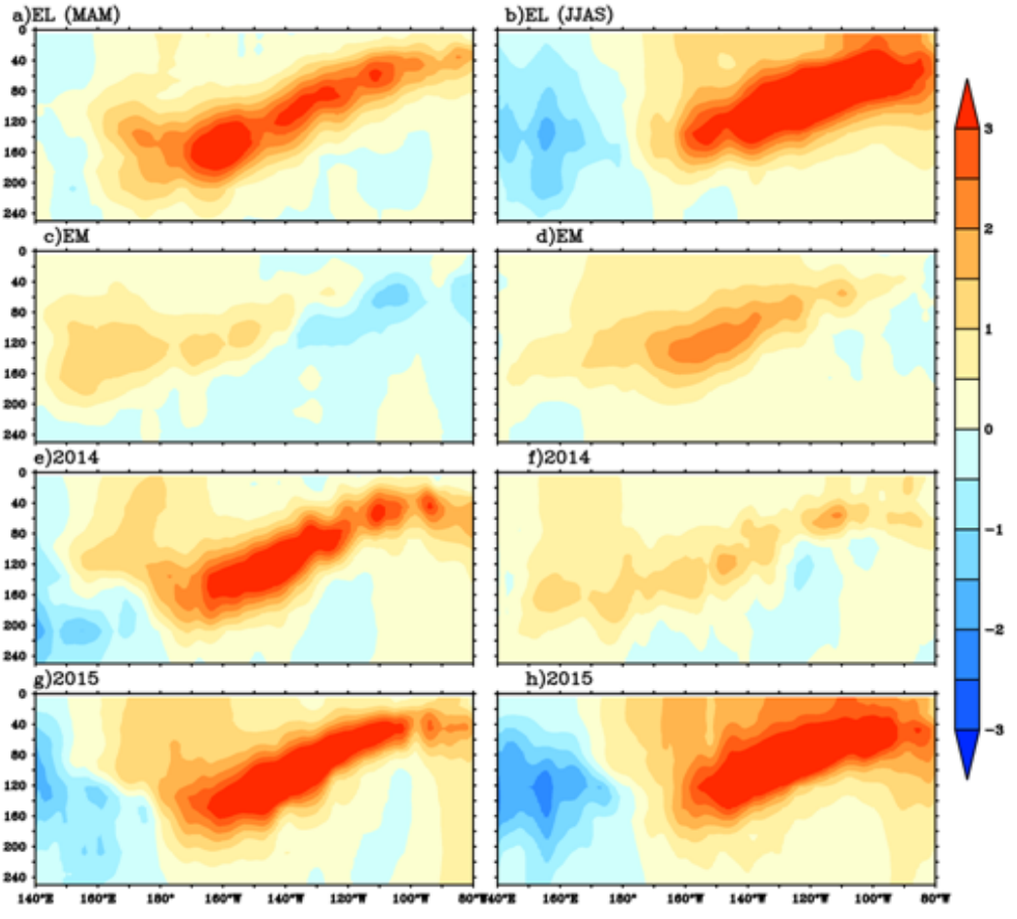

Figure 2.10 Longitude-depth of subsurface temperature anomalies (°C) during March to May (MAM, left panels) and June to September (JJAS, right panels) for different El Niño types: conventional El Niños (a,b), El Niño Modoki (c,d), 2014 (e,f) and 2015 (g,h) from Had-EN4

Chapter 3

Synoptic Features of Southwest Monsoon During 2015

Medha Deshpande, Mata Mahakur, Shilpa Malviya, Snehlata Tirkey, Malay Ganai, S. P. Ghanekar and P. Mukhopadhyay

3.1 Low pressure systems associated with 2015 southwest monsoon season

During the SWM season of 2015, 11 low pressure systems (LPS) formed out of which as many as 8 were intensified into depressions and cyclonic storms (Figure 3.1). Generally, 6-7 LPS with categories depressions and storms, with a standard deviation of 2, forms during the boreal monsoon season. Out of the eight systems, there were two cyclonic storms namely 'Ashobaa' during 7-12 June and 'Komen' during 26 July – 2 August. On average, 13-14 LPS forms (standard deviation 2.5) with average life span of 5 days. It shows that the number of low's (less intense LPS) were less during this monsoon. Although, the number of LPS and its duration is positively correlated with seasonal rainfall but their variability does not clearly explains the interannual variation in rainfall. It would be worth comparing the frequency and characteristics of these synoptic scale systems with those of climatological normals. Cyclone Ashobaa appeared as a depression over the east-central Arabian Sea and lay centred at 0830 hours IST of 7 June 2015 near latitude 14.5^{o}N and longitude 68.5^{o}E, about 690 km southwest of Mumbai, 740 km south southwest of Veraval. This system initially moved northwards and then north-northwestwards and west-southwestwards before landfalling off the Oman coast. The observed track as reported by IMD (ref: www.imd.gov.in, IMD report on Cylonic Storm Ashobaa, 2015) is shown in Figure 3.2. Ashobaa attained the stage of Cyclonic Storm (CS) on 8 June 0300 UTC with a minimum central pressure of 994 hPa and remained in the stage of CS till 11 June, 1500 UTC before becoming deep depression and further dissipation.

The second CS in the monsoon season of 2015 was 'Komen' (26 July – 2 August 2015). 'Komen' developed over the BoB from a low pressure area which lay over northeast BoB and adjoining Bangladesh and Gangetic West Bengal on 25th July evening and concentrated into a depression over the same area in the morning of 26th July. It followed a semi-circular track over northeast BoB and then crossed Bangladesh coast between Hatia and Sandwip near lat. 22.5°N and long. 91.4°E during 1400 and 1500 UTC of 30th July. After the landfall, it moved initially north-north-westwards, then westwards and west-southwestwards across Bangladesh, Gangetic West Bengal and Jharkhand. It weakened gradually into a well marked low pressure area over Jharkhand and adjoining north Odisha and north Chhattisgarh at 1200 UTC of 2nd August (ref: IMD CS Report on Komen, 2015). This CS briefly attained the stage of cyclonic storm during 29 July 1800 UTC to 30 July 1800 UTC. Other than these periods, it remained in the form of deep depression before being dissipated as depression on 2 August 0900 UTC and thereafter as well marked low over Jharkhand area. CS 'Komen' caused heavy rainfall activity that is mostly confined to the eastern part of India over Gangetic West Bengal, Bihar, Jharkhand region. The enhanced rainfall during the passage of the cyclonic storm manifested in the positive rainfall departure for the week is shown in Figure 3.3 (Source:IMD). The simulation and prediction aspects of Ashobaa and CS are described in Chapter – 5 (see section 5.3).

There were two deep depressions during the season occurred between 22 – 24 June and another over land between 27-30 July. Both the deep depressions were short lived and occurred over northwestern part of India.

Due to the shorter life time and track these systems could not produce widespread rainfall over the country. The above mentioned deep depressions remained active over western and north-western part of the country only. Figure 3.4 shows the vorticity and associated wind streamlines at four representative levels namely 850, 600, 500 and 400 hPa on 24 June for the deep depression of 22-24 June over Gujarat and adjoining areas. It may be noted that the centre of circulation hardly shows any southward tilt, which is one of the characteristic features of monsoon depressions. The depressions of 20-21 June, 10-12 July (over land), 4 August (over land) were also very short lived and had shorter tracks. These depressions mostly gave localised heavy rainfall and fail to produce wide spread rainfall over the core monsoon zone of the country. In fact the land depression of 4 August has caused an extremely heavy rainfall event over Khandwa, Madhya Pradesh and this will be discussed later in detail. The depression for the period 16-19 September was the only one which showed longer lifetime and track and caused wide spread rainfall over the central Indian region. The vorticity of the depression on 18 September is showed in Figure 3.5. It is interesting to note that the centre of circulation for this event shows a southward tilt with height. The passage of this system has significantly reduced the overall rainfall deficit over the country which is reflected in the weakly departure plot of Figure 3.3.

As evident from the above discussion, besides just one westward moving depression during September, all other depressions and deep depressions were either of shorter duration, smaller track and confined either to western, north-western part of the country or to the east and north-east region. As a consequence, the major portions of the central India and Gangetic plains have received deficient rainfall. Although Vidarbha, Chattisgarh and Jharkhand have come under normal category, they are in the negative side of the normal. Figure 3.6 (Source IMD) shows the skewed rainfall variation very clearly with all the sub-divisions of north-eastern states are normal, west Rajasthan shows excess and Saurashtra and Kutch shows normal rainfall distribution for the whole season. It may be worth noting that while the frequency of the synoptic systems was less than that of the climatological normals, northward displacement of most of these systems was a common factor during SWM 2015.

3.2 Moist instability and convection during Southwest monsoon season 2015

As it is evident from the above discussion that monsoon 2015 mostly produced weather systems of shorter time scale. To provide further insights, the IMD-NCMRWF gridded rainfall product (Mitra et al. 2013) is analysed. Based on the 10 years of climatology, 2-10 day bandpass filtered variance of rainfall is named as synoptic scale and 10-90 day filtered variance of rainfall is called Intra-seasonal Oscillation (ISO) scale variance. Figure 3.7 shows the plot over the Indian region for the percentage ratio of synoptic to total variance (Figure 3.7a), ISO to total variance (Figure 3.7b) and the percentage ratio of ISO scale to synoptic scale variance for JJAS. Figure. 3.7a shows around 70-80% synoptic scale variance with respect to total Intraseasonal variance (ISV) which is much higher than the climatology (Goswami et al. 2014). In contrast, the ISO variance is found to be much lower and the ratio of ISO to Synoptic scale variance is also found to be lower than the normal over central Indian region. This is consistent with the fact that the monsoon season of 2015 mostly experiences more high frequency short lived weather systems and relatively lesser number of organised convective systems. These features are also described in Chapter 1 (Section 1.6) and Chapter 5 (Section 5.2).

To get further insight into the strength of the monsoon current, we have computed the mean sea level pressure difference between two points namely 9°N,77°E and 22°N, 69°E for the whole season and a similar plot is made for the normal monsoon year of 2013 (Figure 3.8). It is evident from Figure 3.8a (for 2015) and Figure 3.8b (for 2013) that the pressure gradient is less in 2015 and it falls rapidly beyond July as compared to 2013.

As the rainfall over central Indian region is much less as compared to normal in contrast to northeastern region, we have analysed the Convective Available Potential Energy (CAPE) and Convective Inhibition Energy (CINE) over two boxes of central India and Northeast India respectively (Figure 3.9). It is clear that the mean CAPE over central India is much less (Figure 3.9a) for the 2015 season as compared to that of northeast (Figure 3.9b). Further, the CINE over central India is found to be much higher than that of northeast. This clearly shows that the central Indian region was having less moist instability and northeast Indian region was having more moist instability. This could be one of the key reasons behind week organized convection and propagation over central India. Consistent with CAPE, we have computed moist static energy (MSE) for the two contrasting years of 2015 and 2013 (Figure 3.10). It is clearly seen that the MSE was higher over the central Indian region for the year 2013 as compared to 2015. Lastly we would like to throw some insights in the cloud and rainfall distribution over the central Indian region. Figure 3.11 shows the scatter plot of JJAS rainfall with Outgoing Longwave Radiation (OLR). It shows a skewed distribution indicating dominance of rainfall lesser than 50 mm day-1 category. It also shows that even deeper clouds with OLR less than 180 Wm^{-2} did not produce many heavy rainfall events. This needs further analysis as to why the deeper convection did not produce heavy rainfall events. Whether there is any role of aerosol, etc?

All these analyses indicate that the moist instability vis-à-vis the moist convection was weak over central Indian region for the season 2015. However there was dominance of embedded mesoscale systems, which has caused localized heavy rainfall in some region which has led to an inhomogeneous rainfall distribution.

3.3 An event of localised heavy rainfall over Khandwa during 4 August 2015

In association with the land depression of 4 August, very heavy rainfall was reported at Khandwa (21.83°N,76.34°E) in Madhya Pradesh. The heavy rainfall is reasonably captured by near real time GPM IMERG rainfall time series (Figure 3.12). Maximum rain occurred between 1200Z and late afternoon of 4 August. As per IMD sources, the 24 hour accumulated rain reported on 0300Z of 5 August was 29 cm.

The IR channel brightness temperature at 1700 IST from INSAT 3D shows localised deep convective cloud with cloud top brightness temperature reaching up to -80°C (Figure 3.13). The localised nature of the convection is triggered by strong low level convergence (Figure 3.14a) and prevalent vorticity provided by the existing depression (Figure 3.14b).

3.4 Typhoons over the West Pacific

This year having witnessed a strong El Niño, west Pacific showed unprecedented Typhoon activity with total number of typhoon becoming 17 and 4 of them were the super typhoons. A list of Typhoons over the west Pacific during JJAS period is mentioned in Table 3.1. The tracks of the super typhoons show (Figure 3.15) that most of them have moved westward initially but recurved towards north or northeastward direction due to which the remnants of these systems did not enter over Bay of Bengal. The west-Pacific typhoon characteristics are also discussed in section 5.2.3 of Chapter 5.

3.5 Onset of Monsoon over Indian region and influence of intense synoptic systems of northwest Pacific Ocean on the advancement of Bay of Bengal branch of monsoon as observed during 2015

During 2015, the onset of Indian summer monsoon over Southeast Bay of Bengal / North Andaman Sea (SBAS) region occurred on 16 May, 4 days in advance than the normal time (20 May). While it set-in over

Kerala on 5 June with a delay of 4 days against the normal date (1 June). Many agencies predicted that in 2015, the Kerala onset would likely to occur little early (forecast by Skymet Weather Services Pvt. Ltd was around 27-29 May, www.skymetweather.com, that of India Meteorological Department, Pai and Rajeevan, 2009, was 30 May ± 4 days and of Extended Range Prediction (ERPS) Group of I.I.T.M., Joseph et al., 2015, was 31 May ± 4 days), while Ghanekar et al. (2010), predicted it as normal (1 June ± 5 days). Refer Section 5.3 of Chapter 5 for details of simulation aspects. The monsoon covered entire country (northwest India) on 26 June, 19 days earlier than the normal date of 15 July.

The advance of monsoon onset over SBAS occurred in absence of formation of any well-marked system over Indian region. However, it is interesting to note that during 2015, the seasonally northward migrating oceanic branch of near-equatorial Inter Tropical Convergence Zone (ITCZ) over Indian monsoon region showed remarkable interactions with two intense synoptic systems which formed over northwest Pacific Oceanic region viz. Super Typhoon (STy) NOUL (3-12 May) and STy DOLPHIN (6-19 May),. Figures 3.16a and b, respectively, show their Tracks (taken from the website of Co-operative Institute for Meteorological Satellite Studies). Both these systems showed a re-curving path and their successive formation influenced the northward migration of Bay branch of the Indian monsoon. The influence is prominently seen when these systems reach to their peak intensity or exhibit re-curvature.

Figures 3.17 and 3.18 present 06 UTC IR INSAT 3A Satellite Cloud Imageries for selected dates (Taken from website of India Meteorological Department) to show their influence. It was noticed that during their westward passage, the Bay branch is seen to be suppressed / fragmented / located at southern latitude. When these systems started exhibiting a re-curving path, the Bay branch is seen to be activated / got well organized / showed a rapid northward movement. As such, when STy NOUL was moving westward towards Indian region, under its influence on 7 May, the Bay branch is seen to be tagged by the system and running at a southern latitude (Figure. 3.17a). When the system started showing a re-curving path, the Bay branch showed a sudden northward movement as seen on 10 May (Figure. 3.17b). After weakening of STy NOUL, its influence on the Bay branch was lost after 12 May. By this time, STy DOLPHIN was moving westward towards Indian region and the cloud organization over the Bay region got fragmented (suppressed). Instead, the organization is seen at southern latitude (Figure. 3.18a) and with re-curvature of the system, the clouds started moving northeastwards towards the Bay. Due to this, the Bay branch got activated and well organized (Figure. 3.18b) and the onset over SBAS took place on 16 May 2015. From the cloud picture for 19 May it can be seen that the monsoon clouds from the Bay region were been dragged further northeastward (Figure. 3.18c) due to the movement of the system.

Table 3.1 Individual (West Pacific) Storm Summary

Winds in knots, pressure in hPa, category is based on Saffir-Simpson scale
(http://weather.unisys.com/hurricane/w_pacific/2015/index.php)

#	Name	Date	Wind	Pres	Cat
1	Tropical Storm KUJIRA	20-24 JUN	45		-
2	Typhoon-4 CHAN_HOM	30 JUN-12 JUL	120		4
3	Typhoon-1 LINFA	02-09 JUL	65		1
4	Super Typhoon-4 NANGKA	03-18 JUL	135		4
5	Typhoon-2 HALOLA	13-26 JUL	90		2
6	Tropical Storm TWELVE	23-25 JUL	40		-
8	Super Typhoon-5 SOUDELOR	30 JUL-08 AUG	155		5
9	Tropical Depression FOURTE	02-04 AUG	30		-
10	Tropical Storm MOLAVE	07-13 AUG	50		-
11	Typhoon-4 GONI	14-25 AUG	115		4
12	Super Typhoon-5 ATSANI	14-25 AUG	140		5
13	Typhoon-3 KILO	01-11 SEP	105		3
14	Tropical Storm ETAU	06-09 SEP	55		-
15	Tropical Storm VAMCO	13-14 SEP	35		-
16	Typhoon-3 KROVANH	14-20 SEP	105		3
17	Super Typhoon-4 DUJUAN	21-29 SEP	125		4

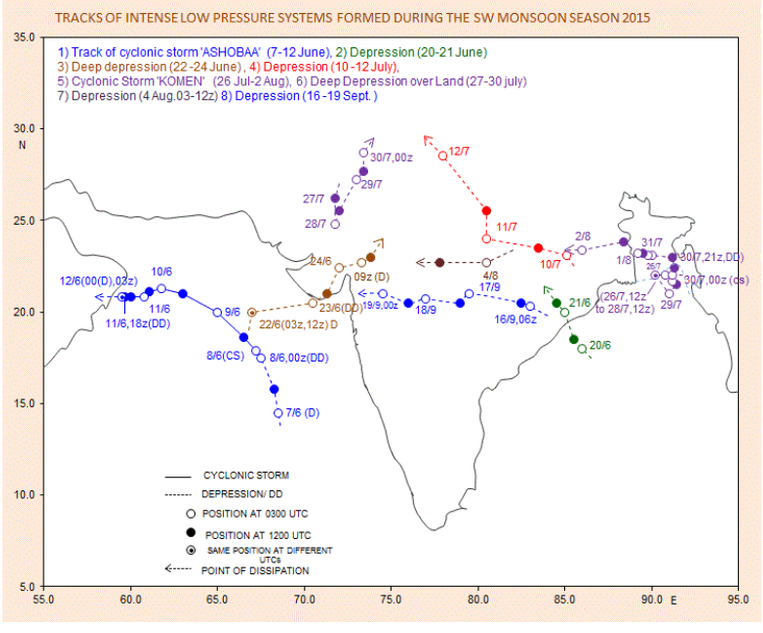

Figure 3.1 Tracks of Low pressure systems formed during the SWM season 2015 (Courtesy IMD)

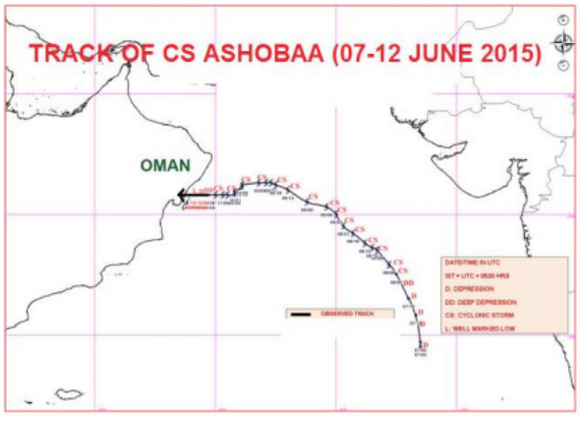

Figure 3.2 Observed Track of cyclonic storm Ashobaa (IMD report on Cyclonic Storm Ashobaa, 2015).

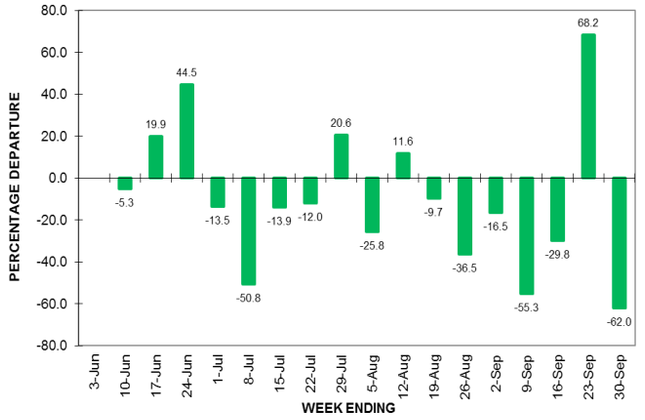

Figure 3.3 Weekly rainfall departure during JJAS of 2015. Red circle indicates the week of cyclone 'Komen' and the blue circle shows the rain received during the passage of September depression.

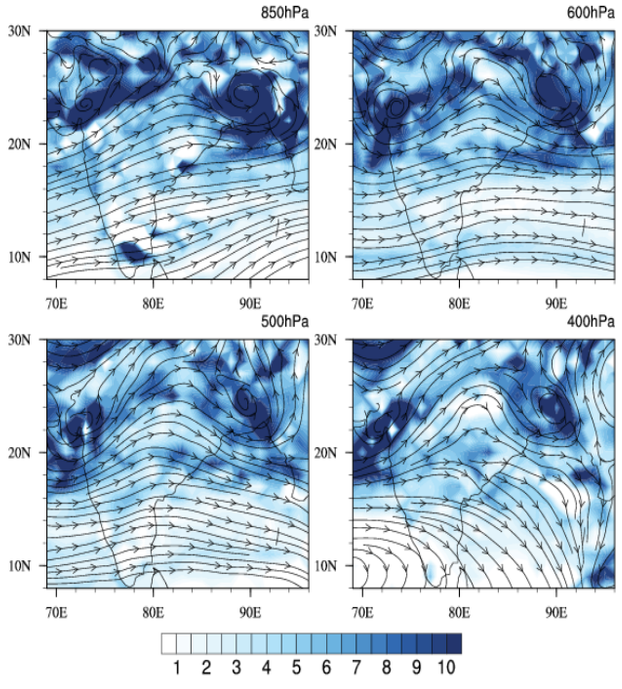

Figure 3.4 Vorticity (x10^{-5} s^{-1}) and streamlines at 850, 600, 500 and 400 hPa over Indian region during 22-24 June 2015.

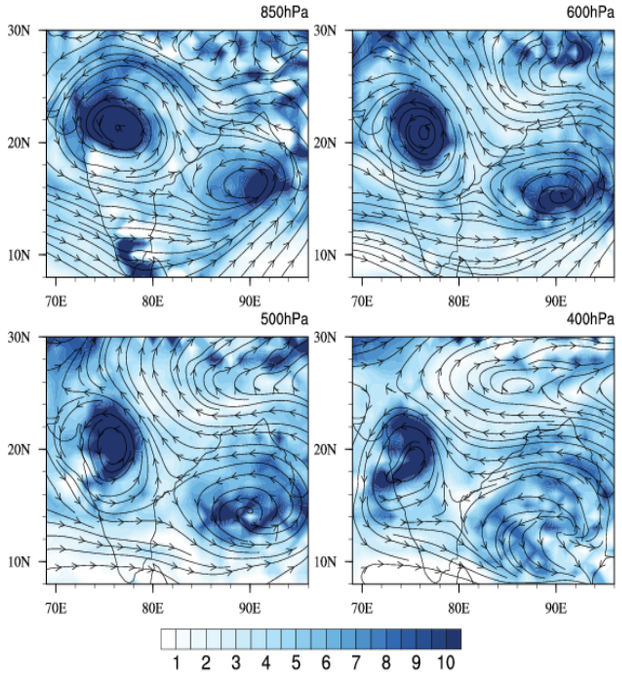

Figure 3.5 Vorticity (x10^{-5} s^{-1}) and streamlines on 18 September 2015 associated with the depression of 16-19 September.

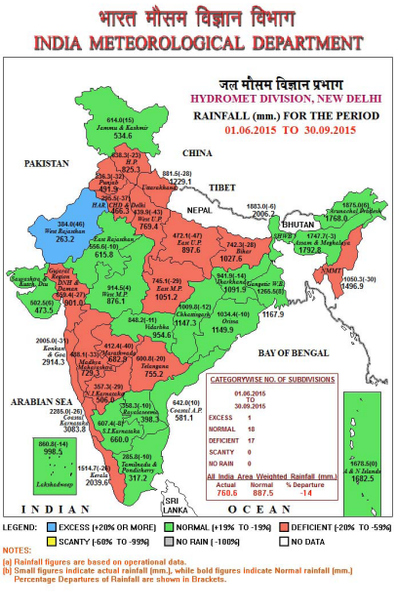

Figure 3.6 1 June to 30 September 2015 rainfall (mm) distribution in each sub-division of India.

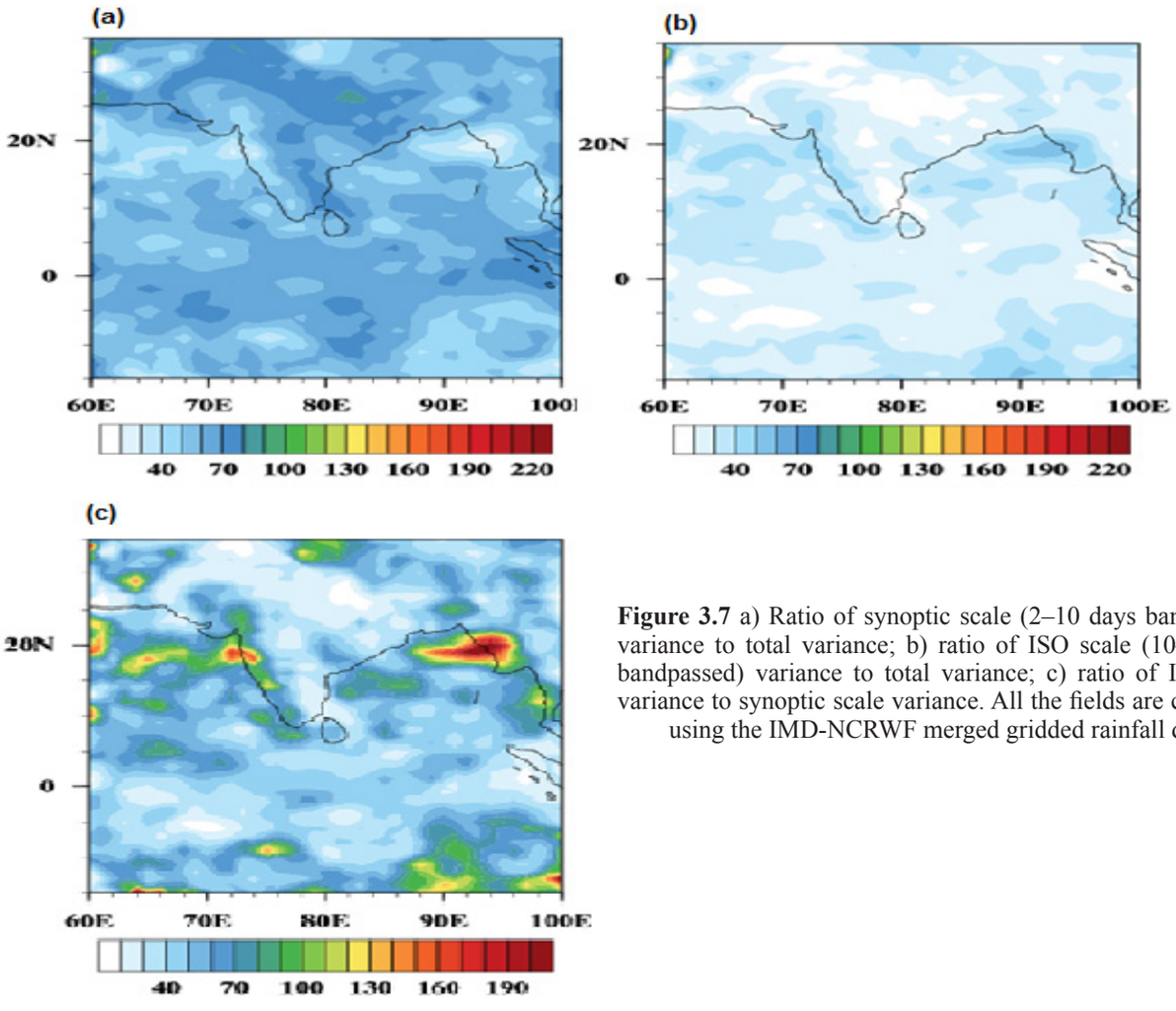

Figure 3.7 a) Ratio of synoptic scale (2–10 days bandpassed) variance to total variance; b) ratio of ISO scale (10–90 days bandpassed) variance to total variance; c) ratio of ISO scale variance to synoptic scale variance. All the fields are computed using the IMD-NCRWF merged gridded rainfall data.

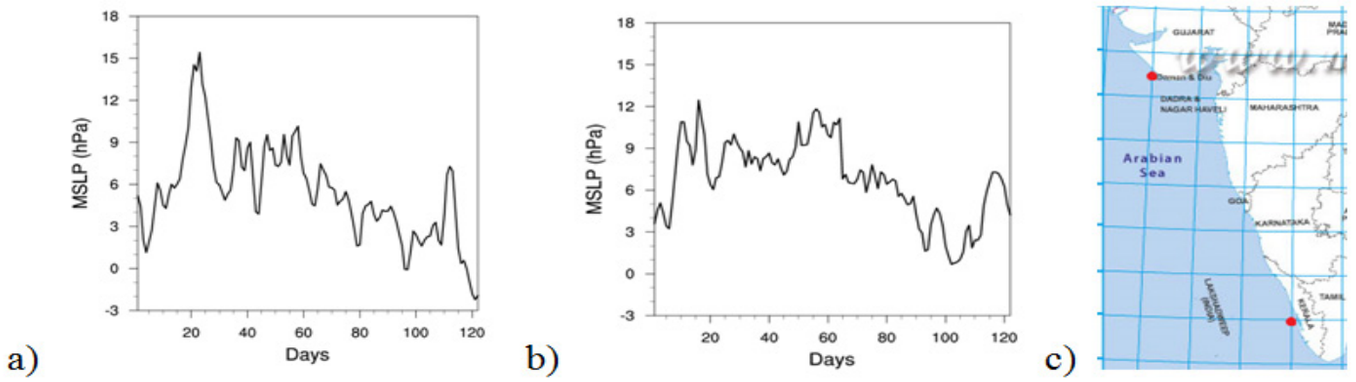

Figure 3.8 Daily evolution of mean sea level pressure difference based on ERA interim data between 9°N,77°E and 22°N, 69°E: a) for 2015, b) for 2013, c) the points considered for computation.

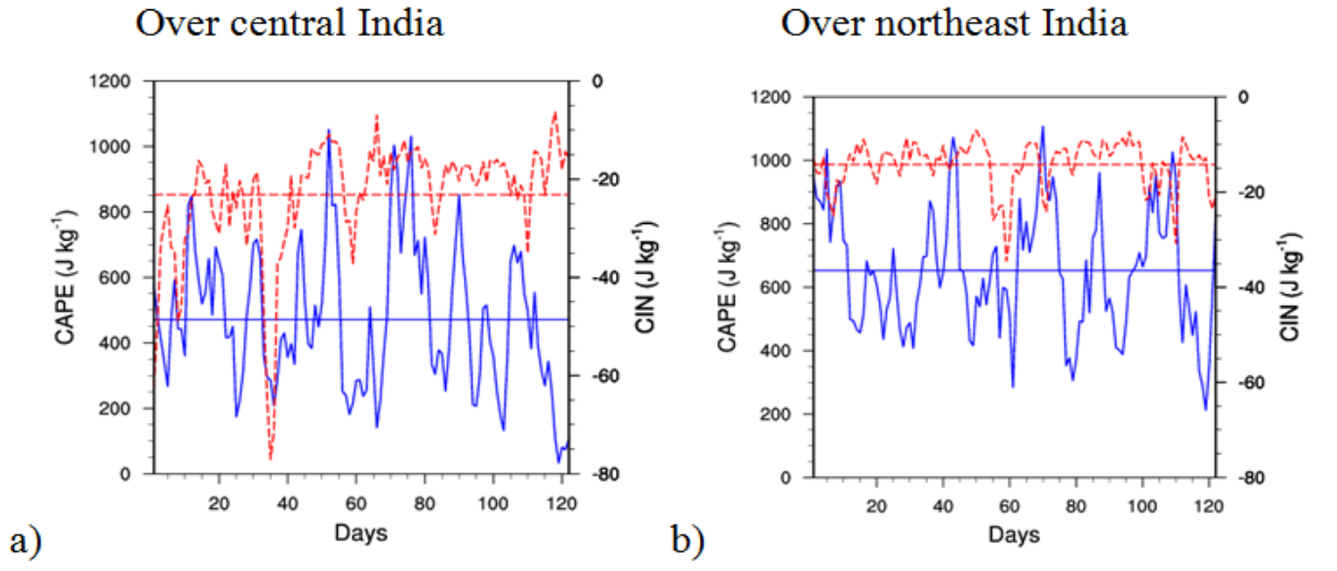

Figure 3.9 Daily CAPE and CINE computed for, a) the central Indian region covering 18°-25°N, 75°-83°E and b) for the northeastern Indian region covering 22°-29°N, 90°-96°E. Blue line represents CAPE, red line stands for CINE.

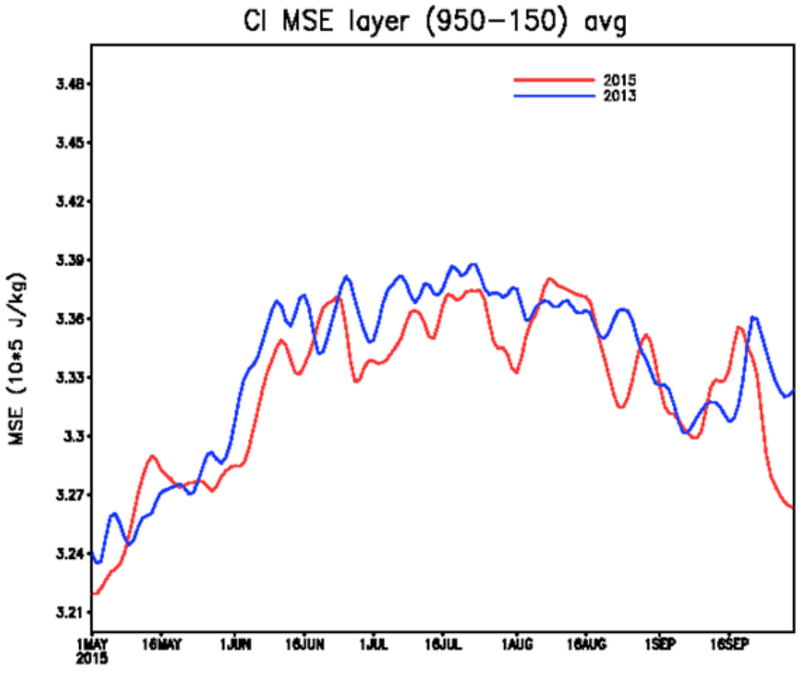

Figure 3.10 Seasonal (JJAS) evolution of moist static energy for the year 2013 and 2015 over Central Indian region.

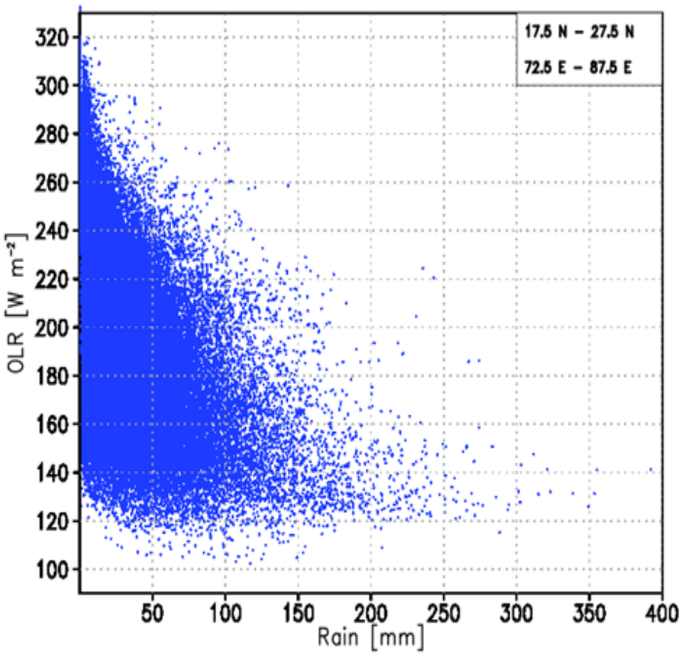

Figure 3.11 Scatter plot of daily averaged Kalpana OLR (Wm^{-2}) and TMPA 3B42RT (real-time) cumulative rain rate (obtained from 3-hourly values) for JJAS of 2015 for the region covering 17.5°N-27.5°N, 72.5°E-87.5°E. Both these data sets are at 0.25° × 0.25° resolution.

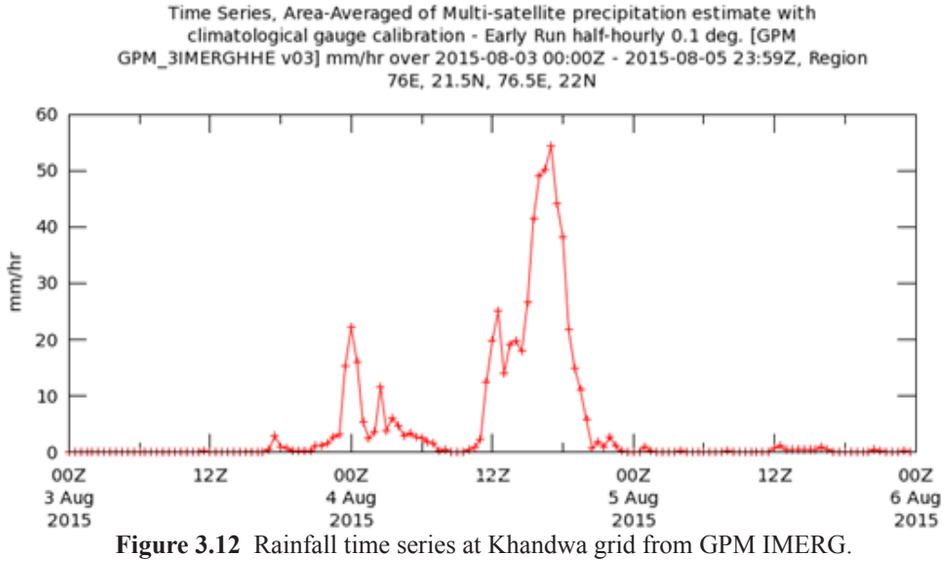

Figure 3.12 Rainfall time series at Khandwa grid from GPM IMERG.

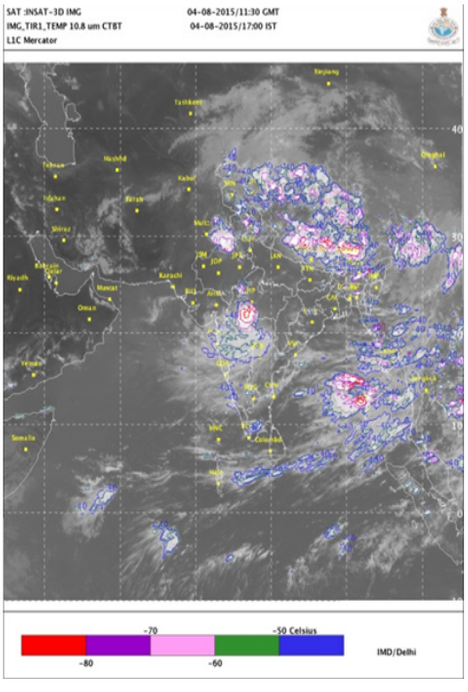

Figure 3.13 INSAT 3D imagery of 4 August 11:30UTC (1700 IST) IR channel brightness temperature.

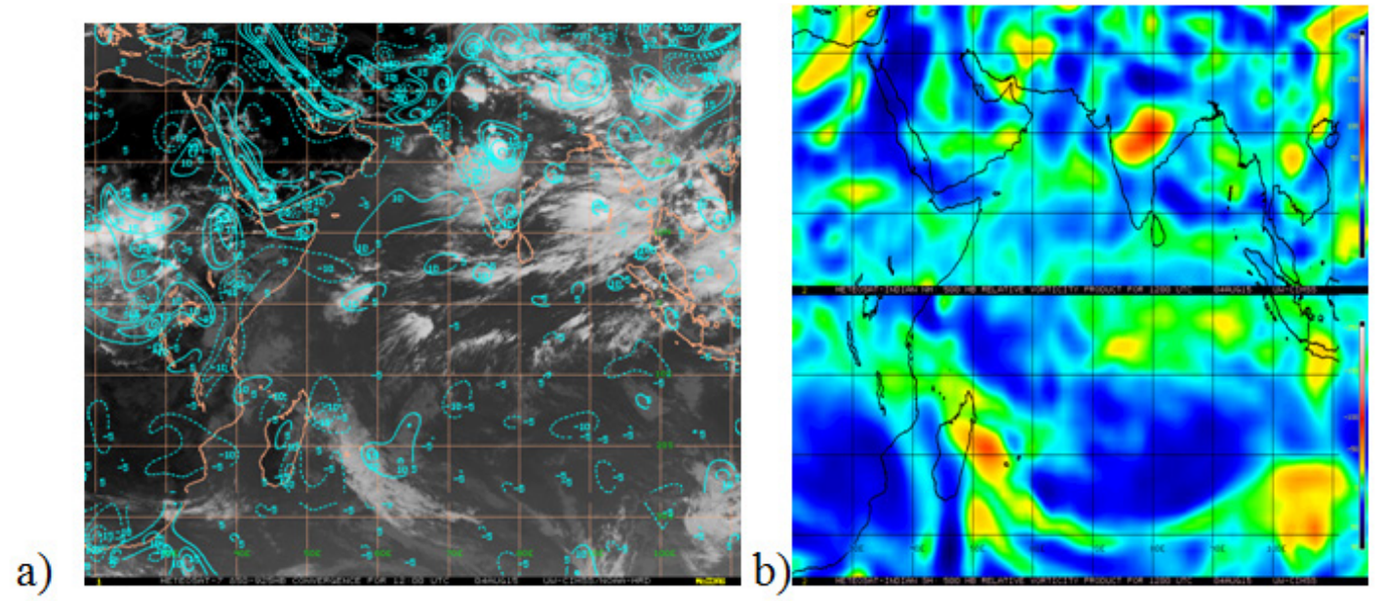

Figure 3.14 a) METEOSAT7 estimated low level convergence (925-850 hPa) in contour (continuous blue line with positive values are convergence and dashed line is divergence). b) 500 hPa relative vorticity (sec 1) on 4 August 1200UTC.

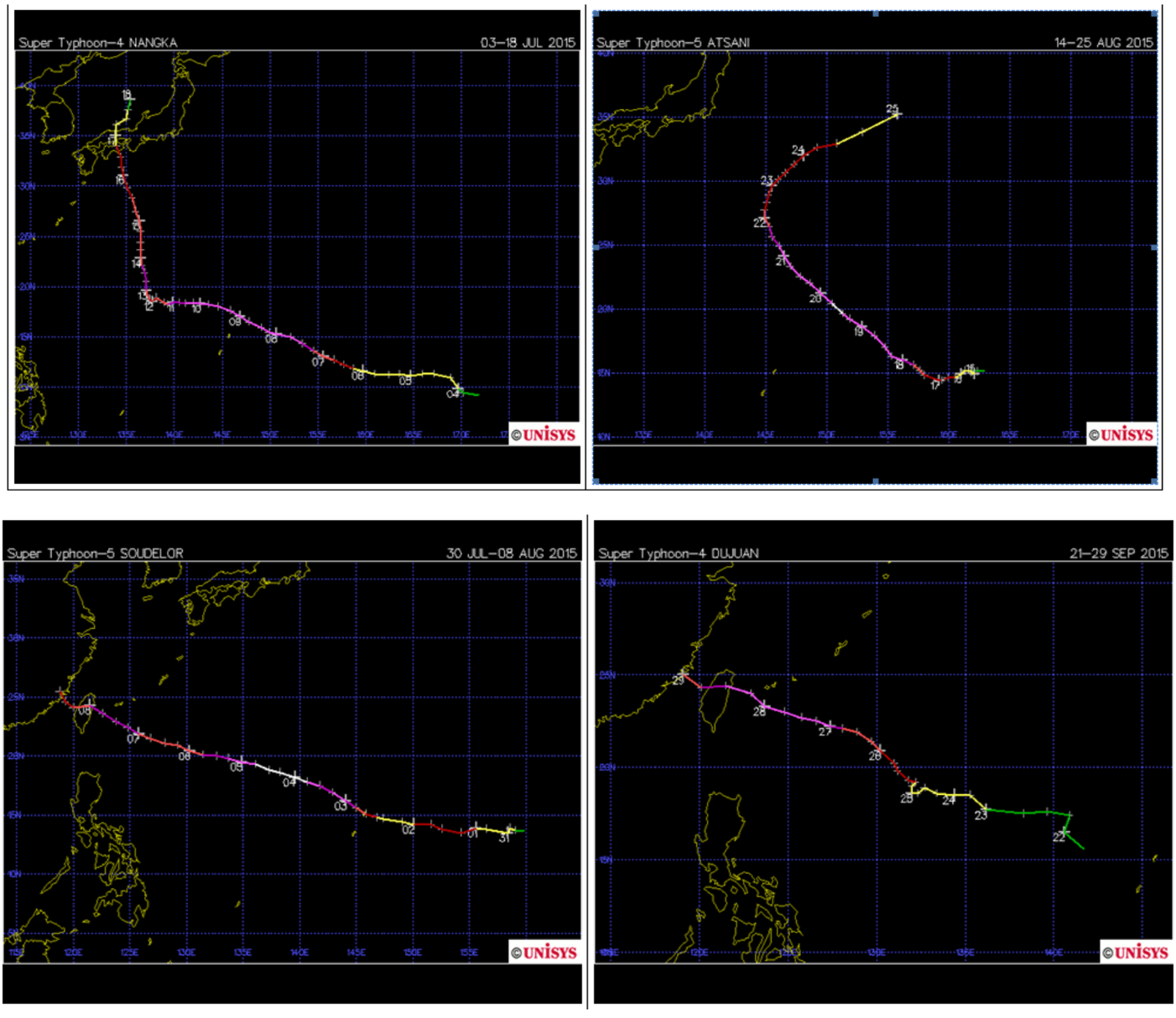

Figure 3.15 Tracks of the super typhoons occurred over the west pacific during JJAS of 2015.

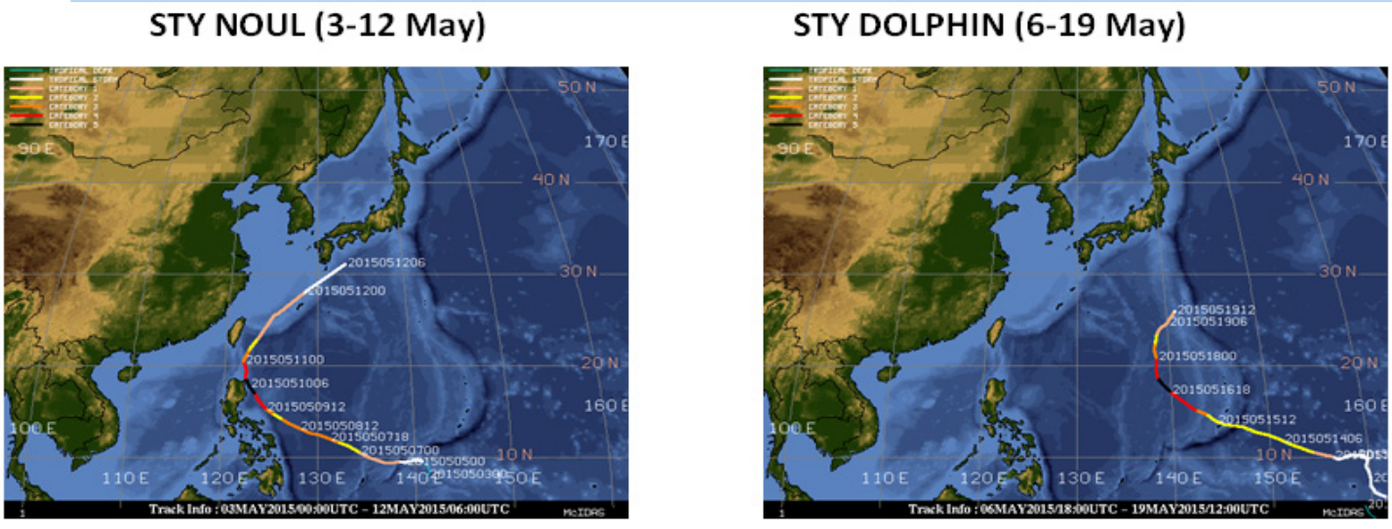

Figure 3.16 Track of the Super Typhoons a) STy NOUL and b) STy DOLPHIN

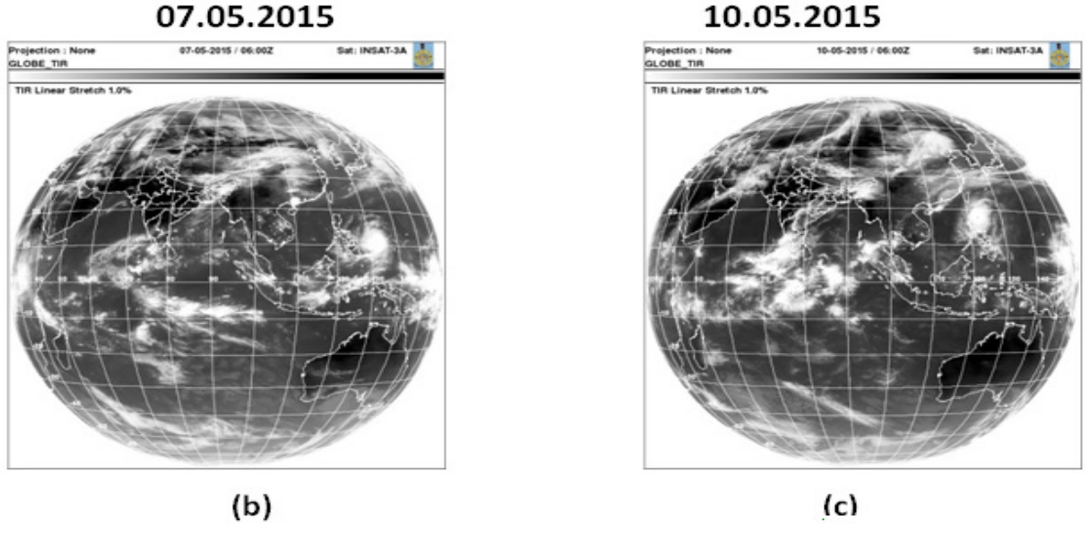

Figure 3.17 INSAT 3A pictures for a) 7 May and b) 10 May 2015

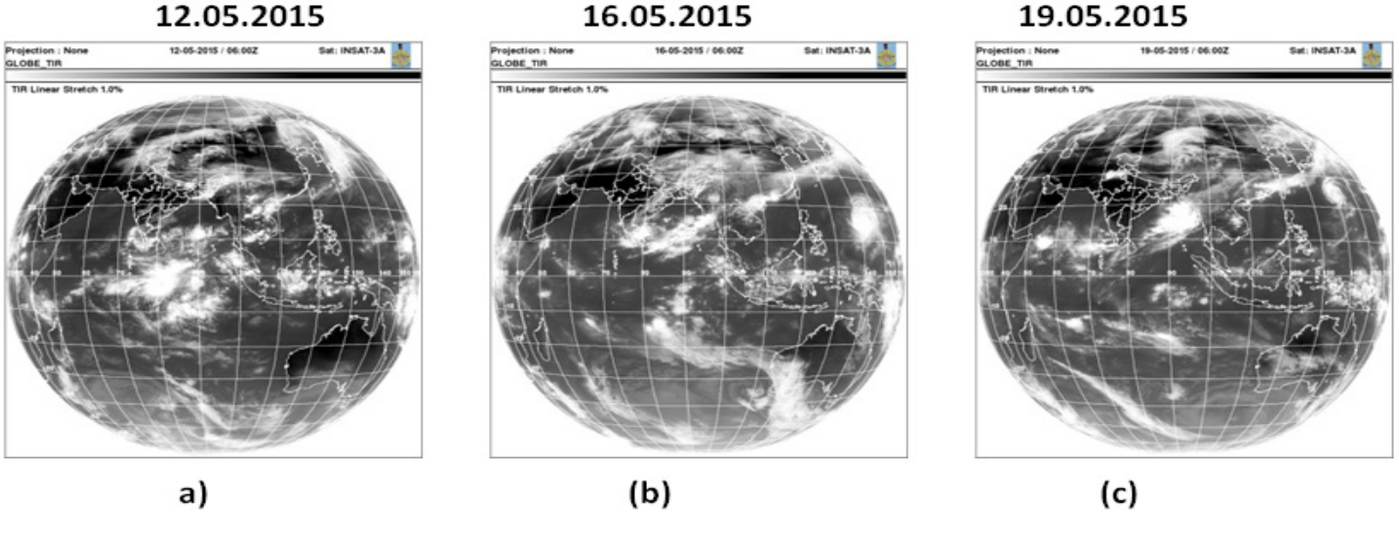

Figure 3.18 INSAT 3A pictures for a) 12 May, b) 16 May and c) 19 May 2015

Chapter 4

Observational Features of Monsoon 2015 from a Local Perspective

Resmi E. A, B. Balaji, Mercy Varghese, Subharthi Chowdhuri, S. Morwal and Thara Prabhakaran

4.1 Observational instruments

This chapter discusses the observed features of SWM 2015 from pre-monsoon to withdrawal phase. Collocated measurements are used to explain the thermodynamic process in coherence with the large-scale features (Table 4.1). Figure 4.1a shows the time series of hourly rainfall from AWS for the JJAS period at Mahabaleshwar. The monsoon showed a very weak beginning in the peninsular Indian region as may be noted from the GPM satellite data on accumulated rainfall during the first week of June (Figure 4.1b). Maximum rainfall was observed during end of June when a low-pressure system was present over the Arabian Sea (Figure 4.1a).

Table 4.1 Summary of the instruments and parameters
(*both from HACPL and IITM, Pune)

Sr. No.	INSTRUMENTS	PARAMETERS
1	Surface Measurements	
HACPL	Automated Weather Station (AWS)	Temperature (^oC), Pressure (hPa), Wind speed (ms^{-1}) and direction (degrees), RH (%) and Rainfall (mm)
	Impact Disdrometer	Rain rate (mm/hr) and instantaneous rainfall (mm)
	Scanning Mobility Particle Spectrometer	Aerosol number concentration (cm^{-3}) and size distribution
	Cloud Condensation Nuclei Counter (CCNC)	CCN (cm^{-3}) at different super saturation
2	Vertical Profile	
Pune	Radiosonde*	Wind speed, direction, temperature, RH
	Microwave Radiometer Profiler (MWRP)	Vertical profile of temperature, humidity, Column-integrated amounts of water vapor and liquid water
	Wind Profiler	Wind speed, direction, vertical velocity/fall velocity of hydrometers and signal to noise ratio
3	Radar	
	X Band, Mandradev	Reflectivity - spatial and vertical cross section
4	Lightning Location Network (LLN)	Lightning density

4.2 The pre-monsoon convective activity

The surface winds were from northeast and southwest direction between 0-12 LST and 13-23 LST, respectively, and speed varies from 2-7 ms-1. The average surface temperature was 25^{o}C over HACPL site. The surface observations show the pre-monsoon convective activity was active on several days with (5th, 9th, 13th May 2015) with rain rates greater than 8mm/hr.

In Pune, 13 May 2015 a severe rainfall event was registered which was part of an organized convection. The surface temperature has dropped 2^{o}C over HACPL site. Pre monsoon convective activity was clearly observed from the LLN network. The cloud to cloud lighting and cloud to ground lightning was also an indication of deep clouds in the pre monsoon season. There were north south oriented features and were part of convective clusters that moved inland. Convergence lines were also noted over the state of Maharashtra.

4.3 Transition from pre-monsoon to monsoon season

The transition from pre-monsoon to monsoon season brought a change in winds from easterly to the south westerlies, from 31st May onwards. Relative humidity and mixing ratio also increased, indicating the moistening of the lower atmosphere (2-8 km). Figure 4.3 shows the collocated measurements of surface temperature, horizontal wind speed from AWS, disdrometer- rainfall and relative humidity from radiosonde observations. The surface temperature gradually reduces in coherence with the progression of monsoon. The rain episodes are associated with a simultaneous increase in wind speed. The vertical extent of the convection is directly linked with the water vapor in the lower and middle atmosphere. The cross section of relative humidity explains the moistening during the pre-monsoon up to 8 km and in the first week of May as well as end of May with the starting of the monsoon season.

4.4 Extremely heavy rainfall over Mumbai on 19 June 2015 and associated convection as seen through radar

Extreme heavy rainfall was observed over Mumbai on 18 June (28 cm) and 19 June (30 cm) 2015. Doppler Weather Radar situated at IMD, Colaba (18.9013ºN, 72.8076ºE, and 100 m) monitored the associated cloud system continuously. Satellite cloud imagery on 19th June indicated the presence of low pressure system over Bay of Bengal (BoB) and Cyclonic circulation (CyCir) over Arabian Sea (AS). On 19th June the different radar products indicated (i) development of convective and stratiform clouds over AS associated with CyCir, (ii) Organization of Convection over AS and over land (iii) Winds becoming SSW to SW with height supporting advection of cold air which strengthened the observed cyclonic circulation (iv) Surface rainfall intensity indicated widespread stratiform rainfall with embedded convective rainfall distribution and (v) accumulated rainfall distribution indicated west to east gradient in the rainfall distribution. The Skew-T diagram on 17th June indicated moist adiabatic stratification up to 400 hPa, freezing level at 550 hPa, low CAPE and low updrafts. Thus, deepening and Strengthening of CyCir due to cold air advection and the clouds tops limiting up to 6 km and with ageing transforming into stratiform clouds indicates (Figure 4.4) a good example of efficient warm rain processes during the heavy rainfall event on 18 and 19 June 2015.

The radar products on 21st June (after the heavy rainfall event) indicated winds becoming SW to S/NE with height supporting warm air advection in the higher levels and divergence of winds in the lower levels which are responsible for the weakening of the prevailing Cyclonic circulation.

4.5 The meteorological features for the period 5 July- 5 August 2015

The monsoon trough was situated close to the foothills and an anomalous anticyclone over the central Indian region at 850 hPa was present during July. The reduced rainfall over the peninsular region is also reflected in the observations taken over Mahabaleshwar (Figure 4.5) and Pune. There were three different periods in July with higher wind speeds as observed at Mahabaleshwar with AWS and over Pune with a prototype wind profiler (Astra Microwave Ltd. operating at 1280 GHz). The wind profiles up to 8 km (note that the observations are not corrected for rain and bias corrections yet to be applied) are presented, which also

include the precipitating cases, where SNR is high due to the precipitation echo (Figure 4.6).

CAIPEEX aircraft observations were conducted during the month of July and 75 hours of airborne observations of aerosol and cloud microphysics, raindrop measurements, GHG and aerosol chemistry documented the extreme dry to wet transition over the triangular area between Kolhapur, Solapur and Mahabaleshwar. Several observations of the inversion layer and the cloud properties in collocation with the Ka-band radar were conducted. The X-band radar was also operated during 2-3 days in collocation with the aircraft observations. Due to subdued convection over the region, the cloud effective radius decreased sharply across the WG to the rain shadow region and there were shallow clouds in the first half of the experiment. The land depressions formed in the second half along with the a few influences from the western disturbances favored more moisture transport over the region. Winds enhanced in the second half, moist convection and rainfall increased. CAIPEEX aircraft observations in the second half of the month indeed concentrated on several of the convective clusters making their way over inland areas in association with the moisture transport.

4.6 The features for the period 5 August- 5 Sept 2015

Even though the rainfall activity was subdued over major parts of India, scattered and isolated rainfall episodes are observed most of the days in August 2015. Fairly widespread rainfall events are also observed for a few days (5 Aug 2015, 11 Aug 2015 and 13 Aug 2015). SWM revived in the last week of August. The cross section of liquid density from the microwave radiometer and equivalent potential temperature (ΘE) shows that the depth of the clouds was between 2-7 km over Pune (Figure 4.7). Rainfall on the lee ward side of the Ghats has received rainfall from shallow clouds as well as the midlevel stratiform (4-6 km layer) clouds. In the first week of September, the surface temperature started increasing and relative humidity decreased with a change in wind direction. Isolated rainfall events are associated with thunderstorms.

4.7 End of monsoon season

The Indian summer monsoon circulation has revived in the mid of September. AWS measurements at Mahabaleshwar showed a systematic increase in westerly wind speed during this period and towards the end of September, easterlies strengthened (Figure 4.8). The measurements with wind profiler and radiometer showed these features in the first half of September (Figure 4.9). The mid level winds have also increased and there were stratiform clouds and thunderstorms recorded over Pune and a severe thunderstorm were recorded on 12th September.

The storm identified by TITAN (> 35 dBZ) count is greater than 120 for the period 3-17 Sept 2015 and have gradually increased over the region (Figure 4.10). The diurnal evolution of the storms showed a peak around 15.30 LST. A case study of rainfall event during a thunderstorm on 12 Sept 2015 over Pune is illustrated with the help of X band radar observations (Figure 4.11). It is part of an organized convective activity. The rainfall received during September was associated with such convective clusters and were more localized.

4.8 Case study: 12th September Thunderstorm over Pune

The thunderstorm observed on 12th September 2015 over Pune was registered by the wind profiler and the radiometer in collocation. The radiometer was used to provide thermodynamic indices as well as the vertical profiles of temperature, humidity and liquid water. The radiometer observed CAPE was > 2000 Jkg-1 CINE was less them 50 Jkg-1, throughout the morning hours and was associated with a moisture convergence. Lifting Condensation Level (LCL) was situated close to 1.8 km. Stratiform clouds were present during the daytime and there were also drizzle associated with these clouds.

The cloud liquid water profiles showed a sudden increase at 15 LST and the corresponding hour average rain rate was 12.9 mm/hr. The rain rate decreased to 11.8 mm/hr during 16 LST. The thermodynamic indices increased beyond the severe thunderstorm limits (KI > 35 and JI >27 and TI > 40) all indicated (Figure 4.13) a clear chance of thunderstorm on the day. Sudden increase in the freezing level just before the initiation of the storm may indicate a sudden surge of warm and moisture in the middle layer. The wetbulb temperature (Twb) =0 level and the freezing level both are at same elevation (5 km) as the thunderstorm initiates, indicating that the whole layer is saturated. Strong instability developed at that point. As there is more environmental dry air entrains in to the storm subsequently, there is more evaporation and the (Twb) =0 level lowered (note that radiometer data also may be not accurate under this condition). The sudden cooling of air and freezing has initiated strong downdrafts and the horizontal wind has decreased beyond this time and momentum is transferred as strong gusts in different layers where condensation and freezing was taking place and cloud and precipitation growth occurred. There was sudden transfer of momentum to lower layers (Figure 4.14). Subsequently, a low level jet is noted in the lower 2 km. The strength of prevailing easterlies above 2 km (in the cloud layer) had decreased significantly during the storm. The signal to noise ratio of the wind profiler showed indications of a melting layer around 4.3 km and indicate subsequent trailing stratiform convection after 2 hours of its initiation. There is also a sudden increase in the wet bulb temperature (Twb) =0 level as convective rainy conditions are over, indicating further warming of middle layers. The observations suggest that there was an overturning circulation, which was important in this case to bring warm and moist air upward (further details of this thunderstorm will be explored in a separate study. It may also be noted that radiometric retrievals under heavy rain conditions also may have errors.)

The aerosol and CCN showed a reduced concentration only during the rainy hours and immediate replenishment was observed as soon as the rain episode got over. Prominent increase in AOD (is observed towards the inland region along the path of depression (16-19 Sept and the associated low pressure system originated over BoB (Figure 4.14). The trajectories at 5 points (from NOAA Hysplit model) showed that there was continued supply of aerosols along south of the track of this system from continental sources of the Himalayan foothills and from northwestern desert regions. The reduced convection along this region favored accumulation of aerosols in this region. It may also be noted that slightly north of this region was also characterized by subsequent lightning activity (Figure 4.15), indicative of high clouds with mixed phase signature.

The key points during the discussion are summarized below:

- The rainfall episodes are accompanied with southwesterly winds and are accompanied by increase in moisture and subsequent reduction in surface temperature.
- Collocated measurements (radiosonde and radiometer) collectively explained the oscillations in winds and associated rainfall events observed over Pune. Vertical extent of the clouds was between 2-7 km from persistent stratiform clouds and a few thunderstorm events were also registered. The mesoscale convective clusters and embedded thunderstorms were noted.
- Heavy rainfall event observed over Mumbai on 19 June 2015 is explained. The convective and stratiform clouds associated with cyclonic circulation are favored by the cold air advection. The depth of the clouds was 6 km indicating possible mixed phase process also present.
- Lightning location network (LLN) explains the cloud to cloud and cloud to ground lightning density and its direction of propagation. It is gives an indication of presence of deep clouds (more than 5 km) in the monsoon region. There were several mesoscale convective clusters such episodes brought more rainfall from the isolated convective cells than from extended stratiform clouds. However, the stratiform convection was more often noted.

- The X band radar observation shows the diurnal cycle of storms (greater than 35 dBZ) during 3-17 Sept 2015. The storm count is above 120 and it peaks around 15.30 LST in the X-band radar range. The horizontal and vertical extent of the heavy rainfall events are also discussed with the help of radar observation.
- Details of a thunderstorm event observed in collocation with the radiometer and wind profiler is documented with some details of the storm initiation and its dynamical interactions.
- The aerosol and CCN concentration showed an immediate replenishment after each rain episodes.
- The consistent increase in the AOD attributed to the continental transport in association with the movement of a depression is illustrated.

Spectral analysis of hourly wind, temperature and rainfall during the entire monsoon season indicated (Figure 4.17) semi diurnal, diurnal, 3 days periodicities from temperature or wind is reflected in the rainfall periodicity. However, for long period effects, wind does not show a coherent periodicity. Temperature and rainfall periodicities at 40 days and 60 days were well correlated.

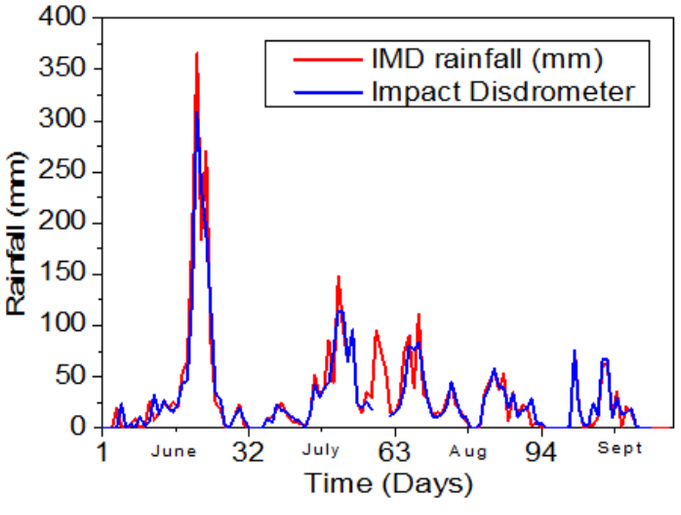

Figure 4.1a. Times series of hourly rainfall for JJAS period at Mahabaleshwar

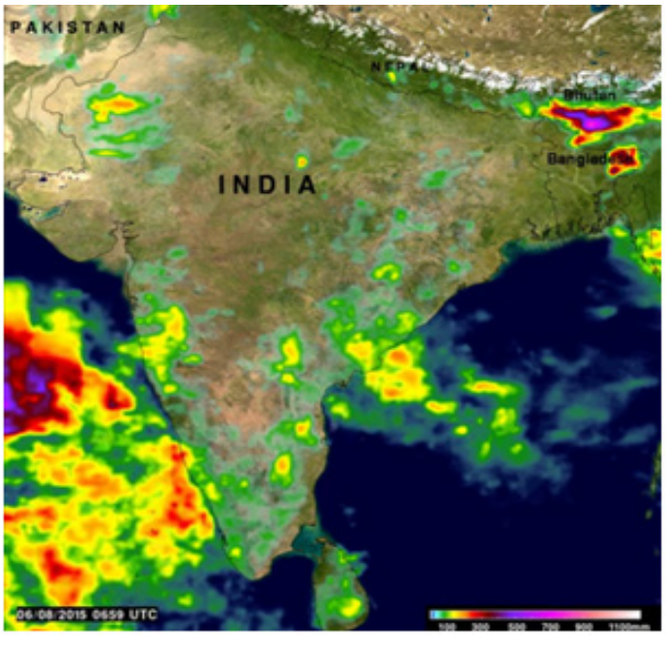

Figure 4.1b. Total rainfall (mm) during 1-8 June 2015 from GPM satellite

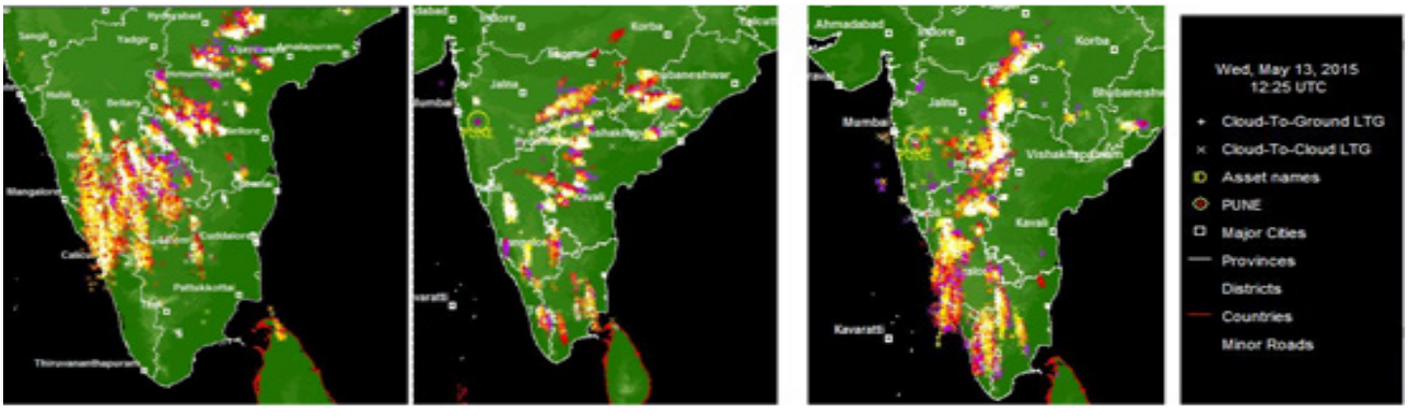

Figure 4.2. The distribution of lightning at 11 UTC from 2- 4 May 2015

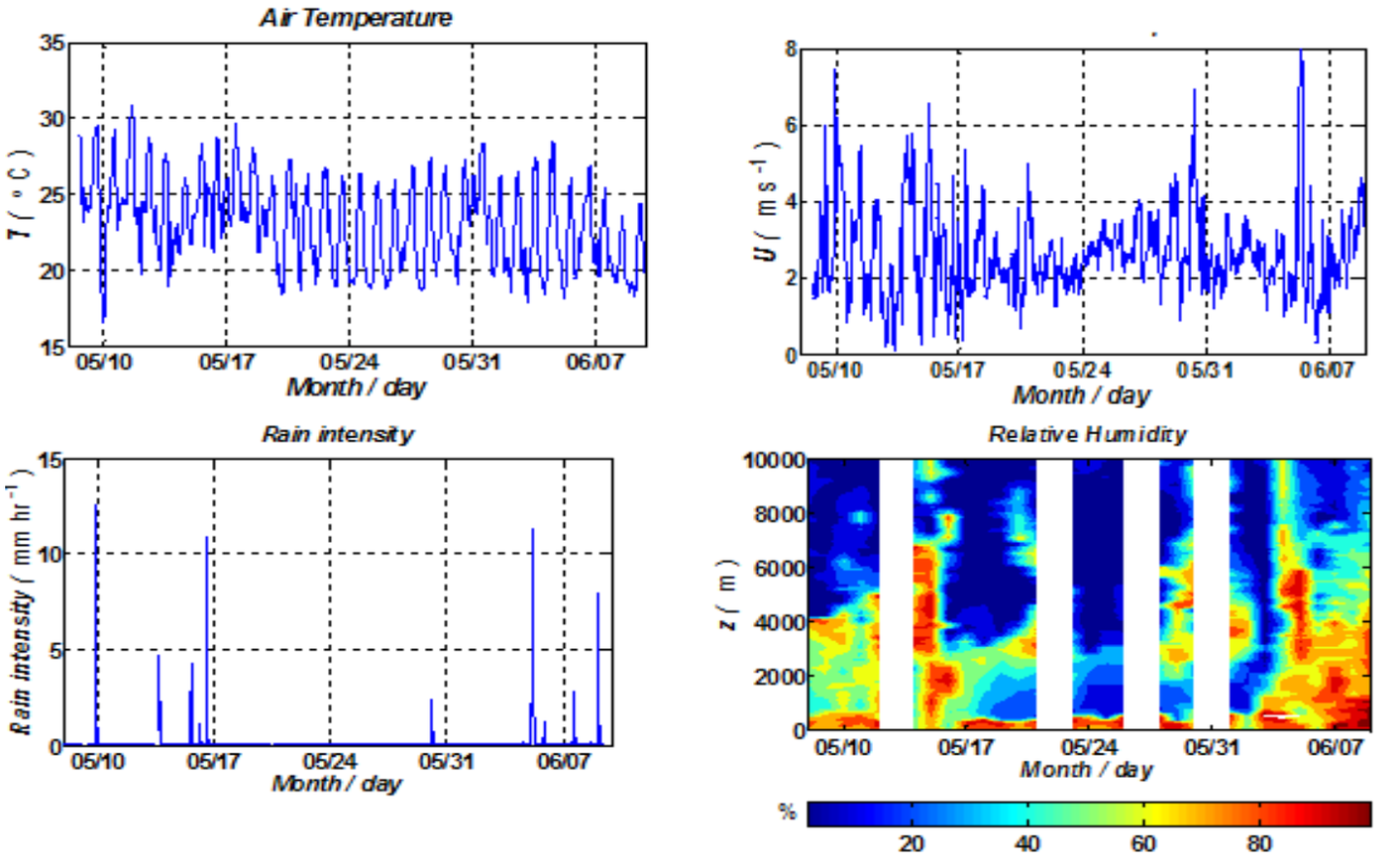

Figure 4.3. Time series of surface temperature, wind speed (AWS), rain intensity (impact disdrometer) and cross section of relative humidity (radiosonde) from HACPL site.

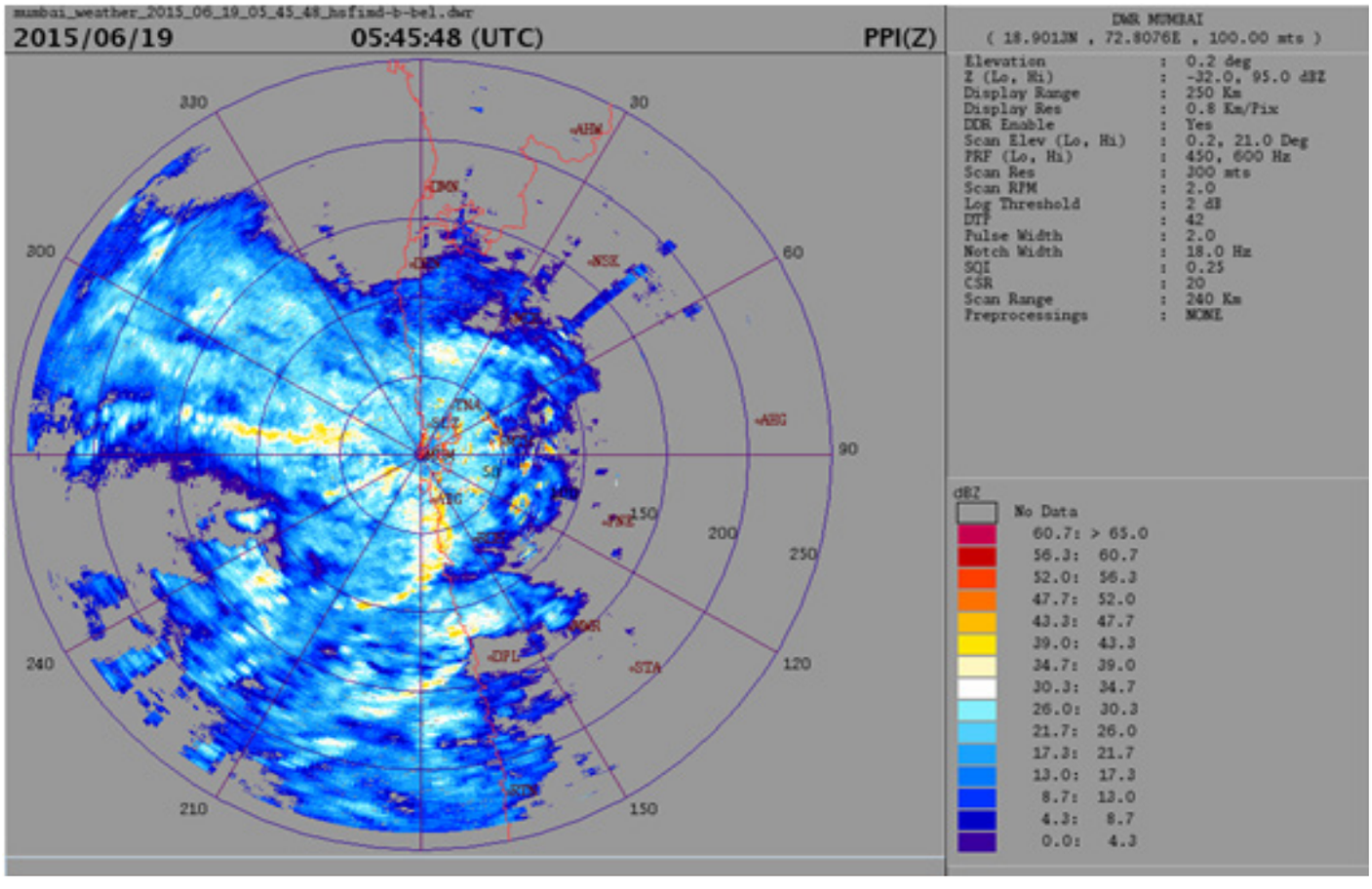

Figure 4.4. PPI (Reflectivity) on 19 June 2015 at 5:45:48 UTC (IMD Mumbai Doppler radar)

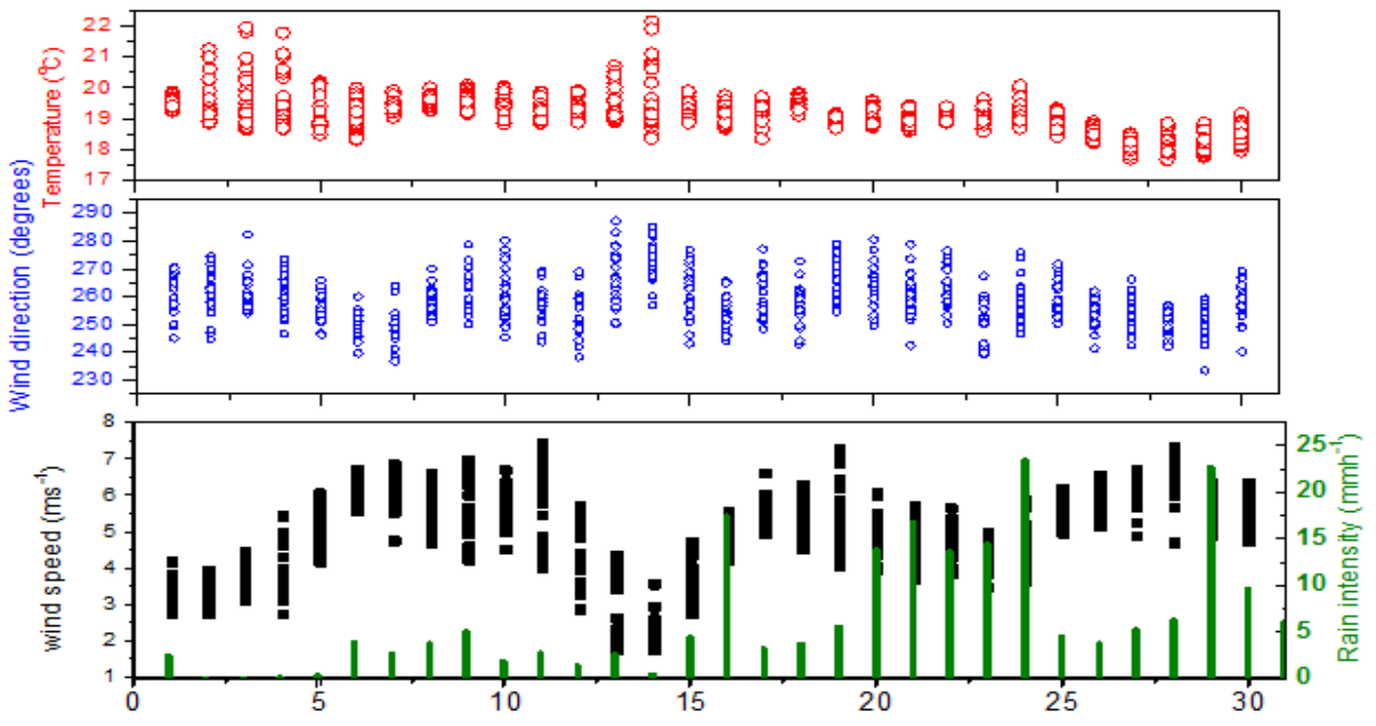

Figure 4.5. Wind speed, wind direction, rainfall and temperature observations at Mahabaleshwar during July. The scatter shows variation during the day. It may be noted that some day's maximum temperature recorded is quite high and is associated with dry westerly intrusion.

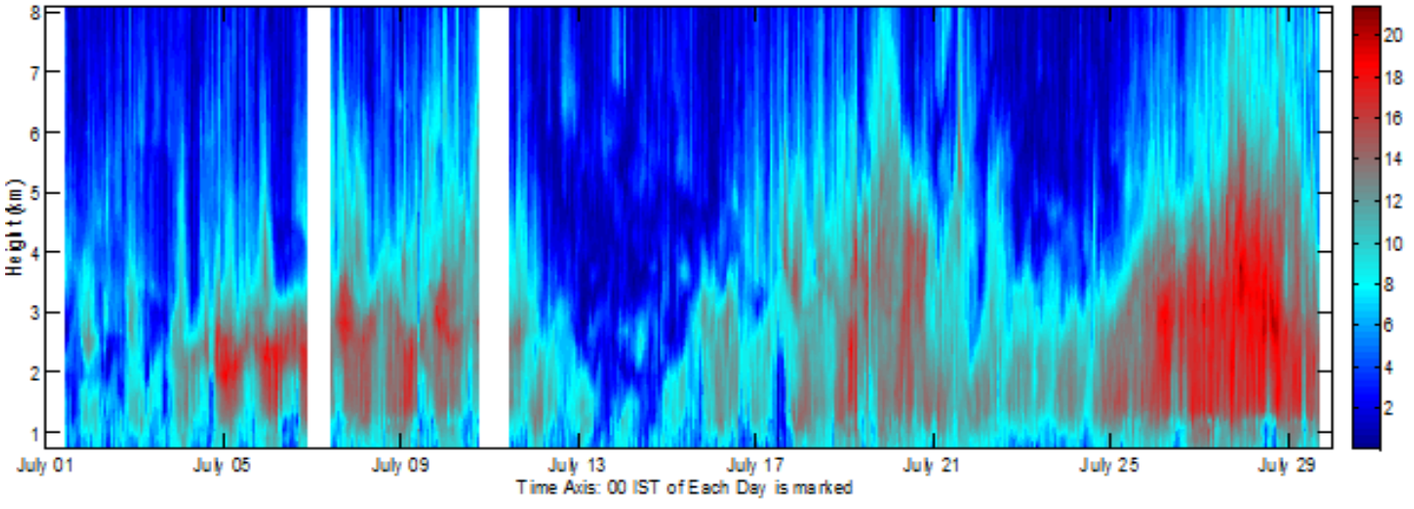

Figure 4.6. Wind profiler observations carried out over Pune with the Astra Microwave Ltd prototype wind profiler operating at 1280 MHz under all weather conditions. (Data is not corrected for rain events.) A systematic variation in winds with the dry/moist conditions may be noted.

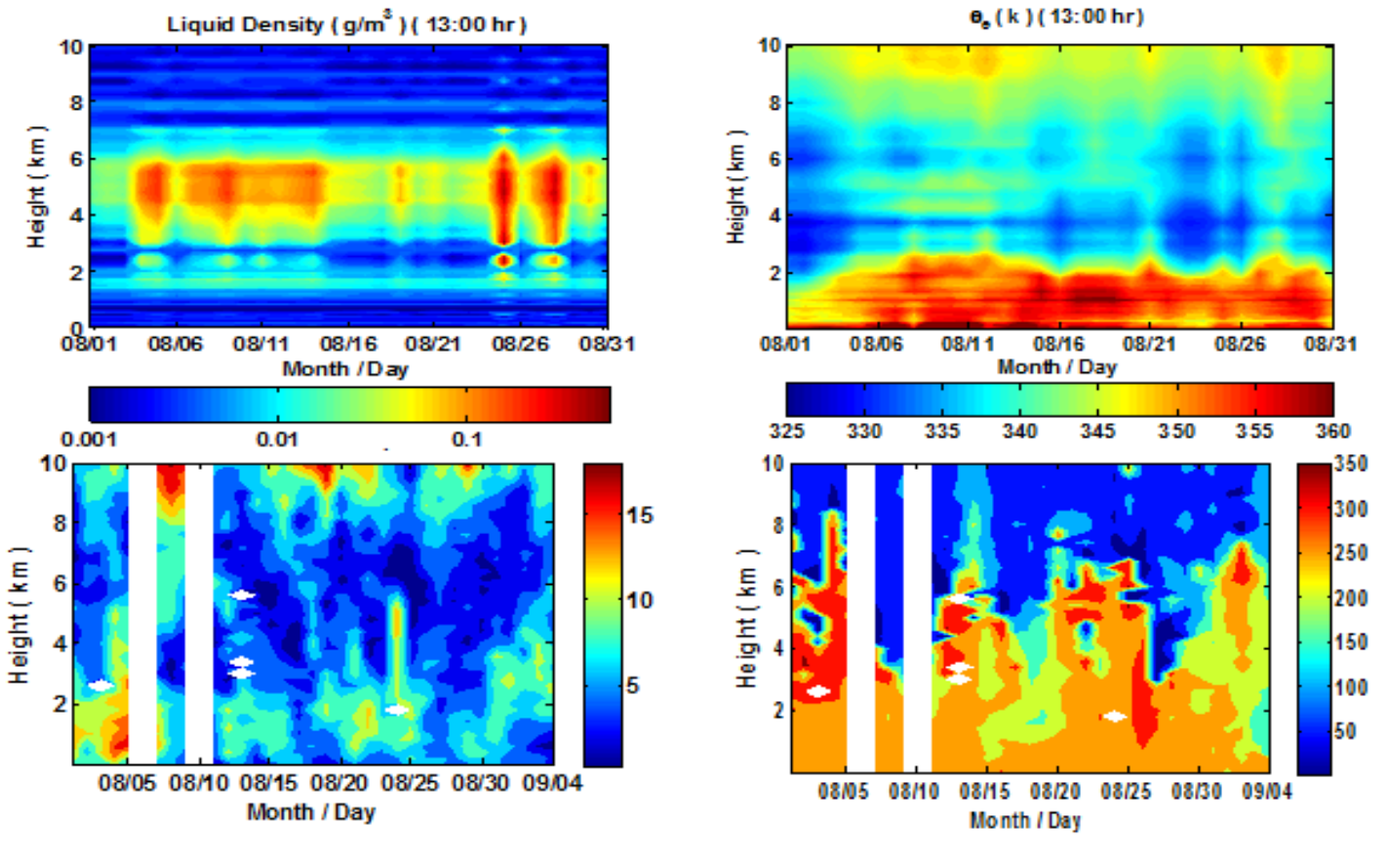

Figure 4.7. Time-height cross section of liquid density (gm^{-3}) and theta ΘE (K) (upper panel, radiometer) and wind speed and direction (lower panel, radiosonde) from IITM, Pune. Liquid density and ThetaE derived from MW radiometer.

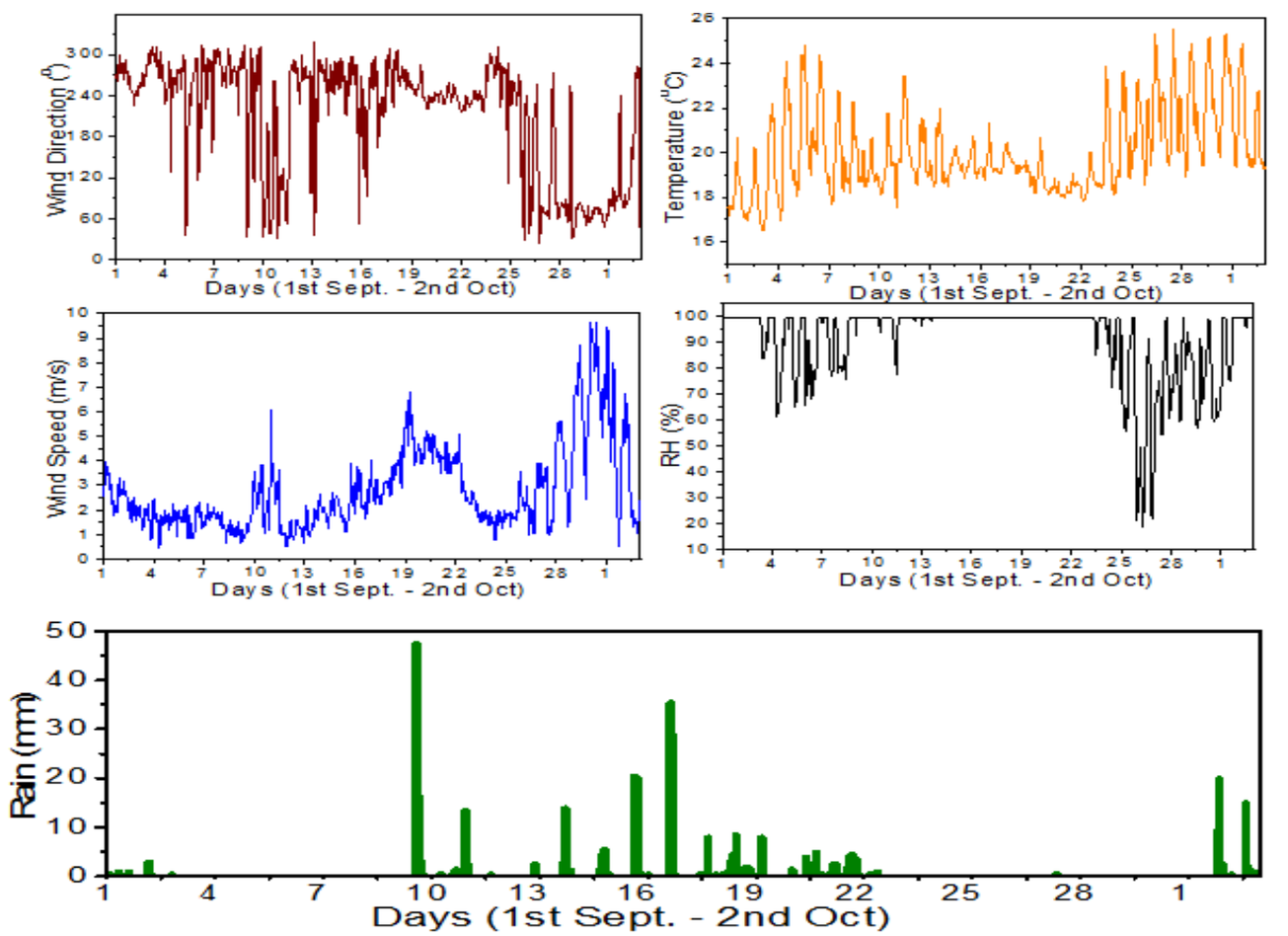

Figure 4.8. Wind direction, temperature, wind speed, RH and daily accumulated rainfall measured over Mahabaleshwar during the month of September. The diurnal variation of various parameters is inherent in these plots.

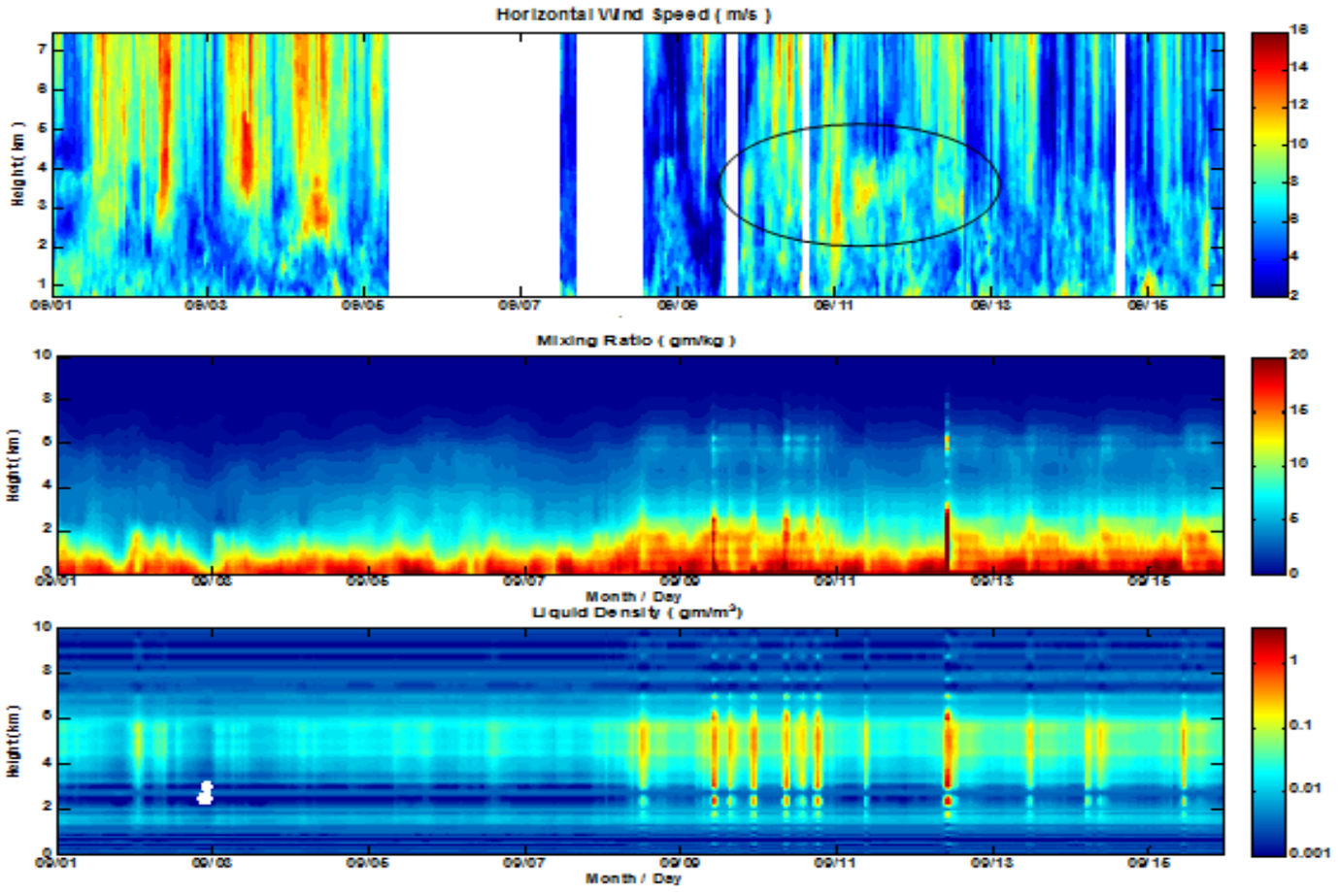

Figure 4.9. Wind speed from wind profiler (ms-1), water vapor mixing ratio (gkg-1) and cloud liquid profiles (gm-3) from radiometer during 1-15 September 2015

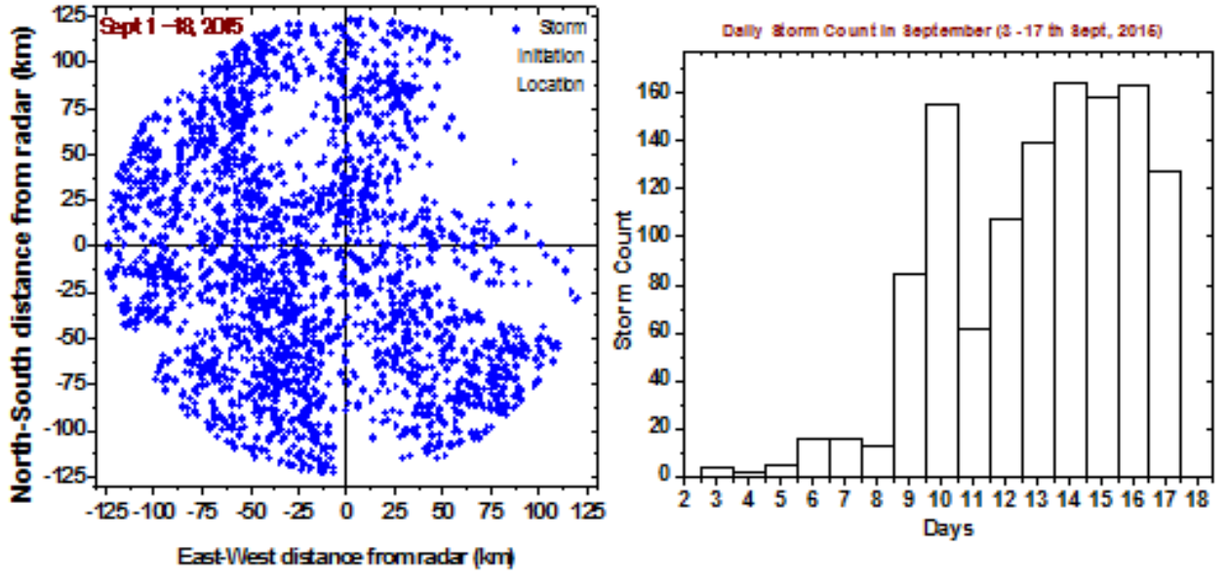

Figure 4.10. Clouds identified with TITAN from X-band radar (> 35 dBZ) data and daily storm count until 18th september. (provided by Mr. Utsav Bhowmik)

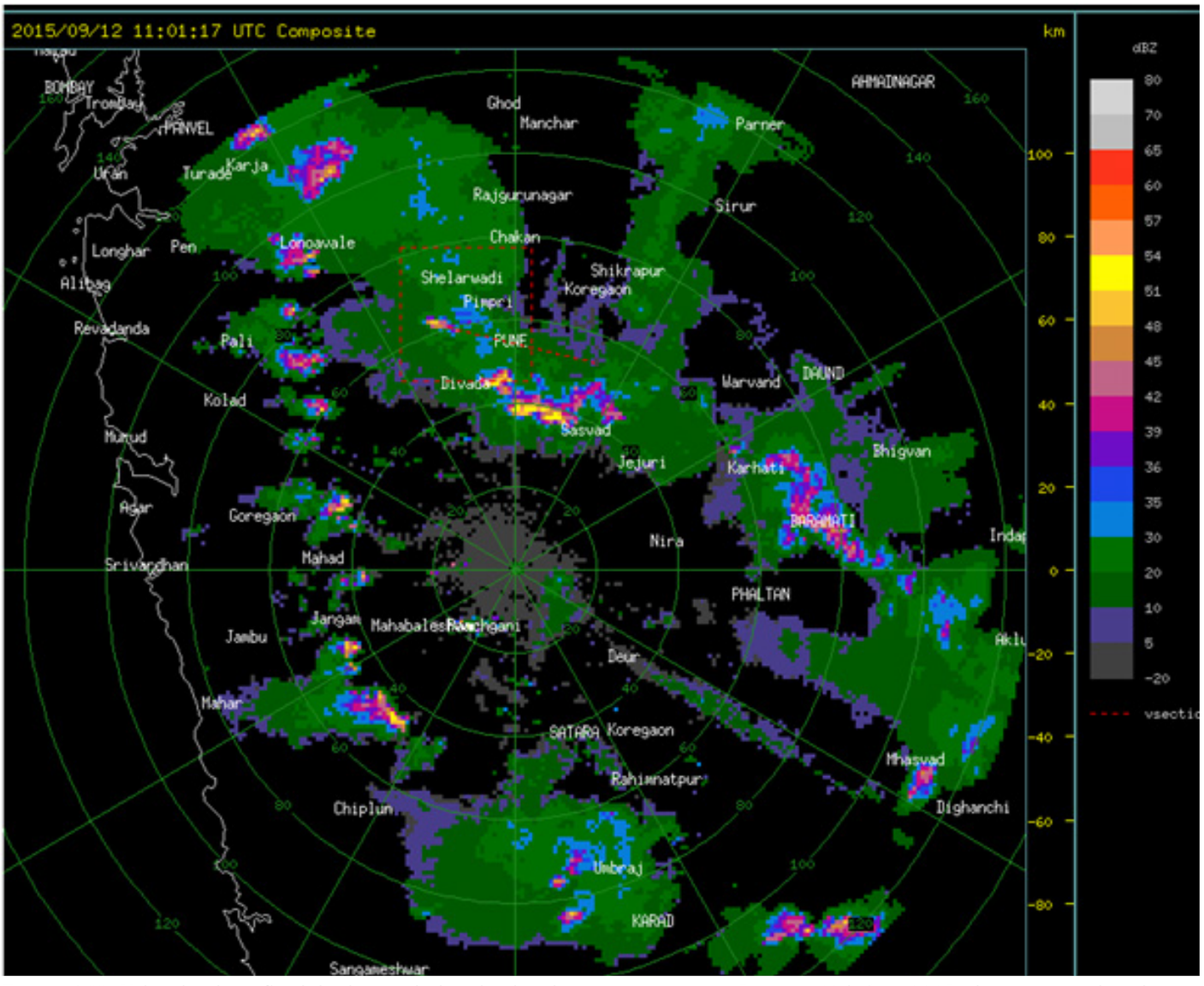

Figure 4.11. X-band radar reflectivity image during the thunder storm event over Pune on 12th Sept 2015, shows convective clusters and explains the localized rainfall (provided by Mr. Utsav Bhowmik)

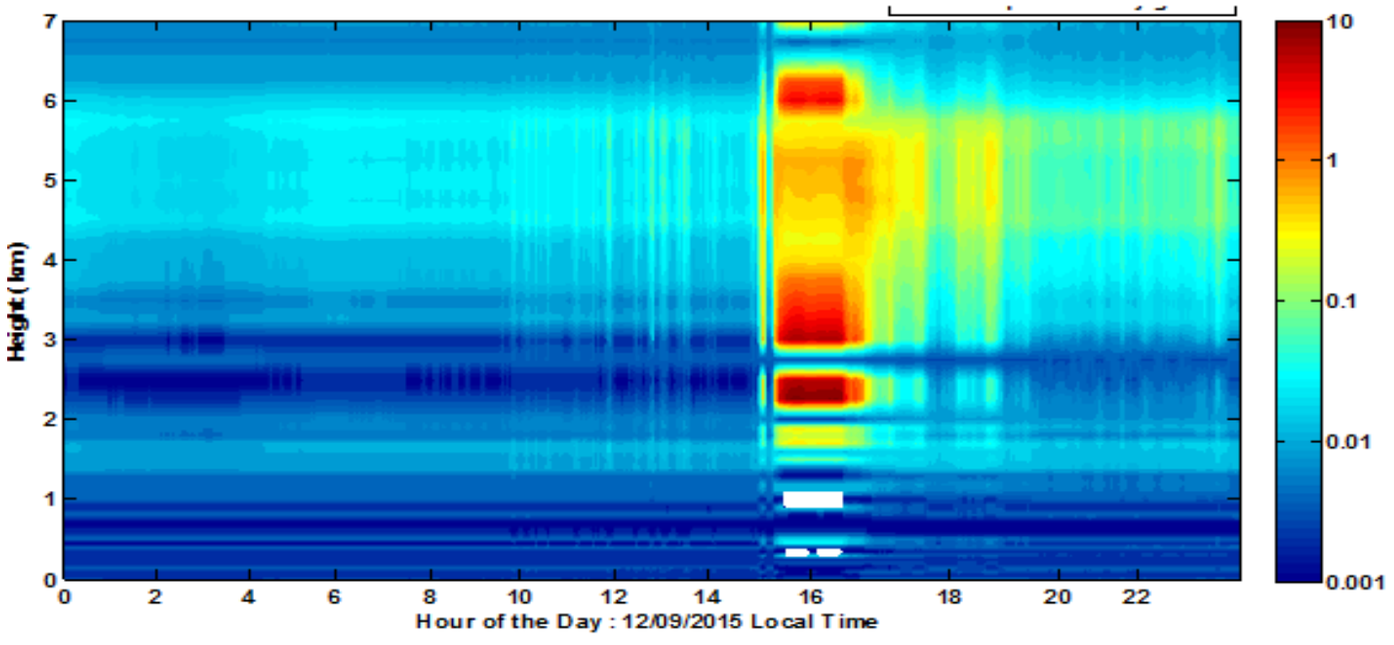

Figure 4.12. Radiometer cloud liquid water (gm-3) during the 12 September thunderstorm event over Pune

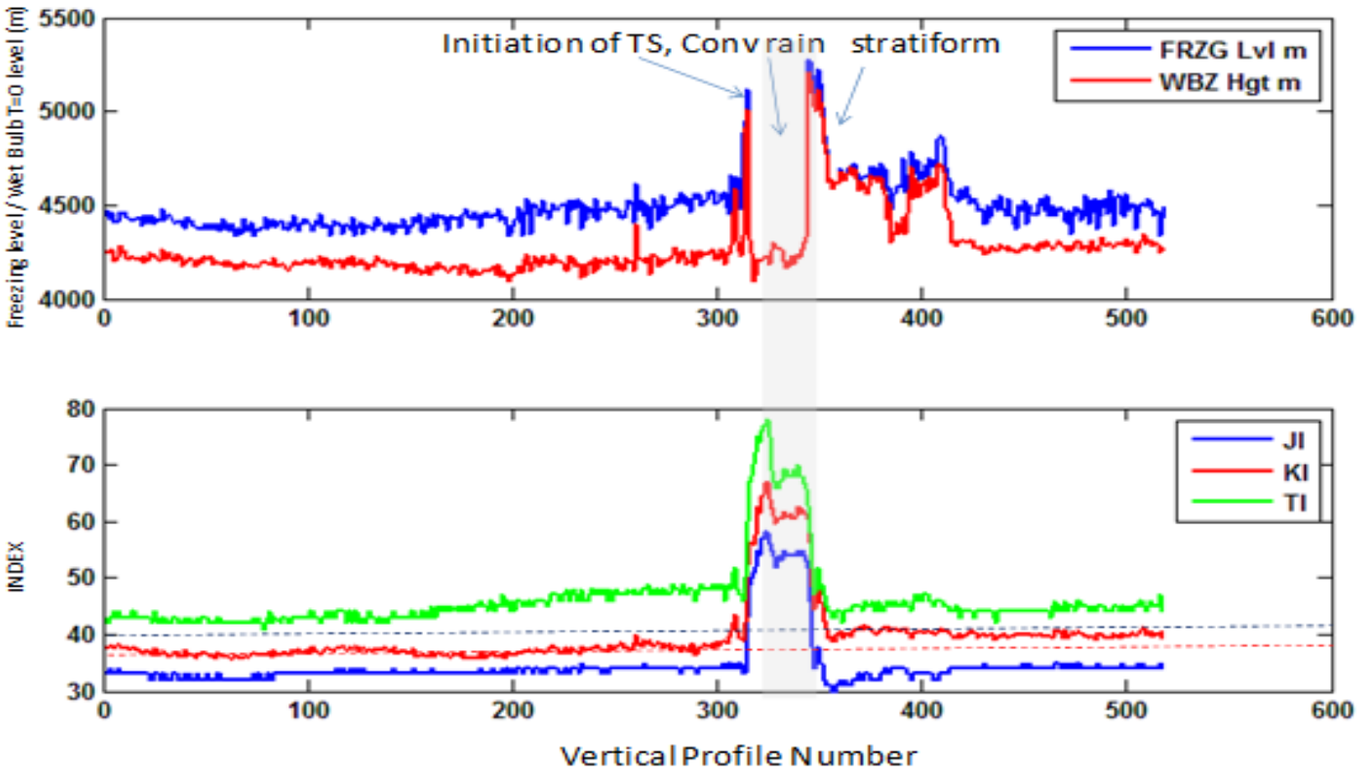

Figure 4.13. Thunderstorm indices such as (KI, TI and JI) derived from radiometer observations on 12 Sept 2015.

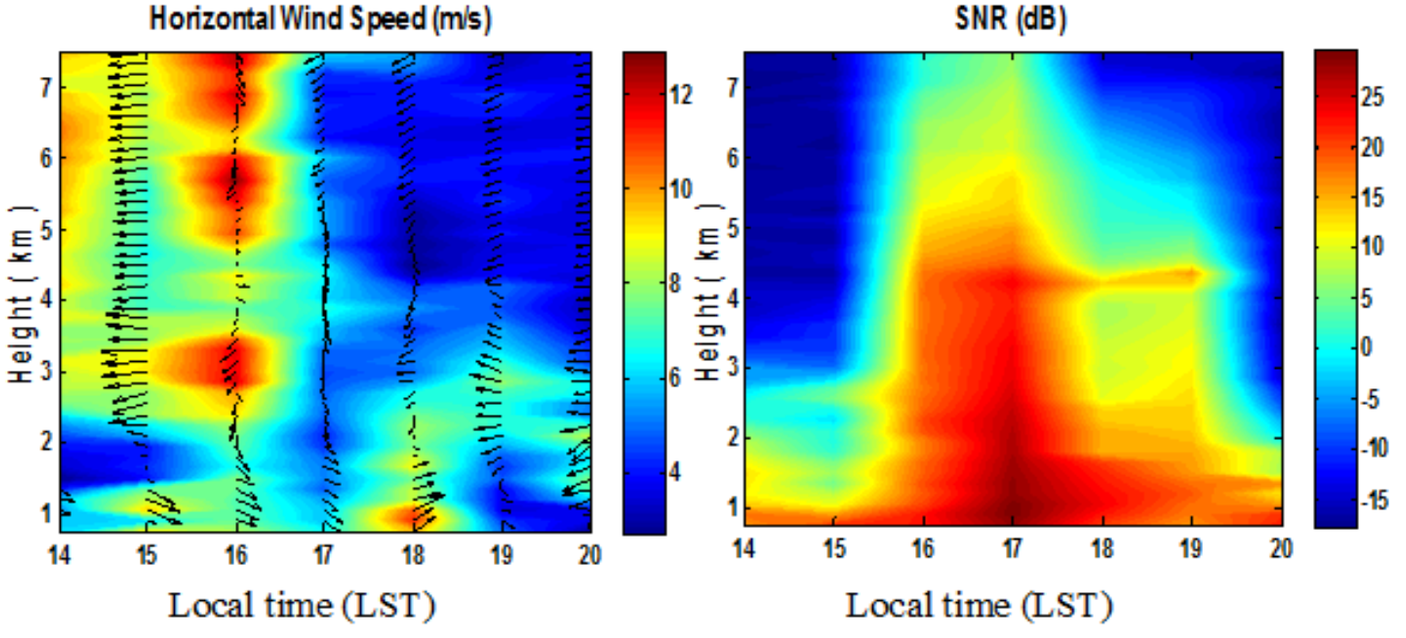

Figure 4.14. Horizontal wind speed and wind vector and signal to noise ratio (SNR) profiles from wind profiler during the 12 September thunderstorm event over Pune

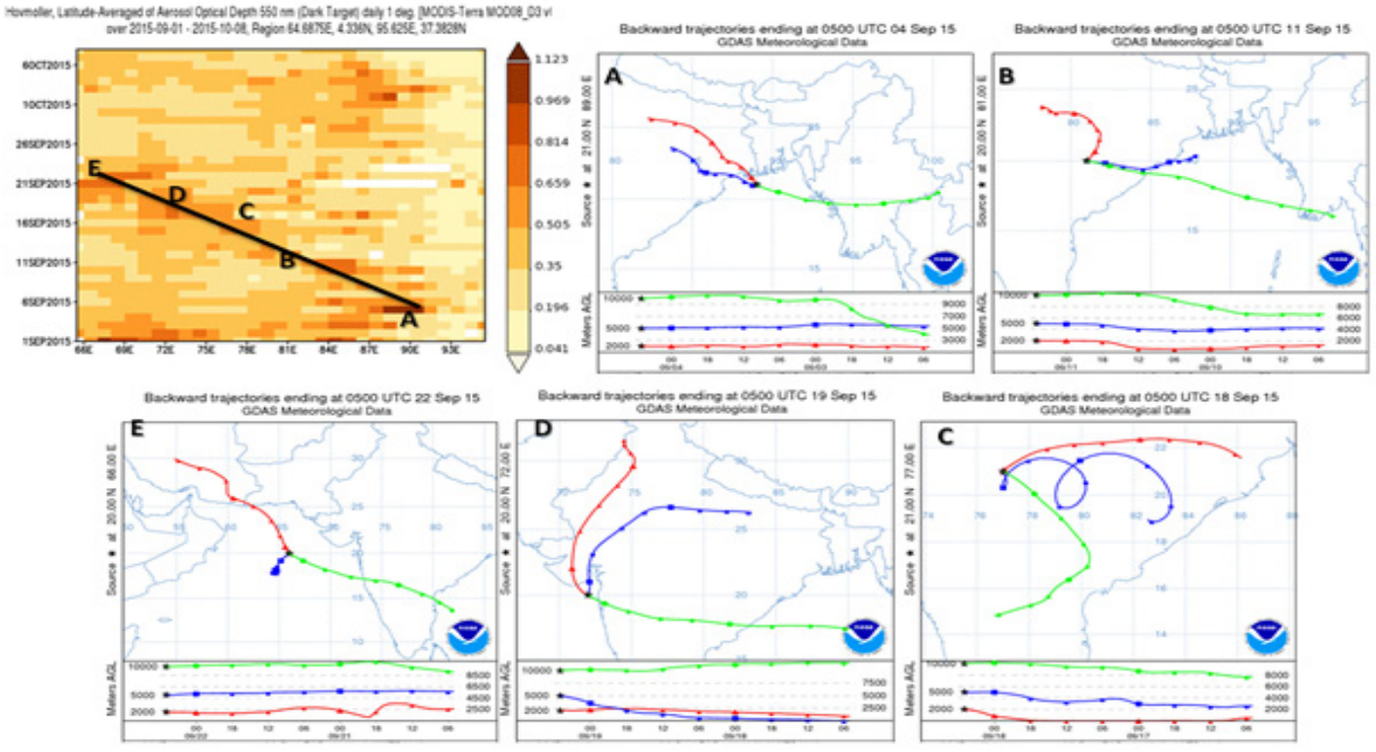

Figure 4.15. MODIS aerosol Optical depth for 1 Sept -8 Oct 2015 and the NOAA Hysplit 2 days back trajectories at selected points indicated as A,B,C, D, and E at three levels (at 2 km, 5 km and 10 km) ending on 4th, 11th, 18th, 19th, 22nd September.

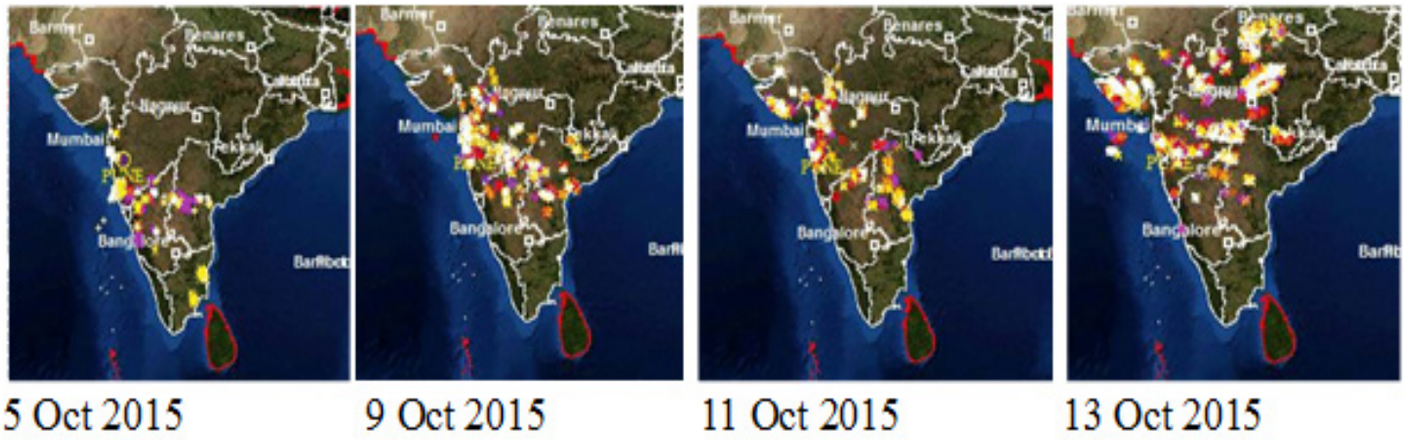

Figure 4.16. The lightning intensity maps during the period of 5- 13th October 2015

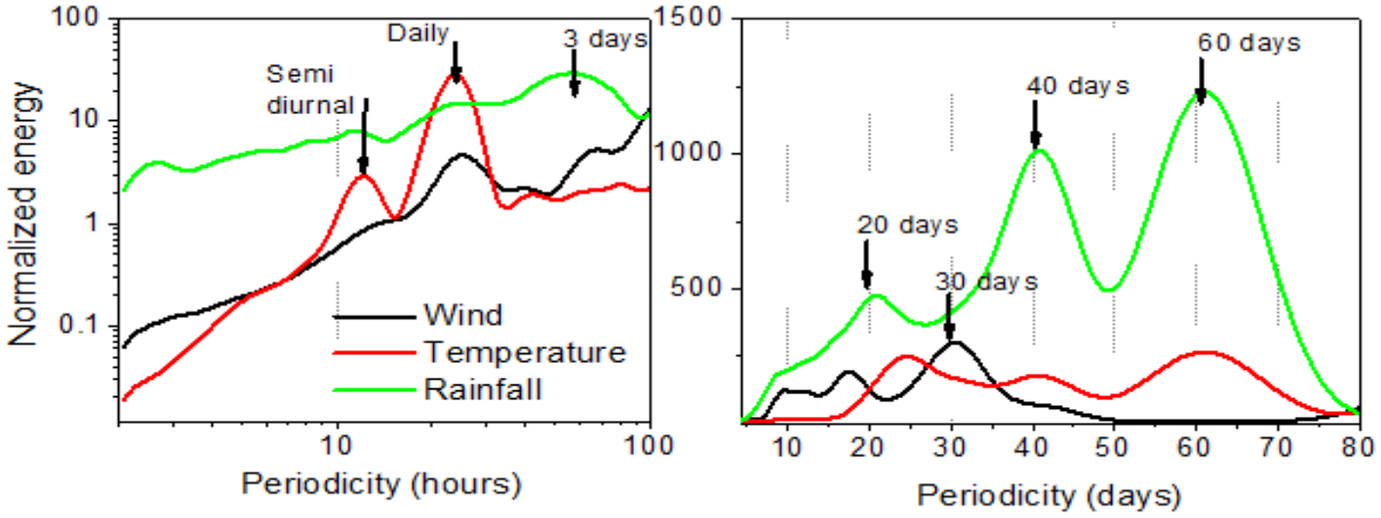

Figure 4.17. Energy spectra of wind, temperature and rainfall measured at Mahabaleshwar

Chapter 5

Performance of the Extended Range Prediction System During 2015 Monsoon Season

Abhilash S., Raju M., Avijit D., R. Phani, S. Joseph, R. Chattopadhyay, A. K. Sahai and M. Rajeevan

5.1 Introduction

The year 2015 registered a deficiency in the all India Summer Monsoon Rainfall (ISMR) during June-September season. The country's official weather forecaster, India Meteorological Department (IMD) warned the nation for an approaching drought like situation well in advance. In their seasonal outlook issued in early June, IMD had predicted only 88% of Long Period Average (LPA) rainfall for June-September season for the country as a whole. The seasonal forecast is mainly used for policy makers for long term planning. Due to the limitations of the seasonal forecasts, it should be supplemented with extended range prediction (ERP) of 1-3 weeks in advance. There is continued demand for user-specific predictions as the time and space scales of the predictions vary with stake holders. Realizing the importance and potential usefulness of the ERP, Indian Institute of Tropical Meteorology (IITM) started issuing the ERP on experimental basis since 2013 using an indigenously developed ensemble prediction system (EPS) based on National Center for Environmental Predictions (NCEP's) Climate Forecast System (CFS) (Abhilash et.al., 2014, Abhilash et al., 2015, Borah et.al., 2014, Sahai et al., 2015). The present report discusses about the design of the prediction system and strategy adopted for 2015 ERP, observed features of the 2015 SWM season, role of intraseasonal oscillation (ISO) signal in ERP, highlights of the monsoon prediction during 2015 season, performance and skill evaluation of the prediction system and the challenges in the ERP during 2015 season.

5.1.2 Strategy adopted for ERP

We have used different versions of climate forecast system model version 2 (CFS) which are created by changing the model resolution, physics, stand-alone atmospheric component of CFS (i.e.: GFS) forced with bias corrected CFS-forecasted sea surface temperature (SST). This corroborates well with the prime goal of the National Monsoon Mission project, which is to improve the monsoon prediction capabilities of the CFS model. The complementary nature of the CFS versions leads to the development of the CFS based Grand Ensemble Prediction System (CGEPS) for the ERP of active/break spells of Indian summer monsoon rainfall (ISMR). Detailed skill analysis, improved spread-error relationship and probability prediction of CGEPS MME can be found from Abhilash et al. (2015). Real-time implementation of this system and its performance during 2014 monsoon season can be found from Sahai et al., (2015). In order to give equal weights to all models and to add more diversity we have used 11 members each from CFST126, CFST382, GFST126 and GFST382 for 2015 ERP. The initial conditions have been obtained from NCEP NOMADS server with T574L64 resolution atmospheric assimilation and MOM4 based oceanic assimilation, and which is real-time extension of the CFSR (Saha et al. 2010). Rainfall prediction skill is mostly verified against the IMD-Merged rainfall data sets (Mitra et al., 2009).

5.2 Prominent observed features linked to ERP during 2015

5.2.1 Northward Propagation of Monsoon Intraseasonal Oscillations (MISO)

Figure 5.1a presents the observed low frequency component of the large scale MISO. The phase space diagram is generated by calculating the MISO1 and MISO2 from Extended EOF analysis following Suhas etal., (2013) and Sahai etal., (2013). Northward propagating convection band from the equatorial Indian Ocean to the

foothills of Himalayas is the most prominent intraseasonal oscillation signal over Indian region during SWM season. Figure 5.1b depicts the latitude-time plot of OLR anomaly averaged over Indian region (70-90°E). It is clear from the figure that there is absence of enhanced convective activity during the entire season of long duration. The OLR anomaly is mainly characterized by three fast propagating active spells of very short duration and is mainly dominated by extended suppressed convection during the season. This fast propagation of the enhanced (active) phase of convection from the southern peninsula to foothills through central Indian region during June is prominent in Figure 5.1(b). During June, July and August, three fast propagating convective spells covered the half cycle in about 12-15 day (Figure 5.1(a)). This implies that the monsoon active phase was comparatively fast propagating, while the break phase was slow propagating during 2015 SWM season. The analyses of progpagation characteristics of SWM convection carried out in section 1.6 of Chapter-1 also support the above diagnosis. These characteristics of large scale MISO very well corroborates with the behavior of active/break spells during below normal monsoon years, as shown by Sharmila et al. (2015).

5.2.2 East-West propagation of convection and Madden Julian Oscillations (MJO)

Another large-scale low frequency intra seasonal component affecting Indian monsoon rainfall is eastward propagating MJO. Figure 5.2a shows the longitude-time plot of OLR anomaly averaged over 5°S to 5°N. Wheeler and Hendon (2004) constructed the RMM index for monitoring the MJO and the RMM indices for 2015 monsoon season is obtained from Australian Bureau of Meteorology. The RMM phase diagram in Figure 5.2c along with hovmoller plot shows eastward propagation of active and suppressed phases of convection. Strong MJO signal was present during June to the mid July and MJO covered one full cycle from in due course. It is clear from both figures that the suppressed phase of convection was prevailed over Indian Ocean to western Pacific from early July to end of September. As seen from the MJO phase diagram, MJO signal was very weak during this period. Figure 5.2b is same as Figure 5.2a except the OLR is averaged over 10°N to 25°N. This figure primarily depicts enhanced and suppressed phases of convection associated with the westward moving 10-20 days oscillation over the Indian Monsoon region. The suppressed convective phase of eastward propagating MJO that was prevalent in the equatorial region during the first half of July seems to have generated westward moving divergent Rossby waves between 10° and 25° N, which are in turn coupled with the northward propagating break anomalies and led to the sustenance of breaks during the end of July and August. This resulted in the subdued rainfall activity during this period as proposed by Joseph et al., (2009). By and large, westward moving enhanced phase of convection of short duration were mostly dominant during 2015 SWM season (See Section 1.6 of Chapter1 for further details).

The enhanced and suppressed phases of MJO well correspond to the above normal rainfall over CI during June and extended break situation in July and August, respectively. This active and break cycle of rainfall over CI has close association to the different phases of MJO as presented by Pai et al. (2009). They have shown that 70% of the active phases are associated with MJO phases 3-6 and 83% of the break phase occurs when MJO is in phase 7,8,1,2. During the period of extended break situation over Indian regions, MJO was in very weak phase over 7,8,1,2. In the month of June 2015, the MJO was strong and present over Phase 3-6 and during the period the rainfall over Indian region was above normal. The active and break phases of rainfall over Indian region during 2015 SWM season is a close prototype suggested by Pai et al. (2009). The later part of the season does not give any strong signal of MJO with weaker amplitudes lying inside the circle (Figure 5.2c).

The wind over central equatorial Pacific is strong, without any clear propagation. Since El-Nino induced

SST anomalies were strong, the MJO signal was not clearly seen along the date line. The JJAS season shows that once the ENSO associated features were strong, it does not allow MJO to propagate across the maritime continent region. Figure 5.3 shows the reconstructed anomaly fields of velocity potential at 200hPa associated with MJO using RMM1 and RMM2 averaged over 7.5°S-7.5°N. Interestingly the upper level does not show any signal of MJO propagation after the onset phase. This also supports our hypothesis. For the 2015 SWM season, extended range MJO forecast from IITM was disseminated in real-time. The lack of propagation was clearly evident in the IITM extended range forecasts initiated from several initial conditions after the end of June.

5.2.3 Western Pacific Storms

Figure 5.4 shows the storm track over Western Pacific during the month of June, July, August and September 2015 (Also refer Table 3.1 in Chapter-3). The association of Western Pacific storm tracks and Indian summer was discussed and well documented by several studies (Krishnamurthy et al., 1977, Rajeevan et al., 1993, etc). Rajeevan et al (1993), Vinay Kumar et al., (2005), Mujumdar et al ., (2007) and Pattnaik and Rajeevan (2007)) shown that recurving storm tracks in Western Pacific which formed east of 150°E has a negative impact on the Indian Summer Monsoon rainfall and typhoons forming over China Sea and moving westward has a positive impact on the monsoon.

The monthly distribution of typhoon activity in Figure 5.4 shows that there were not as much of typhoon activity over Western Pacific in the month of June. This was followed by active typhoon activity in the month of July and August with 5 storms each and all of them re-curved northward. September witnessed 4 storms over Western Pacific and all of them re-curved northwards. Corresponding monthly rainfall anomaly over Indian region was mostly positive in the month of June and followed by large negative anomaly in the month of July, August and September. This is in agreement with earlier findings of the close association of below normal summer monsoon rainfall and re-curving storms over Western Pacific.

5.3 Highlight of ERP during 2015 monsoon season

5.3.1 Real-time dissemination of the ERP and observed rainfall over Central India

Figure 5.5 shows the observed daily rainfall anomaly over Central India during 2015 SWM season. It is clear from this figure that monsoon entered into a break phase from 25 June and extended till the mid July. Followed by an above normal rainfall activity for a short duration mainly associated with a synoptic system moved over Central India (from IMD all India weather report). Then monsoon entered into an extended break situation from last week of July to first half of September. Again monsoon revived over CI around 20 September.

The extended range prediction of daily rainfall is challenging mainly due to the random nature of the forecasts beyond 10 days. As mostly forecasted rainfall patterns are found to be shifted in phase and intensity with respect to observed rainfall. Realizing this inability of most ERP systems available today, dissemination of the forecasts to the end users is extremely important and critical. Figure 5.5 also highlights the extended range forecast disseminated based on the CGEPS from selected initial conditions (ICs). From 31st may IC, it was forecasted that low pressure system over Arabian Sea is likely to intensify and move towards Oman coast and may dissipate around 11th June. The CGEPS successfully predicted track and landfall location of the cyclonic storm named Ashobaa 12 days in advance and will be discussed later. From 5th June IC, we have forecasted the establishment of offshore trough along the west coast by 17th June and subsequent propagation of SWM over Central Indian as a feeble current. From 20th June IC, the CGEPS was successful in predicting the subdued rainfall activity and break situation from first to third week of July. The large scale revival of rainfall during the last week

of July was well predicted from 10th July IC. The possibility of extended break like situation starting around 10th August were well predicted in advance. It is also evident in the figure that, the occurrence of large scale MISO related rainfall activity around 20th September over central India were well predicted from 3rd September IC.

5.3.2 Onset prediction

The onset of Indian summer monsoon (ISM) is generally associated with an increase in rainfall over the southern state of Kerala along with the seasonal reversal in the tropospheric temperatures, low-level winds over Arabian Sea and strong vertical wind shear over the Indian subcontinent. Although the date of ISM onset over Kerala (MOK) does not have considerable correlations with subsequent progression of ISM to northern India and the seasonal mean rainfall (Bansod et al. 1991), the timing of MOK can have significant impact on agricultural productivity. A delay in the onset of the ISM by a few weeks affects the initiation of agricultural activity while an early onset might not be utilized to its full advantage without an advanced forecast.

During 2015, ISM made its onset over Kerala on 04 June, 4 days after its normal date. Based on Joseph et al., (2015), the extended range prediction group of Indian institute of Tropical Meteorology, predicted the MOK date from 16 May initial conditions to be 29 May (Figure 5.6). The criterion makes use of the persistence in rainfall over Kerala and magnitude and depth low level Westerlies over Arabian Sea to identify the MOK date. The difference between the predicted and actual MOK date was found to be 6 days. This may be attributed to the increased rainfall over Kerala due to the pre-monsoon thundershowers, which the model predicted realistically.

5.3.3 Prediction of Ashobaa cyclone during the onset phase

The cyclonic storm Ashobaa formed over the central eastern Arabian Sea in from the with onset vortex in association with the southwest monsoon onset over Kerala. It developed into a low pressure system on 5th June and system initially moved in a north-northwesterly direction and concentrated into a depression over east central Arabian sea on 7th June. Under the favorable large scale setting, the system intensified into a cyclonic storm named "Ashobaa". It maintained the intensity till 10th June and later under the influence of high vertical wind shear, interaction with land and intrusion of dry air from western side, it weakened into a deep depression on 11th June. It further weakened into a depression and then a well marked low over the northwest Arabian coast off the coast of Oman on 12th June (Also refer section 3.1 of Chapter 3). Figure 5.7 shows the observed (pink line) and forecasted track from each ensembles members (green line) and ensemble mean (blue thick line) from 31st May IC. It is found that the extended prediction system well captured the track of the Ashobaa cyclone. At a lead time 13 days, the present ensemble prediction system captured the track of the cyclone reasonably well. It was forecasted that the cyclonic system may hit the Oman coast as a feeble low around 12th June at a lead time of 13 days. Hence the present extended range prediction shows some success for the cyclogenesis prediction at lead time of more than 10 days.

5.3.4 Pentad lead deterministic and probability prediction

Since potential predictability of dynamical prediction of daily rainfall beyond 10 days decreased below useful limit, some kind of averaging is required to extend the predictability limit. We employed pentad averaging (5 day average) to filter some of the high frequency weather noises. Then the forecast is issued for 1st pentad to 4th pentad lead over a large area. Further to add value to the deterministic forecasts, probabilities of different categories were also generated. The categories are defined by clustering the observed rainfall into above normal (AN), below normal (BN) and Near Normal (NN) using the tercile classification method. Each category has an equal climatological probability of 33.33%. By taking into account the proportion of the

model's ensemble members falling into the respective categories, corresponding probabilities for each forecast category are generated for five homogeneous zones of Indian Subcontinent as defined in Borah et al. (2014).

For brevity averaged rainfall prediction over MZI (See Borah et al. 2014) for P1 to P4 lead is shown in Figure 5.8. The top panel in each subplot shows the predicted pentad average rainfall anomaly (black bar) along with the corresponding observed anomaly (pink line). The percentage occurrence probability, in the forecast, of three categories of rainfall namely the active, break and normal is given in the lower panels of each sub plot. It is clear from the Figure 5.8 that, there was some mismatch in the phase and intensity of the observed and predicted rainfall especially in the P3 and P4 lead. Hence the generations of the forecasts, understanding its potential, its inherent inability while interpreting the raw forecast product are fundamental to the ERP system. The final dissemination of the consensus forecast to stake holders is a demanding job and should be treated as an essential component of the forecasting system. The extended range prediction of Monsoon during 2015 is an example of this successful forecast dissemination.

5.4 Forecast verification

5.4.1 Pentad lead prediction skill

Forecast verification and overall performance evaluation of the prediction system are the last but not the least component in the forecast dissemination string. This step assists the forecasters to rectify the shortcomings in the forecasting system and paves ways for its further improvement. Different skill measures have been used to evaluate the usefulness as well as the accuracy of both pentad lead deterministic and probabilistic rainfall forecast. Forecast skill of the MME from CGEPS is analyzed for pentad-averaged rainfall over 5 homogeneous regions of India. Skill in terms of the CC between the predicted and observed pentad mean rainfall series is computed up to P4 lead.

Figure 5.9 shows the CC between predicted and observed pentad-averaged rainfall over 5 homogeneous regions of India. Except for NEI, the skill of ERP is useful over other 4 homogeneous regions only up to pentad 2. At P3 lead, prediction skill over SPI and NWI shows useful skill. On the other hand, 3 homogeneous regions (MZI, CEI, NEI) was not skillful and significant even at P3 lead. It is observed that, pentad lead prediction skill at P4 lead was strangely lower even CC becomes negative except for SPI region. The negative CC values at P4 lead are mostly because predicted rainfall was in out-off of the observed anomalies as seen in Figure 5.9.

5.4.2 MISO prediction skill

Figure 5.10 shows bivariate CC and RMSE between the predicted and observed MISO indices. It is found that, the limit of useful prediction as measured by a threshold CC of 0.5 for MME during 2015 (black line) was only 17 days and this skill is found to be lower than hindcast skill (red line) by 3 days. The significant reduction of skill in the prediction of large-scale low frequency component of the SWM also hints that the extended range prediction becomes difficult when large scale intraseasonal oscillation is absent or in a weak phase. Since extended range prediction skill is closely linked to the signal associated with ISO, we have calculated the ratio of the synoptic to ISO variance and discussed in following sub sections.

5.4.3 MISO verification from selected ICs

Figure 5.11 shows the phase diagram of MISO monitoring from CGEPS and its verification from observations. The spread of forecast from ensembles is also given in green shades. The large scale reduction in rainfall

over Central Indian region during the first half of July was well predicted from 20th June IC. The MISO monitoring also shows clear absence of reduced rainfall activity over Central Indian region during the period and MISO amplitude over North Indian region was slightly underestimated by the model at 20 days lead. The revival of rainfall during the end of the July was also predicted from 10th July IC. However, it was found from the observation that the enhanced phase of convection propagated fast over Central Indian region and reached foothills by the end of July. The predicted MISO lags behind the observed MISO. The CGEPS well predicted the subdued rainfall activity during August and early September from 25th July and 4th August IC. Both the predicted amplitude and phase propagation well matched the observations during this time interval. From 24th August IC, the CGEPS was not successful in predicting the large-scale revival of rainfall activity over Central Indian region in the third week of September. However, from 3rd September IC, the CGEPS derived MISO has predicted the large scale revival of rainfall activity in the third week of September over Central Indian region. Hence the enhanced and suppressed phases of rainfall activity associated with large scale MISO activity were well monitored using CGEPS system except few unsynchronized propagation phase from predictions as compared to observations

5.4.4 Role of Intraseasonal Oscillation Signal on the lower ERP skill during 2015

Figure 5.12 shows that during 2015 SWM season, the ratio of synoptic to ISO variance becomes very large as compared to their climatological ratio. This means that during 2015 monsoon season, most of the rains bearing systems were dominated with synoptic disturbances with short duration. When these systems are embedded in the background of weak ISO forcing, most of the predictions beyond 10 days were out-off phase with observed rainfall. The typical lifetime and predictability of individual synoptic systems are less than 10 days and are difficult to predict at lead time of more than 10 days. This may be one of the reasons for the lower ERP skill during 2015 SWM season.

5.5 Summary

This chapter assesses the skill of ERP issued by IITM on real-time during 2015 SWM season. The prediction and monitoring of Monsoon Intraseasonal Oscillation on extended range time scale have been carried out using the newly implemented MME based on CFS called CGEPS. The performance of the CGEPS is analyzed for pentad lead predictions over different homogeneous regions of India. Over most of the homogeneous regions, the CGEPS shows useful skill only up to P2 lead except for SPI. The predicted and observed large-scale low frequency component of the MISO is compared for different initial conditions. The CGEPS is able to predict the large scale enhanced and suppressed phases of convection associated with MISO reasonably well. The bivariate correlations and RMSE between the observed and predicted MISO shows that the useful skill is reduced by 3 days compared to the hindcast skill. Further analysis suggests that synoptic scale variance during 2015 SWM season was considerably higher than that of ISO variance. This reduced skill and role of ISO advocates the challenges of ERP in the absence of large scale ISO signal.

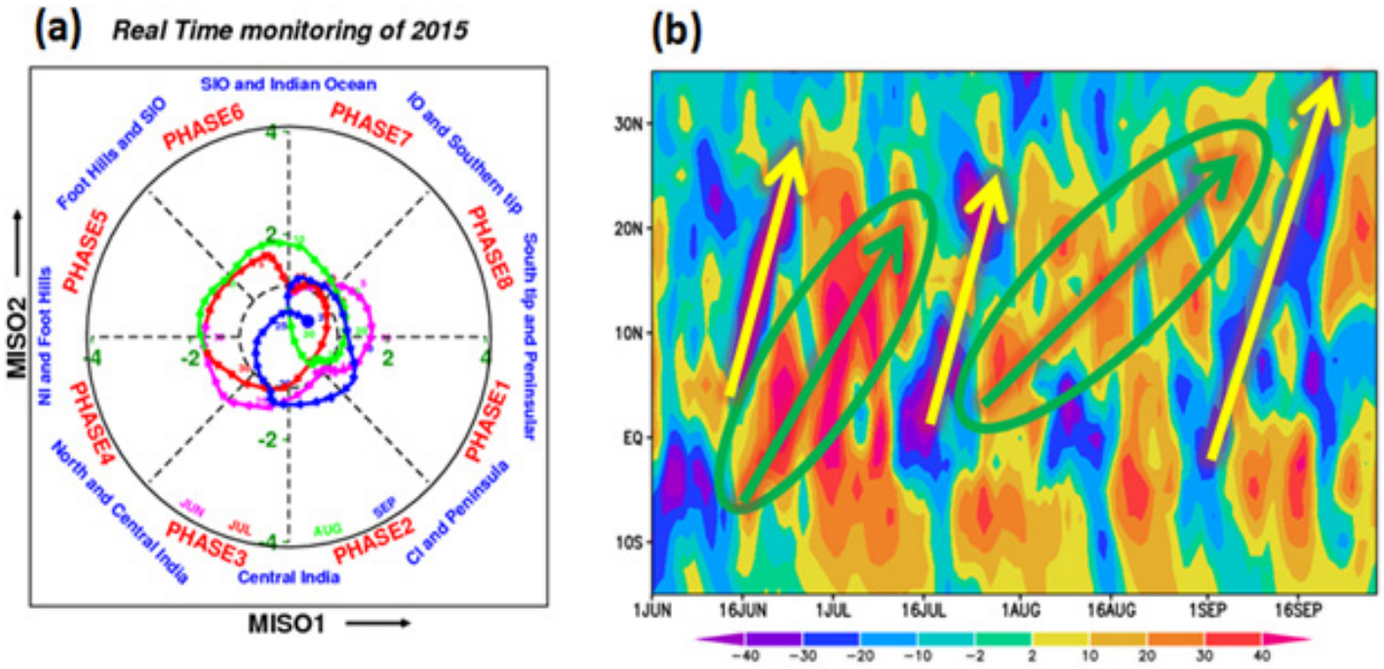

Figure 5.1 (a) Phase diagram of MISO1 and MISO2 showing northward propagation, (b) Hovemoller of OLR (Wm^{-2}) anomalies averaged over Indian Longitudes

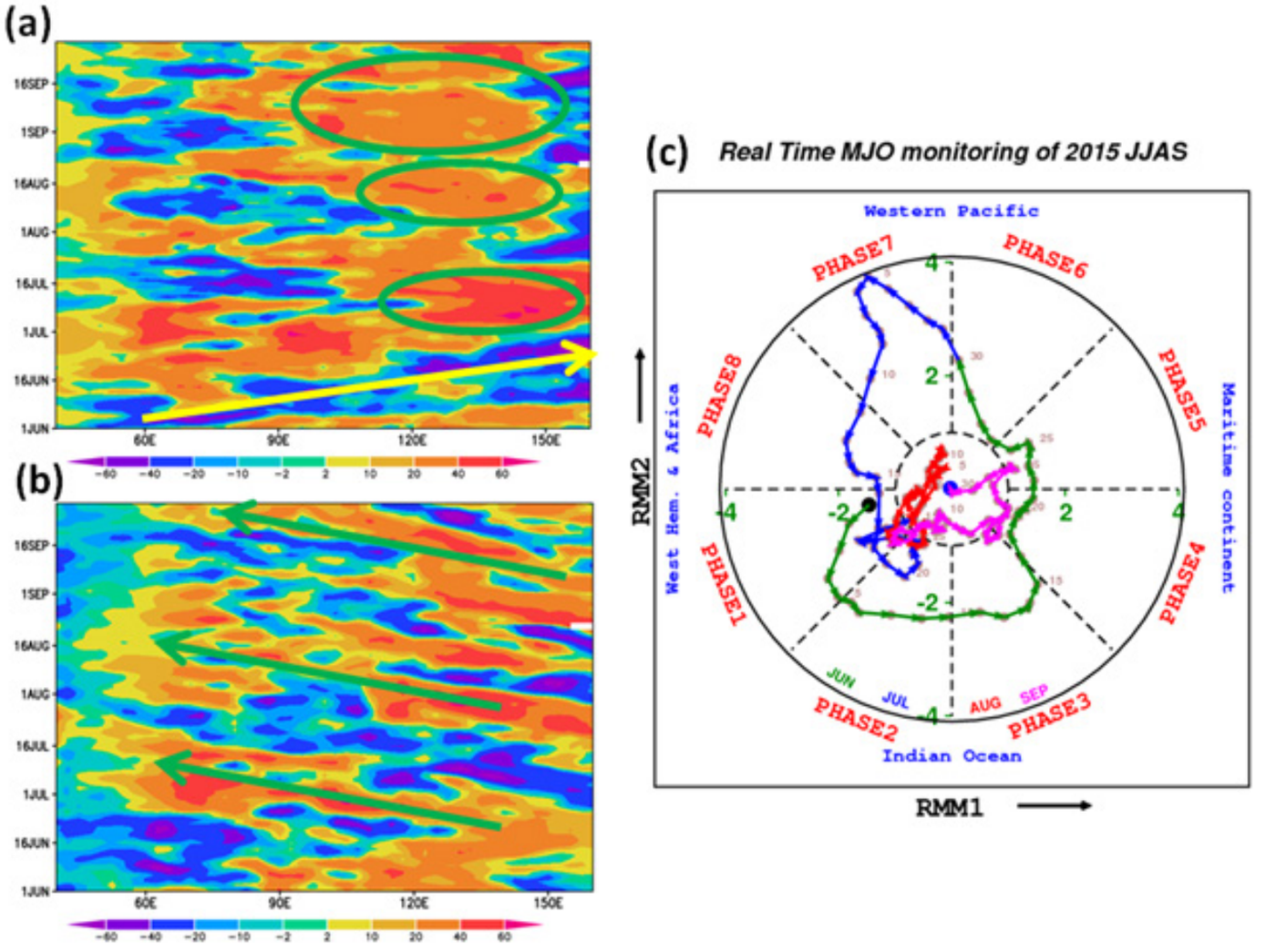

Figure 5.2 (a) Hovemoller of OLR (Wm^{-2}) anomalies averaged over 5°S-5°N and (b) over 10-25°N . (c) Phase diagram of RMM1 and RMM2 showing MJO propagation

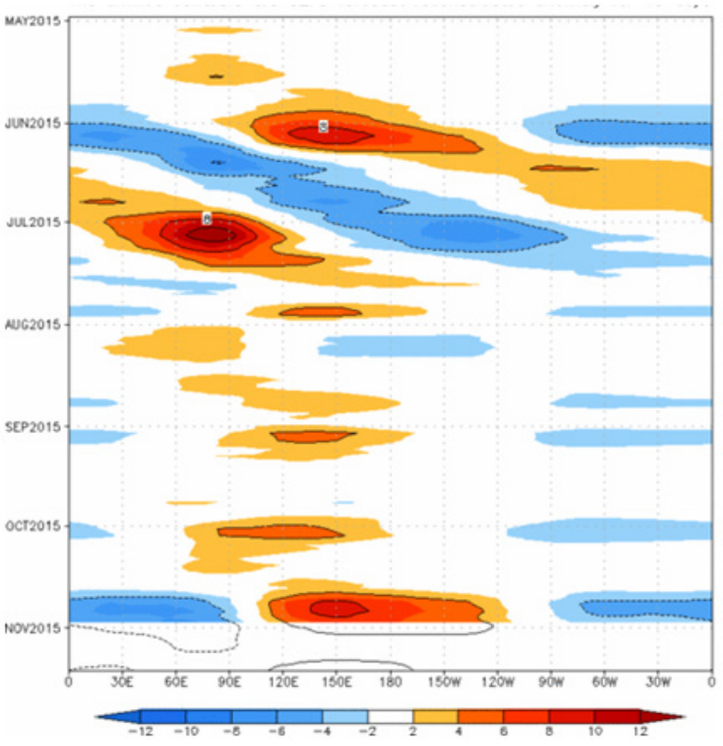

Figure 5.3: The reconstructed anomaly fields of velocity potential at 200hPa associated with MJO using RMM1 and RMM2 averaged over 7.5S-7.5N (Source: CPC, NOAA)

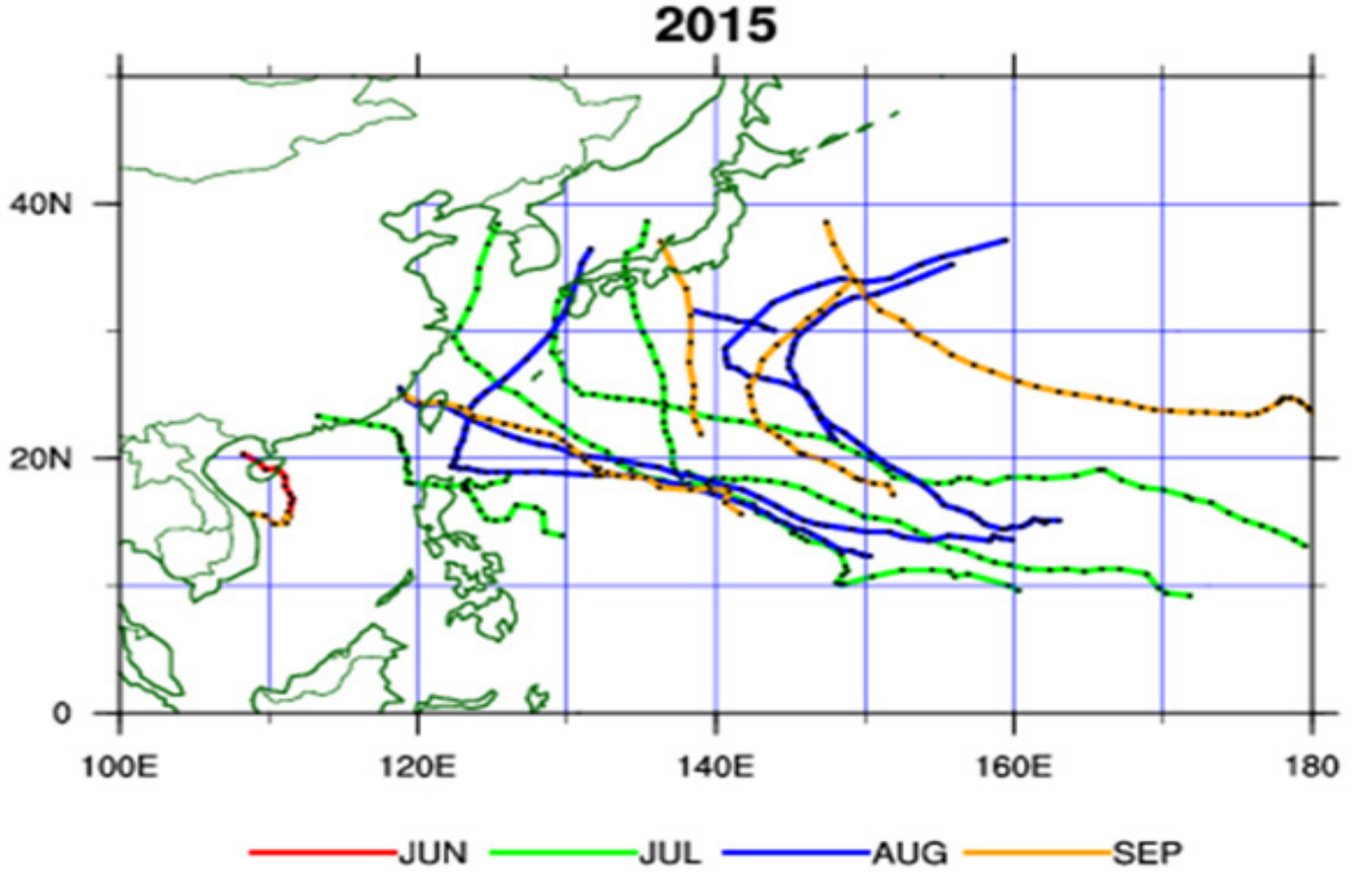

Figure 5.4 Distribution of storm tracks over Western Pacific in the month of June (red), July (green), August (blue) and September (orange).

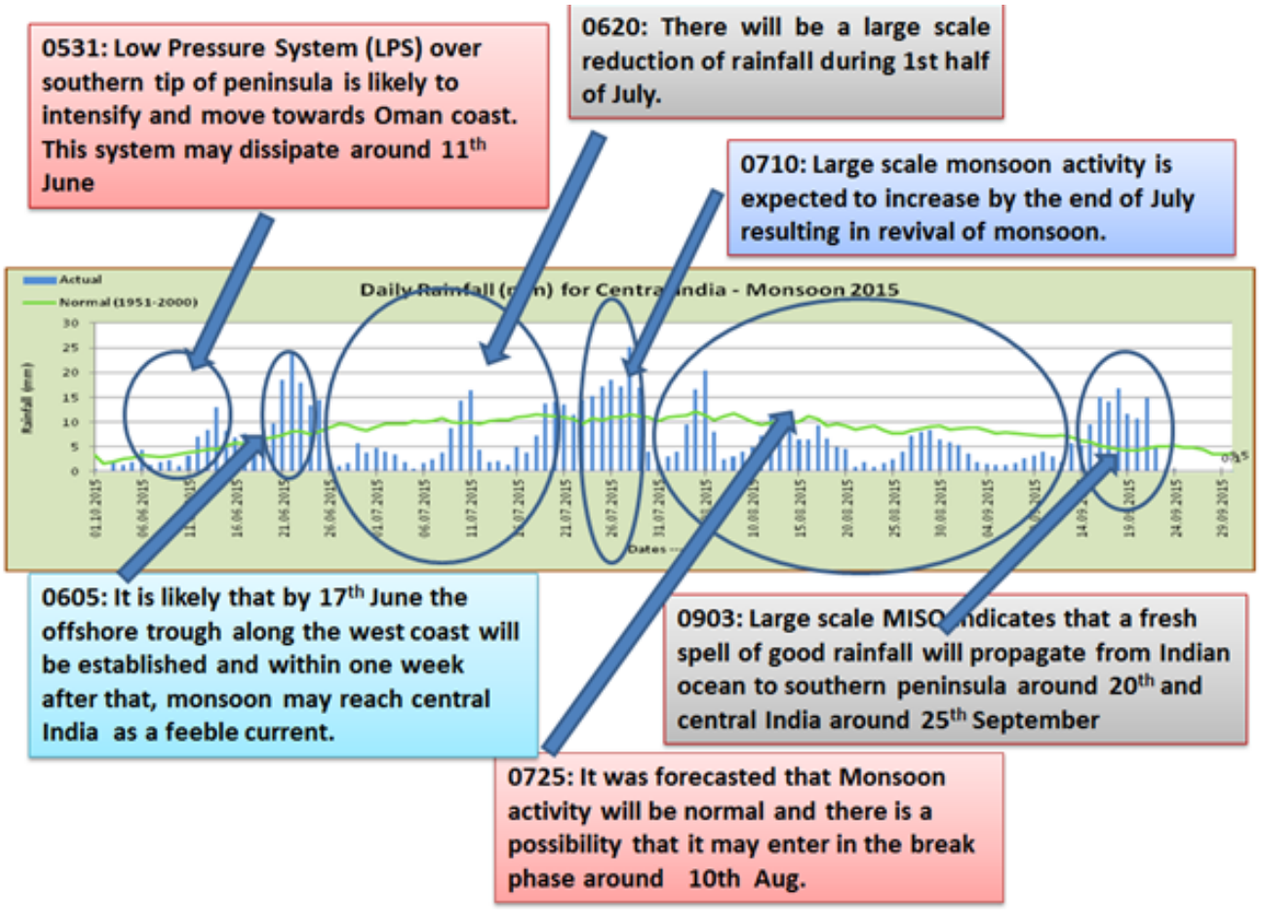

Figure 5.5 Time series of area averaged rainfall over Central Indian region (blue bars) and along with normal rainfall for base period 1951-2000 (green line). Highlights of real-time forecast issued from selected Initial Conditions are also shown

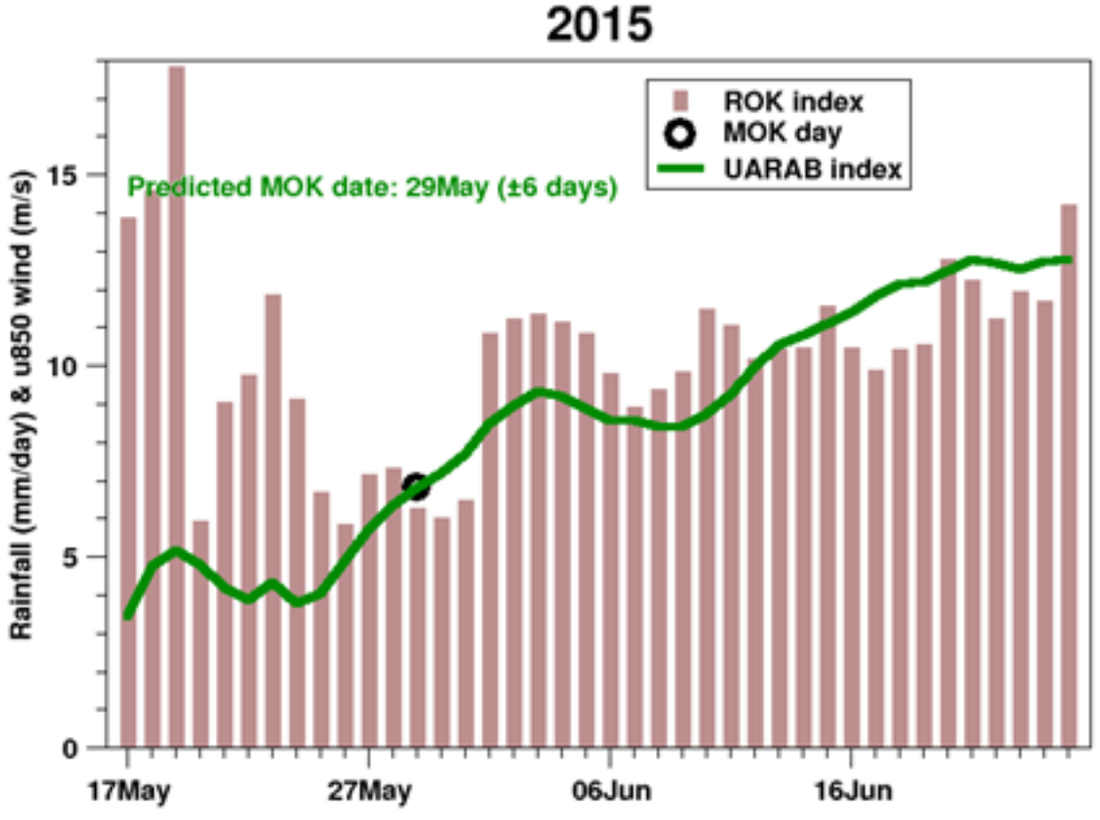

Figure 5.6 The evolution of rainfall and low level wind indices used for predicting the MOK date.

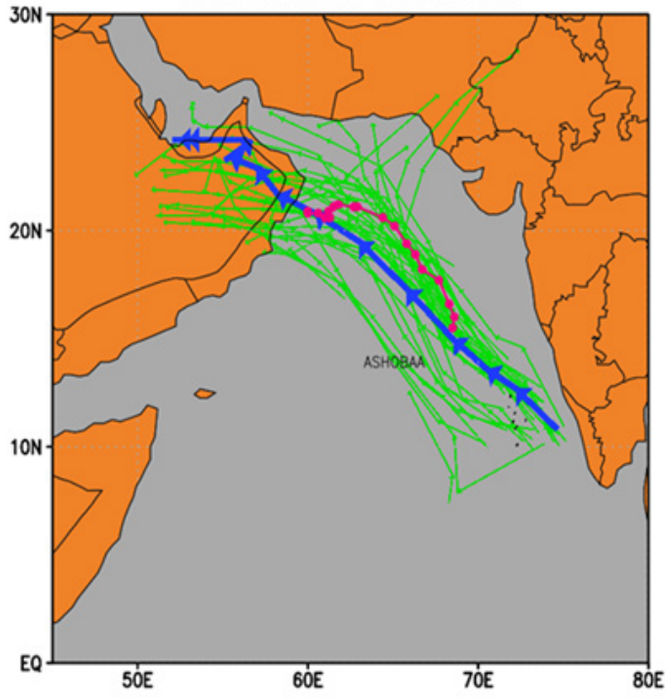

Figure 5.7 Forecasted track of Ashobaa cyclone from the ensembles (green line), ensemble mean (Blue solid line) and the observed best track (pink) is also given.

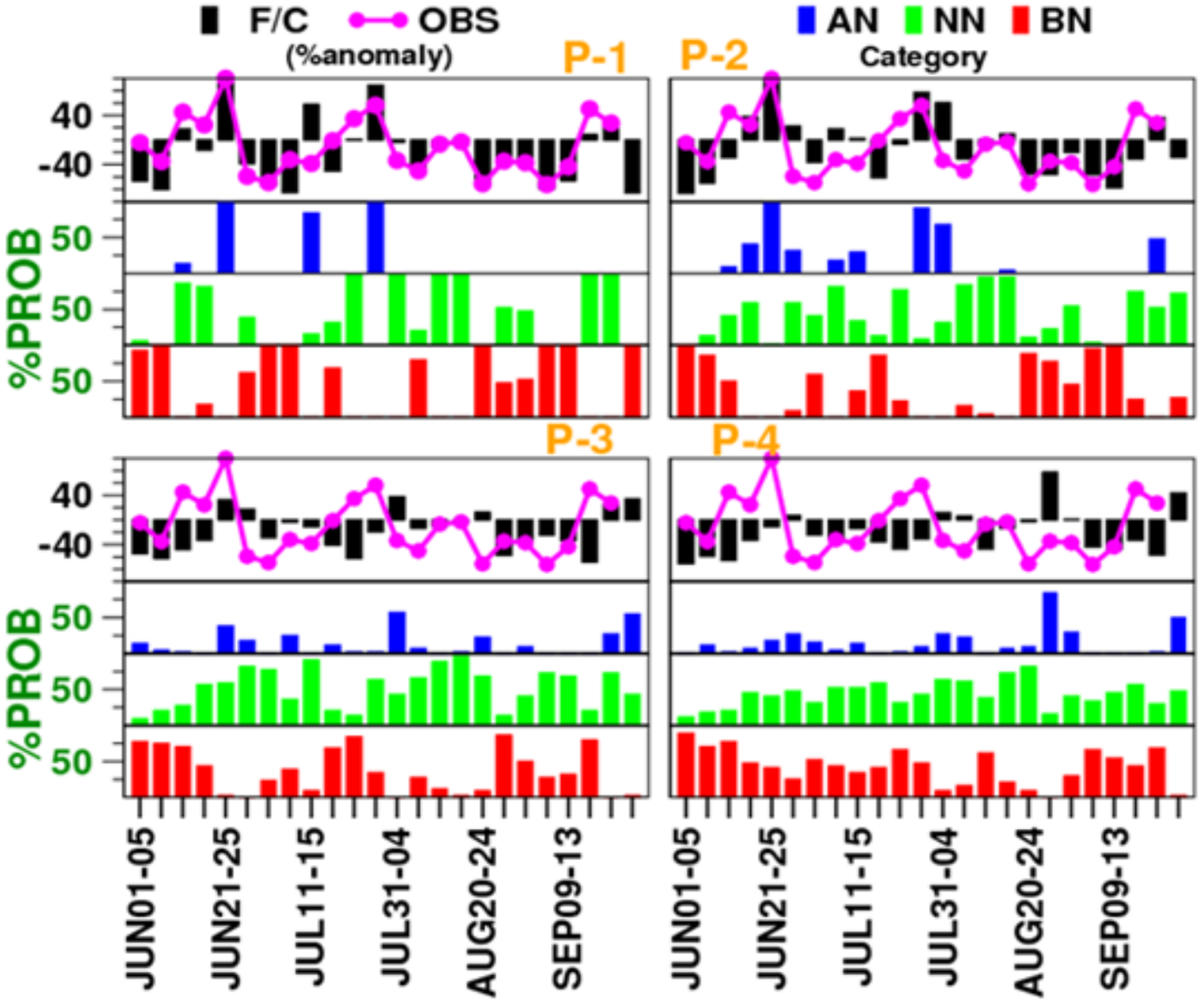

Figure 5.8 Area averaged deterministic and probability prediction over MZI region

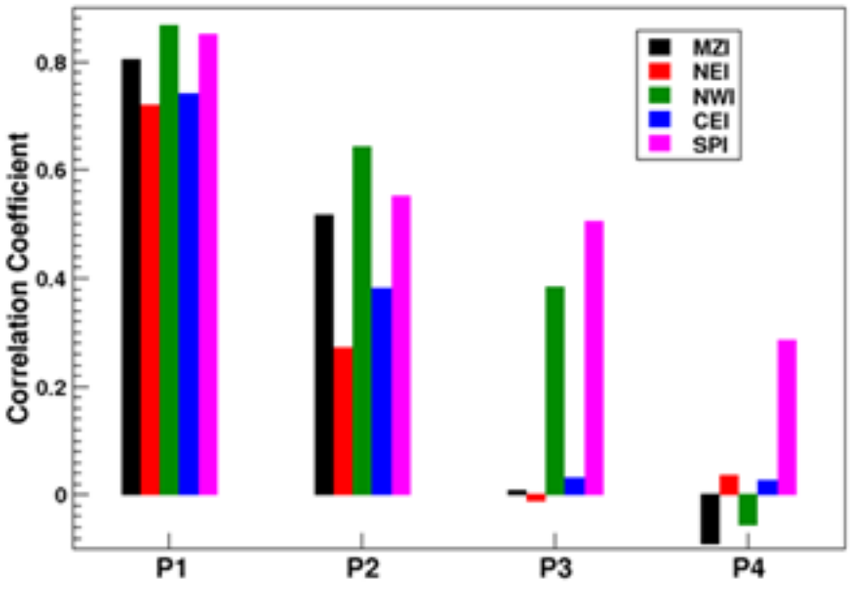

Figure 5.9 Correlation coefficient between the predicted and observed rainfall anomaly over homogeneous regions of India

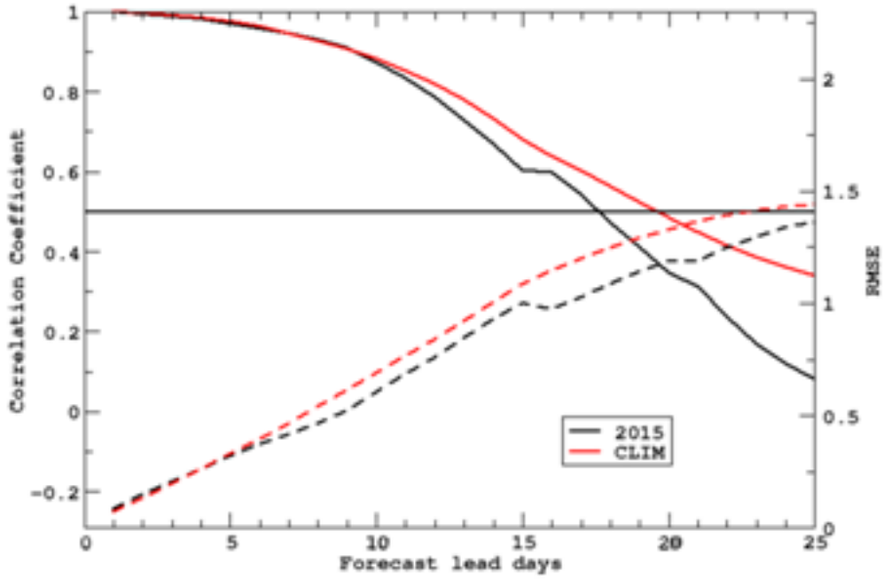

Figure 5.10 Bivariate correlation and RMSE of predicted and observed MISO indices during 2015.

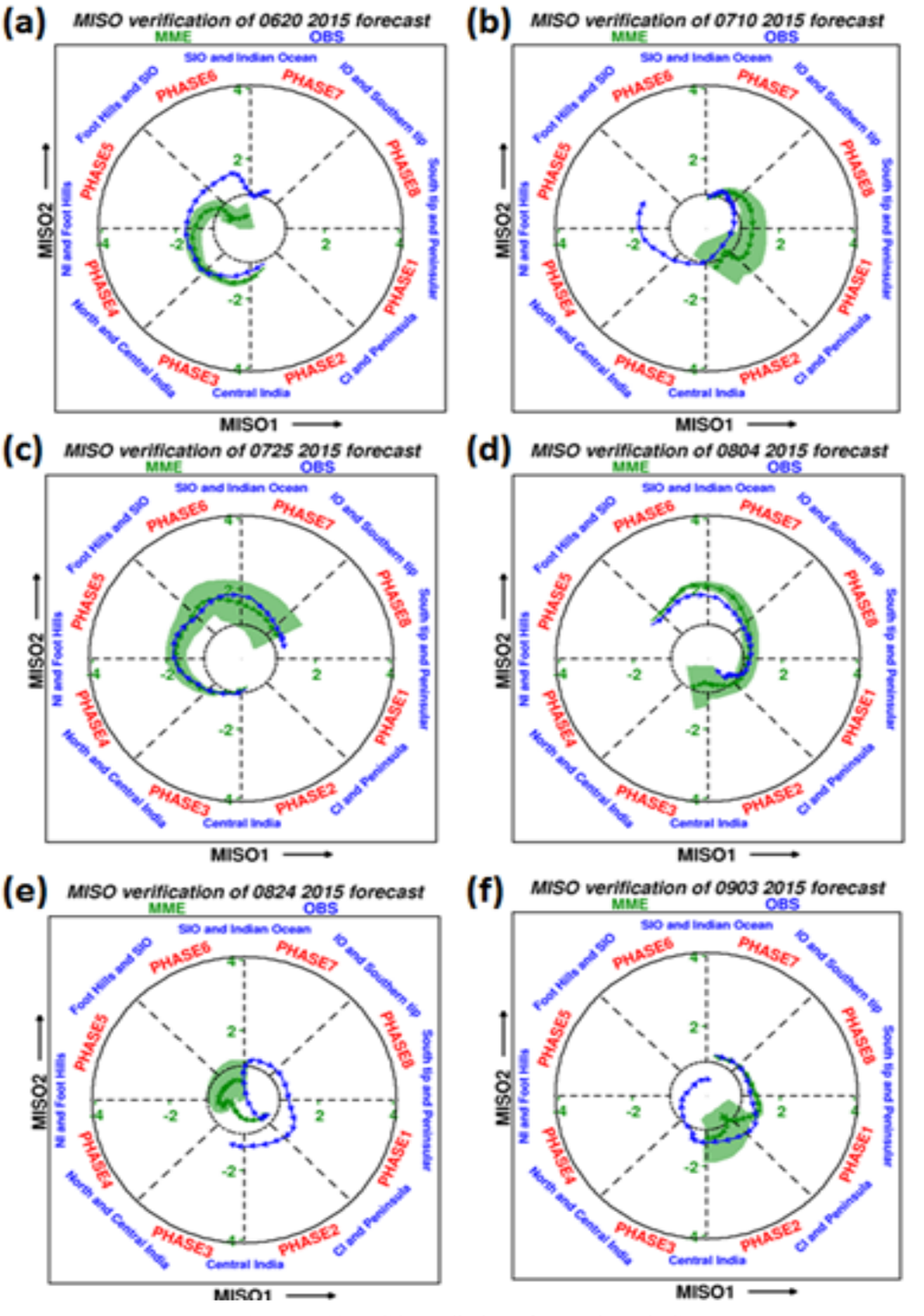

Figure 5.11 MISO predictions from selected ICs

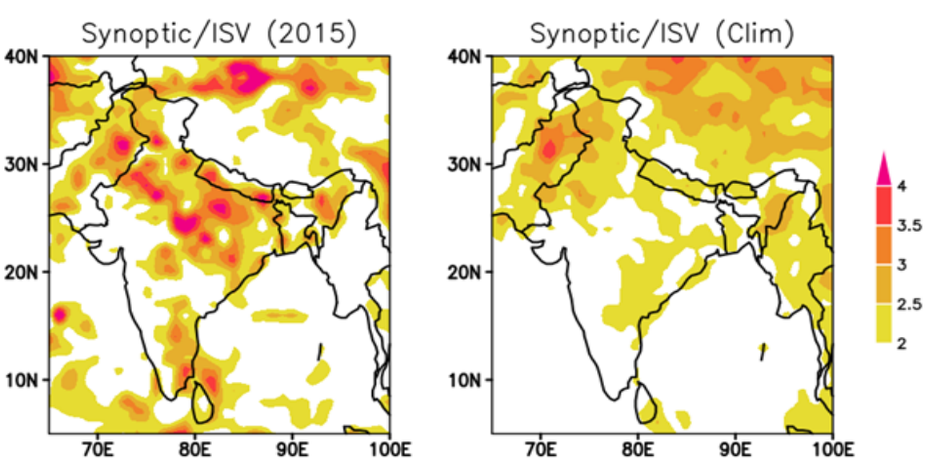

Figure 5.12 Ratio of the synoptic to ISO variance in the observed rainfall during 2015 and from climatology

Chapter 6

Long Range Forecast of the Indian Summer Monsoon using Climate Forecast System

Ankur Srivastava, Maheswar Pradhan, Gibies George, Ashish Dhakate, Kiran Salunke, and Suryachandra A. Rao

Since 2011, Indian Institute of Tropical Meteorology (IITM) has started providing experimental real-time seasonal forecasts of the Indian Summer Monsoon, as well as other major climate phenomenon such as El-Niño and Indian Ocean dipole. These forecasts are based on the high-resolution version of state-of-the-art Climate Forecast System Version 2 (CFSv2), which provides an atmospheric resolution of about 38 km in the horizontal.

6.1 The Climate Model

The National Centers for Environmental Prediction (NCEP) CFSv2 is an improved version of the NCEP CFSv1 (Saha et al., 2006) with advances in model resolution and model physics (Saha et al., 2014). This model has been used for the seasonal and extended range forecast of the Indian Summer Monsoon Rainfall (ISMR) since 2011 at IITM. The CFSv2 is a fully coupled atmosphere-land-ocean model with a spectral model Global Forecast System (GFS) as the atmospheric counterpart (Moorthi et al., 2001) and Geophysical Fluid Dynamics Laboratory (GFDL) Modular Ocean Model version 4p0d (MOM4) as the ocean model (Griffies et al., 2004). The horizontal resolution of the ocean component (MOM4) is 0.25° between 10°S to 10°N latitude band and gradually increasing to 0.5° poleward of 30°S and 30°N. In addition to the atmosphere and ocean component, the CFSv2 also employs a four layer NOAH land surface model (Ek et al., 2003) and a three layers (one layer of snow and two layers of sea ice) interactive sea ice model (Winton, 2000). The atmospheric component of CFSv2 has 64 sigma-pressure hybrid levels in vertical and the ocean component has 40 vertical layers. In CFSv2, the ocean and atmosphere are coupled without flux correction. The convective parameterization scheme used in the atmospheric component of CFSv2 is based on Arakawa-Schubert scheme, with orographic gravity wave drag and momentum mixing. The atmospheric counterpart of the CFSv2, which is implemented at a spectral resolution of T382 (horizontal resolution of approximately 38km) has been used for generating seasonal forecasts of the ISMR. This is a worthwhile improvement over the original version, which has a resolution of about 100 km.

6.2 Initialization Strategy

The retrospective ensemble prediction (hindcast) runs of the CFSv2 have been performed for a period of 28 years (1981-2008). The model is initialized each calendar month using 10-12 different initial conditions. The atmosphere, land and ocean initial conditions for these runs are obtained from the NCEP Climate Forecast System Reanalysis (CFSR; Saha et al., 2010). The current status of the hindcast runs is mentioned in Table 6.1. The forecasts are generated using an ensemble of minimum 40 members, which are initialized every calendar month using atmospheric initial conditions provided by ESSO-NCMRWF and the oceanic initial conditions provided by ESSO-INCOIS or ESSO-IITM. The model climatology is generated using 28-year hindcast runs which is ensemble mean of 10-12 members (depending on the calendar month used for initialization).

For generating the 2015 forecast, 40 ensemble members corresponding to 40 different initial conditions of the same month were used. The forecast with February IC was done initially using ICs from IITM-GODAS. These ICs could not properly capture the SSTs in these regions and in turn had a very weak El Niño. Thus, we decided to use INCOIS-GODAS ICs, which provided a more realistic estimate of the ocean conditions in the

tropical Pacific. However, the forecast generated using INCOIS February ICs have 20 ensemble members only. So the ensemble considered (for February IC) is a combination of members based both on IITM-GODAS and INCOIS-GODAS. Several experiments were conducted to examine the reasons behind weaker El Niño in IITM-GODAS. The surface salinity restoration to climatology in IITM-GODAS was found to be responsible for the weaker El Niño representation. However without the surface restoration, IITM-GODAS captured the El Niño intensity comparable to the observation (Chapter 2, Figure 2.4).

6.3 Model Skill and performance

The skill scores of the model for the forecasting of seasonal rainfall over the country as a whole at two different lead periods ('3' to '1' months with February and April Initial conditions, respectively) are given in the Table 6.2. The forecasts at these two lead times are found to have better prediction skill which is in line with the recent study by Chattopadhyay et al. (2015), where they have shown that the prediction skill of the SWM rainfall in CFSv2 is better when the model is initialized with ICs from February month. The performance of the model for the period 1981-2008 is given in the Figure 6.1. It is interesting to note that the model could forecast the deficient monsoon years in the past with very good skill. The experimental forecasts with February & April ICs are shared with IMD for operational use. The seasonal forecasts from CFS for the 2015 SWM rainfall over the country as a whole are also given in the table. The spatial maps of the observed and model forecasted anomalies of seasonal mean rainfall over India are provided in Figure 6.2 and the forecast spread of all India land rainfall is shown in Figure 6.3. As it turned out, 2015 SWM season was deficient and the country as a whole received 86% (departure from the long term mean) rainfall. Observed and forecasted rainfall departures are closer with April IC but the time evolution is better with February IC.

The spatial maps of the observed & forecasted global SST anomalies are shown in Figure 6.4. Also, the monthly evolution of the observed & forecasted Niño 3.4 index is shown in Figure 6.5. The year, 2015 is recorded as a strong El-Niño year with SST anomalies in the Niño 3.4 region hovering around 2°C. The model with February IC was able to forecast a moderately strong El-Niño; however, the magnitude was slightly under-predicted (Figure 6.5). But the forecast with April ICs has a very good correspondence with the observed SST anomalies in the tropical Pacific & the Niño 3.4 index is very close to observations. The model with both the ICs predicted neutral dipole mode conditions (figure not shown), and as it turns out, no significant dipole mode conditions have been observed till date.

It is interesting to note that forecasts issued by other leading international centers (e.g., NCEP of USA and ECMWF of Europe) could not predict below normal/deficient monsoon signal even with zero lead time even though they could simulate strong El Niño. NCEP forecast, which uses the original version of CFSv2, did not show any signal of possible below normal monsoon over India. Same was the case with European Centre for Medium-Range Weather Forecasts (ECMWF). The success story of the forecasts issued by IITM can mainly be attributed to the high-resolution coupled model implemented at IITM, which is one of its kind, and realistic forecast of El-Niño conditions in the tropical Pacific Ocean.

Table 6.1 The initialization strategy for each calendar month for the reforecast (hindcast) runs.

MONTH	IC Days	UTC	ENSEMBLES
JAN	06,11,16,21,26	00 & 12 UTC	10
FEB	5,10,15,20,25	00 & 12 UTC	10
MAR	2,7,12,17,22,27	00 UTC	06
APR	01,06,11,16,21,26	00 & 12 UTC	12
MAY	01,06,11,16,21,26, 31	00 & 12 UTC	14
JUNE	05,10,15,20,25,30	00 & 12 UTC	12
JULY	05,10,15,20,25,30	00 & 12 UTC	12
AUG	04,09,14,19,24,29	00 & 12 UTC	12
SEP	05,10,15,20,25,30	00 & 12 UTC	12
OCT	03,08,13,18,23,28	00 & 12 UTC	12

Table 6.2 The skill scores & corrected RMSEs of All India land rainfall as simulated by CFSv2T382 with February and April initial conditions and the model forecasts of the seasonal (JJAS) mean rainfall for 2015.

Initial conditions (IC) of	JJAS		Forecast for 2015 (% of LPMA)
	C.C (1981-2008)	Corrected RMSE (% of LPMA) (1981-2008)	
February	~ 0.55	7.4%	91%
April	~ 0.39	8.3%	86%

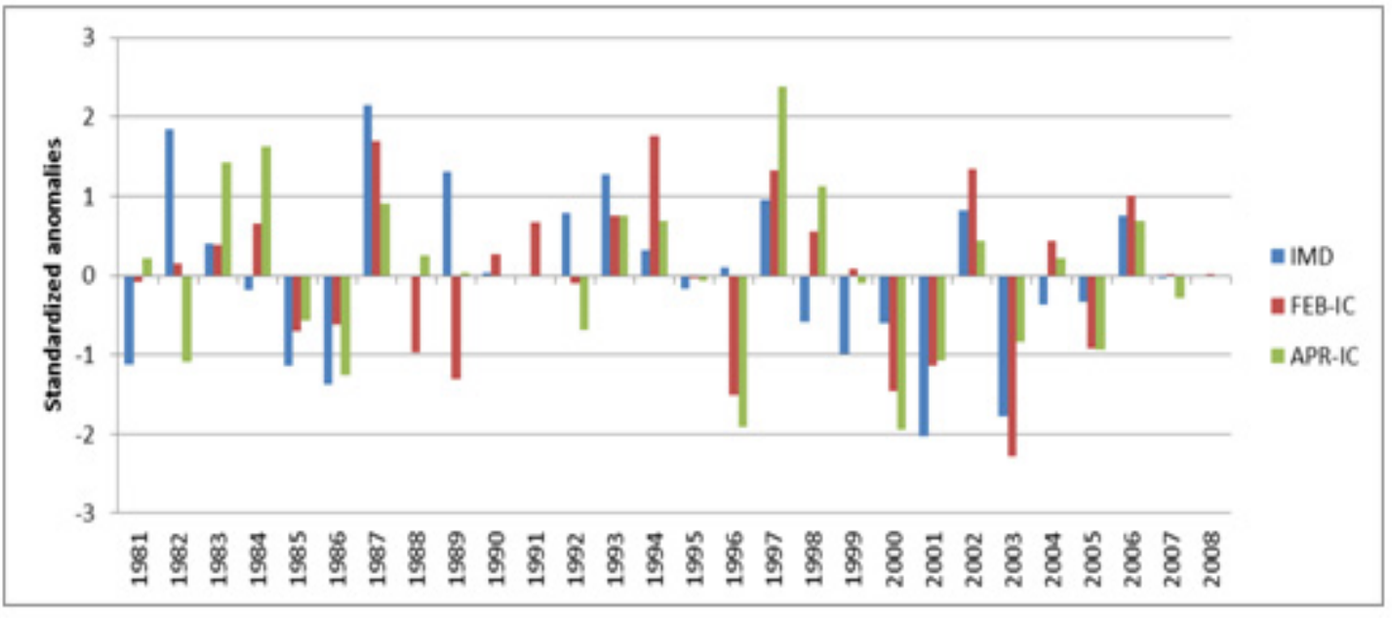

Figure 6.1 Inter-annual variability of the standardized all India summer (JJAS) monsoon rainfall anomalies in T382 reforecast runs along with observations for February & April initial conditions. The observation data is provided by IMD, Pune.

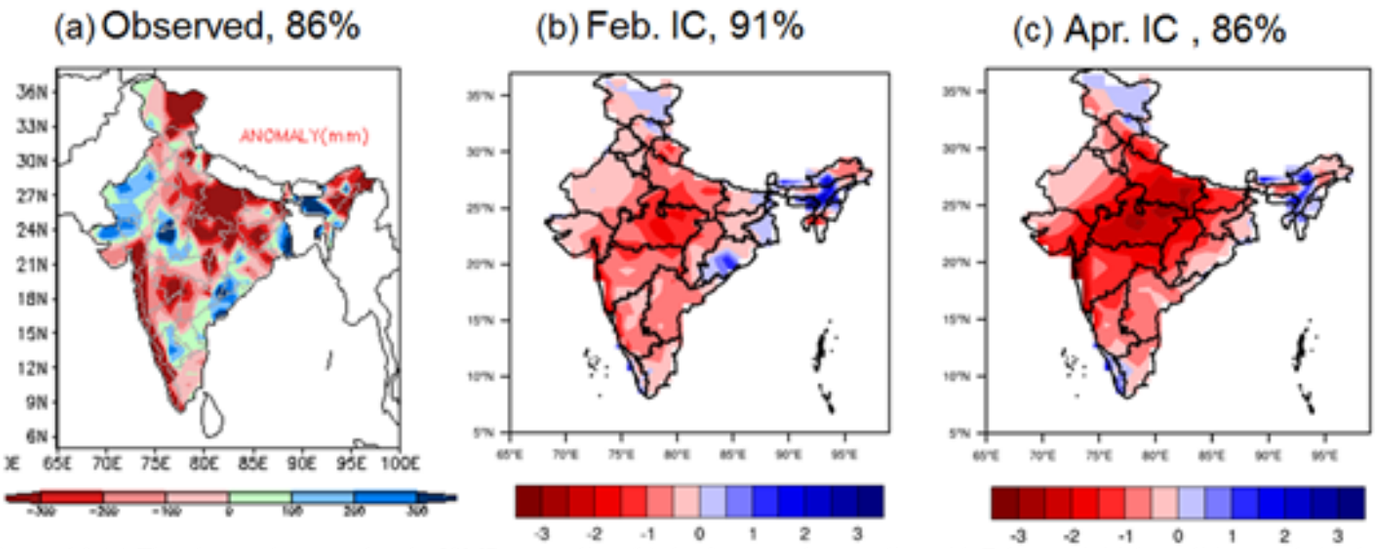

Figure 6.2 (a) The observed accumulated AISMR anomalies, (b) the forecasted anomalies with February initial conditions and, (c) the forecasted anomalies with April initial conditions for the year 2015. The departures from long term climatology are gives as percentages. The observation figure is provided by IMD, Pune.

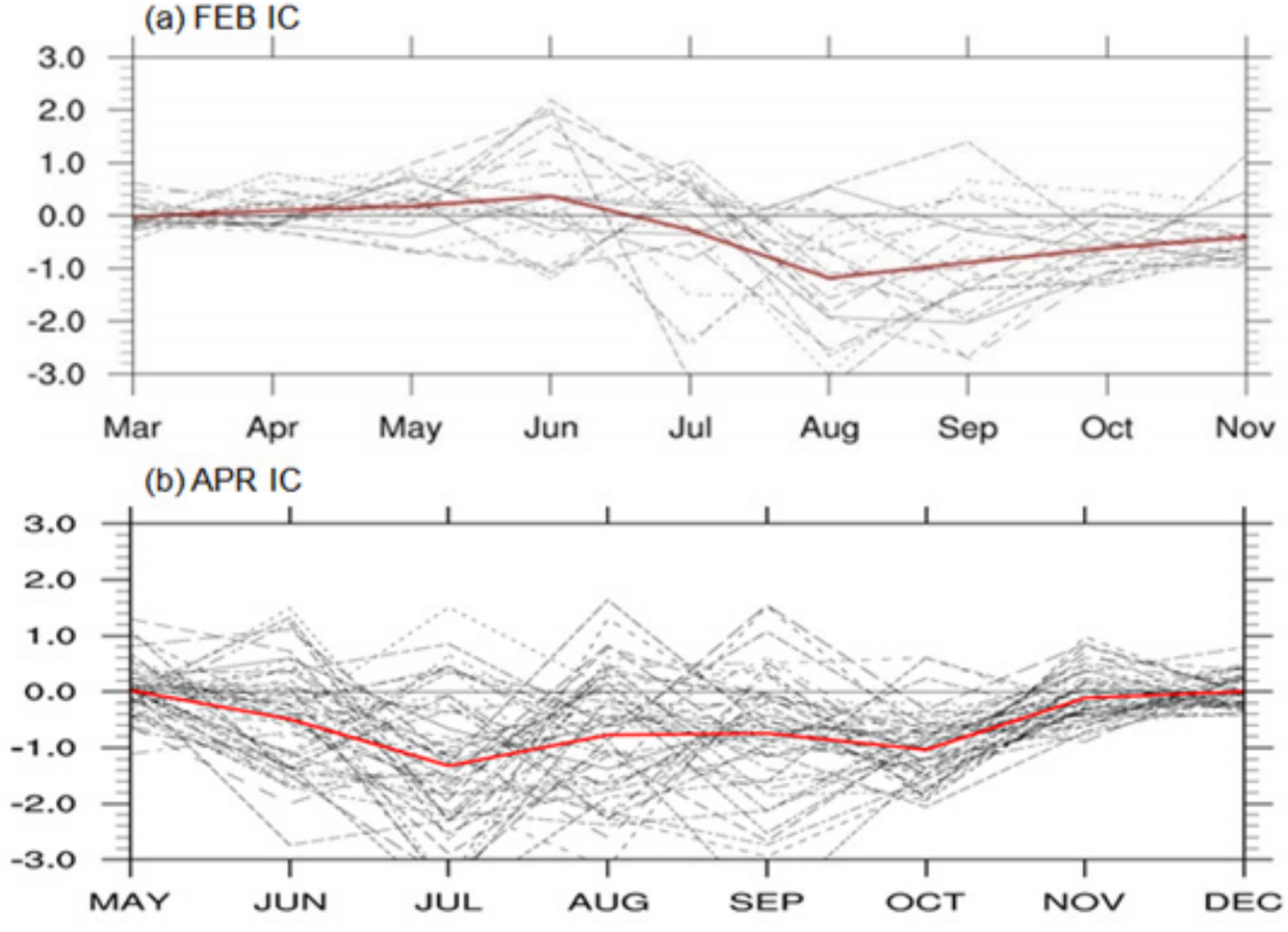

Figure 6.3 The forecast spread of all India land rainfall anomalies for 2015 with (a) February IC and, (b) April IC. The red line is the ensemble mean and the black dotted lines are the individual ensemble members.

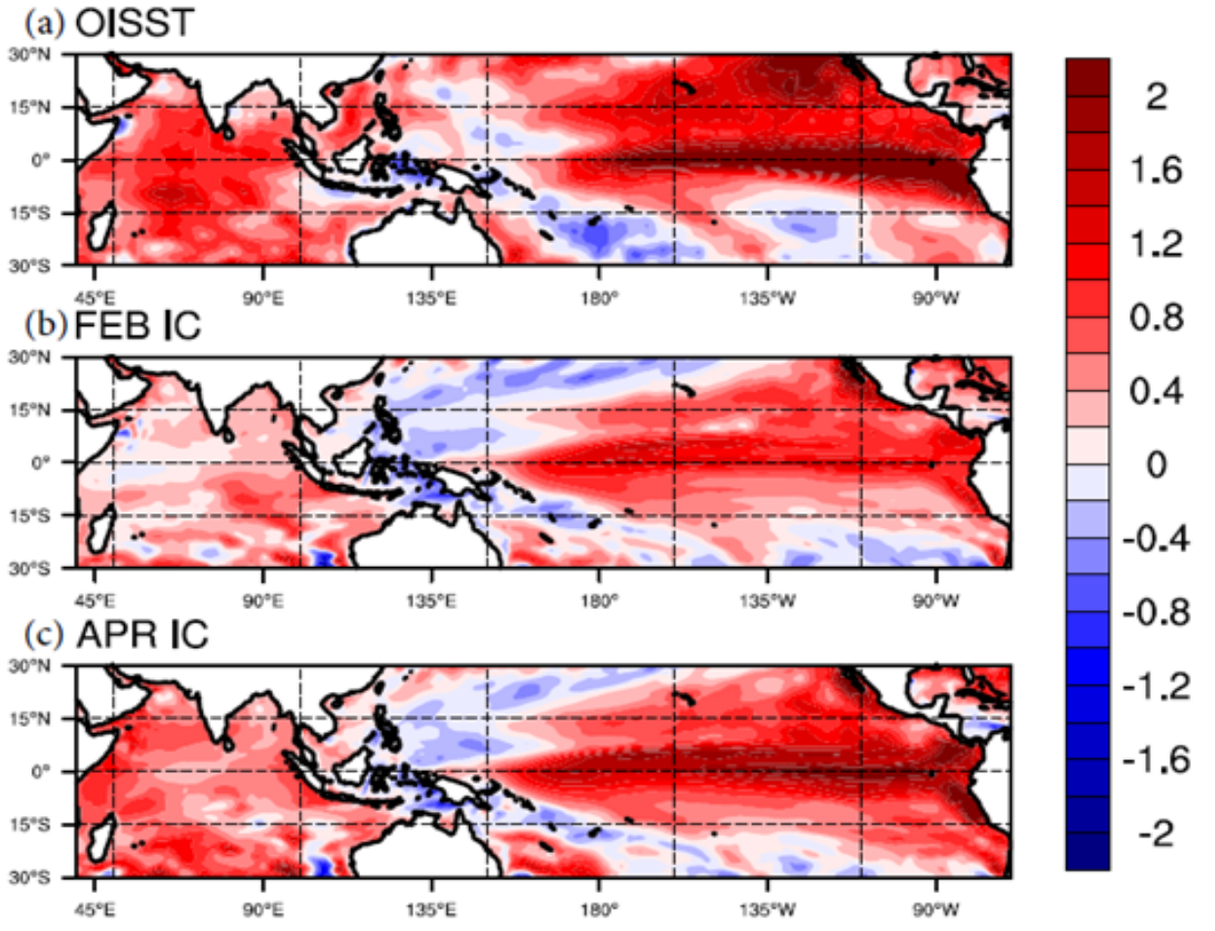

Figure 6.4 The seasonal (JJAS) mean SST anomalies (°C) for the year 2015 (a) in observations; (b) with February initial conditions & (c) with April initial conditions. Observational data is the NOAA OISSTv2 data provided by the NOAA/OAR/ESRL PSD, Boulder, Colorado, USA, from their web site at http://www.esrl.noaa.gov/psd/.

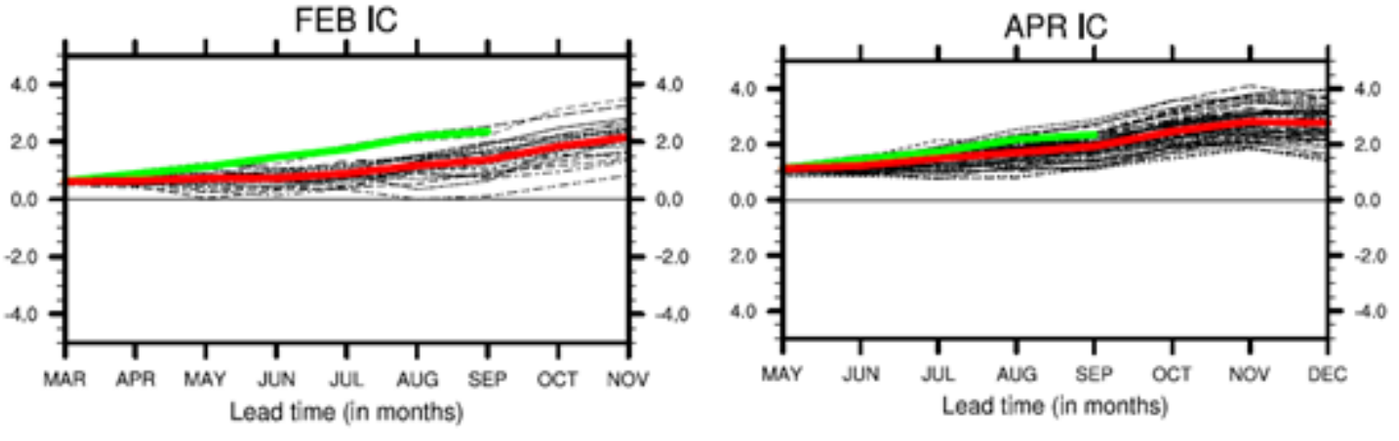

Figure 6.5 The monthly evolution of the Niño 3.4 index as forecasted with February and April initial conditions (solid red line) and the forecast spread (black lines). The observed Niño 3.4 index calculated from OISST is shown as the green line.

Summary

The deficient rainfall during the 2015 SWM season suggested a strong influence of evolving El Niño, particularly during the second half of July. This is consistent with the strengthening of El Niño signal in the tropical Pacific and meridional SST gradient in the Indian Ocean during the second half of the SWM. However, the 16% excess rainfall during June was interesting against the forecast of El Niño related deficient monsoon and the prevailing El Niño conditions. Interestingly, the regional synoptic scale convective activities were more dominant over the Arabian Sea as compared to that of BoB during this year. The modulation of summer monsoon synoptic activities (northward recurving systems), through anomalous regional and remote forcings, seems to be conducive for large-scale convection asymmetry, resulting to skewed rainfall variation, over the Indo-Pacific region. The dominance of frequent tropospheric cyclonic circulations of short duration with shorter track, in the background of a ENSO-related weaker SWM flow, seems to be unfavorable for the evolution of large-scale organized convection. The localized extreme rainfall events, evolving from dominant meso-scale convective circulations embedded in the synoptic and sub-synoptic systems are the unique characteristics of the 2015 SWM e.g. 4th August 2015 event close to Khandwa Madhya Pradesh. The anomalous Walker cell, with a descending branch over the western end of Pacific extending to the Indian subcontinent and ascending branch over the eastern to central Pacific, confirms the footprints of canonical El Niño episode during 2015 SWM. The alterations in the meridional and zonal propagation of convection over Indo-Pacific region confirm the influence of typical El Niño signal. Also contrasting feature of dominance of faster mode of variability during deficit summer monsoon of 2015 is intriguing. The 2015 El Niño evolved very similar to a canonical El Niño such as 1982 and 1997. The subsurface anomalies displayed the dominance of typical recharge discharge mechanism during 2015. Indian Ocean was anomalously warm throughout the summer monsoon season.

The prediction and monitoring of Monsoon intra-seasonal Oscillation on extended range time scale have been carried out using the newly implemented MME based on CFS called CGEPS. The CGEPS is able to predict the large scale enhanced and suppressed phases of convection associated with MISO reasonably well, however the skill score is less compared to the hindcast skill. Further analysis suggests that synoptic scale variance during 2015 SWM season was considerably higher than that of ISO variance which might be responsible for have reduced skill.

It is interesting to note that forecasts issued by other leading centres (e.g., NCEP of USA and ECMWF of Europe) of the world could not predict below normal/deficient monsoon signal even with zero lead time. NCEP forecast, which uses the original version of CFSv2, did not show any signal of possible below normal monsoon over India. Same was the case with European Centre for Medium-Range Weather Forecasts (ECMWF). The success story of the forecasts issued by IITM can mainly be attributed to the high resolution coupled model implemented at IITM, which is one of its kind, and realistic forecast of El-Niño conditions in the tropical Pacific Ocean.

Acknowledgements

At the outset MM and CG wish to express their deep sense of gratitude to Dr. M. Rajeevan, Director, IITM, for his keen interest, motivation, and guidance for successfully conducting the monsoon discussions during boreal summer 2015 as well as for the documentation of the intriguing research results in the form of a scientific report. We also greatly acknowledge the constant support received from the group/program managers, especially Drs. R. Krishnan, A. K. Sahai, Suryachandra Rao, P. Mukhopadhyay, Thara Prabhakaran, G. Pandithurai, and others.

We feel indebted to Prof. (Mrs.) S. Gadgil and Prof. Raghu Murtugudde for their keen interest, encouragement, and guidance in almost every session of the monsoon discussions. The suggestions from Drs. D. S. Pai, A. K. Srivastava, B. P. Jadhav, Sunitha Devi, D. R. Pattnaik, and A. K. Mitra are also greatly acknowledged. We are thankful to Dr. John McGregor for his fruitful suggestions in improving the report. The editors greatly acknowledge the reviewers namely Dr. Terray Pascal and Dr. R. H. Kripalani for providing critical comments/suggestions in improving the readability of this research report. It is also worth mentioning that both the reviewers have interacted closely with the speakers during monsoon discussions.

We express our sincere regards to Mrs. Preethi Bhaskar, Dr. Manish K. Joshi, Dr. Hamza Varikoden, Dr. K. P. Sooraj, and Mr. Bhupendra Bahadur Singh for their constant support throughout the preparation of this research report. We sincerely thank Mrs. Shompa Das, Shri. Abhay S.D. Rajput, Shri. V. Sasane, and Mrs. V. V. Sapre of LIP division for their constant support. We also thank Mr. Harish J. Borse, ICMPO for his valuable help in designing and formatting this report.

The extended range forecasts were issued real-time in close collaboration with ESSO and India Meteorological Department (IMD). The forecast dissemination is prepared by incorporating the inputs from IMD. Thanks are also due to NCEP, USA for providing the initial condition for model integration. Reanalyses datasets from NCEP, MERRA, NCMRWF, and Hadley Centre EN4 are also acknowledged. Some of the sight specific data presented in this report is part of the efforts of PDTC program (CAIPEEX team, HACPL team, Lightning location network group) and Radar team.

We thank one and all the participants of 2015 monsoon discussions and hope that their valuable contributions for stock of scientific knowledge would be very useful for students and researchers as well as the society in general.

- **First Monsoon discussion on May 20, 2015. Theme: Onset and Long-Range Forecast**

1) Large Scale Features (Dr. Hamza Varikoden)
2) Synoptic Scale Features (Mr. S.P. Ghanekar)
3) Observational Features (Mrs. E. A. Resmi)
4) Ocean Features (Dr. C. Gnanaseelan)
5) Extended Range Prediction (Dr. Sushmitha Joseph)
6) Long Range Forecast (Mr. Ankur Srivastava)

- **Second Monsoon discussion on June 25, 2015. Theme: Progress and Future Evolution**

1) Large Scale Features (Mr. Bhupendra Bahadur Singh)
2) Synoptic Scale Features (Dr. Medha S. Deshpande)
3) Observational Features (Mr. Subharthi Chowdhuri & Dr. S. B. Morwal)
4) Ocean Features (Dr. P. Swapna)
5) Extended Range Prediction (Mr. Avijit Dey)
6) Long Range Forecast (Mr. Maheswar Pradhan)
7) Progress of Monsoon (Dr. D. S. Pai, IMD)

- **Third Monsoon discussion on August 04, 2015. Theme: Progress and Future Evolution**

1) Large Scale Features (Dr. K. P. Sooraj)
2) Synoptic Scale Features (Mr. Malay Ganai)
3) Observational Features (Dr. Thara Prabhakaran)
4) Ocean Features (Dr. P. Sreenivas)
5) Extended Range Prediction (Mr. Raju Mandal)
6) Long Range Forecast (Dr. Rajeeb Chattopadhyay)

- **Fourth Monsoon discussion on September 10, 2015. Theme: Performance and Progress**

1) Large Scale Features (Dr. Manish K. Joshi)
2) Synoptic Scale Features (Ms. Tirkey Snehlata)
3) Observational Features (Mr. B. Balaji)
4) Ocean Features (Mrs. Rashmi Kakatkar)
5) Extended Range Prediction (Dr. S. Abhilash)
6) Long Range Forecast (Mr. Ankur Shrivastav)
7) Extreme rainfall event over south-west M.P. (Ms. Shilpa Malviya)
8) Predictions for the second half of summer monsoon season {Prof.(Mrs.) S. Gadgil}

- **Fifth Monsoon discussion on October 12, 2015. Theme: Performance and Progress**

1) Large Scale Features (Dr. M. Rajeevan)
2) Synoptic Scale Features (Dr. P. Mukhopadhyay)
3) Observational Features (Mrs. Mercy Varghese)
4) Ocean Features (Dr. Anant Parekh)
5) Extended Range Prediction (Dr. A. K. Sahai)
6) Long Range Forecast (Dr. Suryachandra Rao)

List of Acronyms

BoB – Bay of Bengal

ERPS – Extended Range Prediction System

ESSO – Earth System Science Organization

IITM – Indian Institute of Tropical Meteorology

IMD – India Meteorological Department

IMDF - IITM Monsoon Discussion Forums

INCOIS – Indian National Centre for Ocean Information Services

LLJ - Level Jet stream

LRSF - Long Range Seasonal Forecast

NCMRWF – National Centre for Medium Range Forecast

NCEP - National Centers for Environmental Prediction

OLR – Out going long-wave radiation

SBAS- Southeast Bay of Bengal / North Andaman Sea

SWM- South-west Monsoon

TEJ – Tropical Easterly Jet

References

Abhilash S., Sahai A. K., Borah N., Chattopadhyay R., Joseph S., Sharmila S., De S., Goswami B. N., Kumar A. (2014) Prediction and monitoring of monsoon intraseasonal oscillations over Indian monsoon region in an ensemble prediction system using CFSv2. *Climate Dynamics*, 42:2801-2815. DOI:10.1007/s00382-013-2045-9

Abhilash S., Sahai A. K., Borah N., Joseph S., Chattopadhyay R., Sharmila S., Rajeevan M., Mapes B. E, and Kumar A. (2015) Improved Spread-Error Relationship and Probabilistic Prediction from CFS based Grand Ensemble Prediction System. *Journal of Applied Meteorology and Climatology*, 54:1569-1578. DOI:10.1175/JAMC-D-14-0200.1

Bansod S. D., Singh S. V., and Kripalani R. H. (1991) The relationship of monsoon onset with subsequent rainfall over India. International Journal of Climatology, 11:809–817. doi:10.1002/joc.3370110707.

Bjerknes J. (1969) Atmospheric teleconnections from the equatorial Pacific. *Monthly Weather Review,* 97:163–172.

Borah N., Sahai A. K., Abhilash S., Chattopadhyay R., Joseph S., Sharmila S., Kumar A. (2014) An Assessment of real-time extended range forecast of 2013 Indian summer monsoon. *International Journal of Climatology,* 35:2860–2876. DOI:10.1002/joc.4178

Chattopadhyay R., Rao S.A., George G., Sabeerali C. T., Dhakate A., Mahapatra S., Salunke K. (2015) Seasonal prediction of Indian Summer monsoon in Climate Forecast System (CFSv2) *Model. Journal of Geophysical Research (Under Review)*

Deshpande A., Chowdary J. S., Gnanaseelan C. (2014) Role of thermocline–SST coupling in the evolution of IOD events and their regional impacts. *Climate Dynamics,* 43:163-174. DOI:10.1007/s00382-013-1879-5.

Ek M. B., Mitchell K. E., Lin Y., Rogers E., Grunmann P., Koren V., Gayno G., and Tarpley J. D. (2003) Implementation of Noah land surface model advances in the National Centers for Environmental Prediction operational mesoscale Eta model. *Journal of Geophysical Research,* 108(D22), 8851. doi: 10.1029/2002JD003296

Fousiya T. S., Parekh A. and Gnanaseelan C. (2015) Interannual variability of upper ocean stratification in Bay of Bengal: observational and modeling aspects. *Theoretical and Applied Climatology.* DOI 10.1007/s00704-015-1574-z.

Ghanekar S. P., Puranik P. V. and Mujumdar V. R. (2010) Application of satellite-derived OLR data in the prediction of the onset of Indian summer monsoon. *Theoretical and Applied Climatology,* 99:457-468.

Good S. A., Martin M. J. and Rayner N. A. (2013) EN4: quality controlled ocean temperature and salinity profiles and monthly objective analyses with uncertainty estimates. *Journal of Geophysical Research: Oceans,* 118:6704-6716. doi:10.1002/2013JC009067

Goswami B. B., Deshpande M. S., Mukhopadhyay P., Saha S. K., Rao S. A., Murthugudde R. and Goswami

B. N. (2014) Simulation of monsoon intraseasonal variability in NCEP CFSv2 and its role on systematic bias. *Climate Dynamics,* 43:2725-2745. DOI:10.1007/s00382-014-2089-5

Griffies S. M., Harrison M. J., Pacanowski R. C., Rosati A., Liang Z., Schmidt M., Simmons H. and Slater R. (2004) *A Technical Guide to MOM4. GFDL Technical report.*

Gruber A. and Krueger A. F. (1984) The status of the NOAA outgoing longwave radiation data set. *Bulletin of American Meteorological Society,* 65: 958–962.

IMD cyclone report '*Ashobaa'* published 2015 (http:/www.imd.gov.in)

IMD cyclone report *'KOMEN'* published 2015 (http:/www.imd.gov.in)

Joseph P.V. and Raman P.L. (1966) Existence of Low-Level Westerly Jet Stream over Peninsular India during July. *Indian Journal of Meteorology Hydrology and Geophysics,* 17:407-410.

Joseph S., Sahai A. K. and Goswami B. N. (2009) Eastward propagating MJO during boreal summer and Indian monsoon droughts. *Climate Dynamics,* 32:1139-1153. DOI 10.1007/s00382-008-0412-8

Joseph S., Sahai A. K., Abhilash S., Chattopadhyay R., Borah N., Mapes B., Rajeevan M. and Kumar A. (2015) Development and evaluation of an objective criterion for predicting Indian summer monsoon onset in a coupled model framework. *Journal of Climate,* 28:6234-6248. DOI:10.1175/JCLI-D-14-00842.1

Koteswaram P. (1958), The Easterly Jet Stream in the Tropics. *Tellus,* 10:43–57. doi: 10.1111/j.2153-3490.1958.tb01984.x.

Kripalani R. H., Kulkarni A., Sabade S. S., Revadekar J. V., Patwardhan S. K. and Kulkarni J. R.(2004) Intra-seasonal oscillations during monsoon 2002 and 2003. *Current Science* 87:327–331.

Krishnamurti T. N. (1971) Tropical east-west circulations during the northern summer. J*ournal of Atmospheric Sciences,* 28:1342-1347.

Krishnamurti T. N., Molinari J., Pan H. L. and Wong V. (1977) Downstream amplification and formation of monsoon disturbances. *Monthly Weather Review,* 105:1281–1297.

Laing A.G. and Fritsch J. M. (1993) Mesoscale Convective Complexes over the Indian Monsoon Region. Journal of Climate, 6:911–919. doi: http://dx.doi.org/10.1175/1520-0442(1993)006<0911:MCCOTI>2.0.CO;2

Lau K. M., Wu H. T. and S. Bony (1997) The role of large-scale atmospheric circulation in the relationship between tropical convection and sea surface temperature. *Journal of Climate* 10:381-392.

Mitra A. K., Bohra A. K., Rajeevan M. N., and Krishnamurti T. N. (2009) Daily Indian Precipitation Analysis Formed from a Merge of Rain-Gauge Data with the TRMM TMPA Satellite-Derived Rainfall Estimates.

Journal of Meteorological Society of Japan, 87A:265–279. doi:10.2151/jmsj.87A.265.

Mitra A. K., Momin I. M., Rajagopal E. N., Basu S., Rajeevan M. N. and Krishnamurti T. N. (2013) Gridded Daily Indian Monsoon Rainfall for 14 Seasons: Merged TRMM and IMD Gauge Analyzed Values. J*ournal of Earth System Science,* 122:1173-1182.

Moorthi S., Pan H. L. and Caplan P. (2001) Changes to the 2001 NCEP operationalMRF/AVN global analysis/ forecast system. *NWS Technical Procedures Bulletin,* 484, pp14. Available at: http://www.nws.noaa.gov/om/ tpb/484.htm.

Mujumdar M., Vinay Kumar and Krishnan R. (2007) Indian summer monsoon drought of 2002 and its linkage with tropical convective activity over northwest Pacific. *Climate Dynamics,* 28:743-758.

Pai D. S. and Rajeevan M. (2009) Summer monsoon onset over Kerala: New definition and prediction. *Journal of Earth System Science,* 118:123-135

Pai D. S., Bhate J., Sreejith O. P. and Hatwar H. R. (2009) Impact of MJO on the intraseasonal variation of summer monsoon rainfall over India. *Climate Dynamics,* 36: 41–55. doi:10.1007/s00382-009-0634-4

Palmer T. N., Brankovic C., Viterbo P. and Miller M. J. (1992) Modelling interannual variations of summer monsoons. *Journal of Climate,* 5:399-417.

Pant G. B. and Parthasarathy B. (1981) Some aspects of an association between the southern oscillation and Indian summer monsoon. *Archiv für Meteorologie, Geophysik und Bioklimatologie,* Ser. B, 29:245 – 251.

Pattanaik D. R. and Rajeevan M. (2007) Northwest Pacific tropical cyclone activity and July rainfall over India. *Meteorology and Atmospheric Physics,* 95:63-72.

Rajeevan M. (1993) Inter-relationship between NW Pacific typhoon activity and Indian summer monsoon on inter-annual and intra-seasonal time-scales. *Mausam,* 44:109–111.

Rajeevan M., Gadgil S. and Bhate J. (2010) Active and Break spells of the Indian summer monsoon. *Journal of Earth System Science,* 119:229-247.

Rasmussen E. M. and Carpenter T. H. (1983) The relationship between eastern equatorial Pacific SSTs and rainfall over India and Sri Lanka. *Monthly Weather Review,* 111:517–528.

Saha S. et al. (2006) The NCEP Climate Forecast System. *Journal of Climate,* 19:3483–3517. doi: 10.1175/ JCLI3812.1

Saha S. et al. (2010) The NCEP Climate Forecast System Reanalysis. *Bulletin of American Meteorological Society,* 91:1015–1057.

Saha S., Moorthi S., Wu X., Wang J., Nadiga S. et al. (2014) The NCEP Climate Forecast System Version 2. *Journal of Climate,* 27:2185-2208. doi:10.1175/JCLI-D-12-00823.1

Sahai A. K, Chattopadhyay R., Joseph S., Mandal R., Dey A., Abhilash S., Krishna R. P. M. and Borah N. (2015) Real-time Performance of a multi-model ensemble based extended range forecast system in predicting the 2014 monsoon season based on NCEP-CFSv2, *Current Science (In Press).*

Sahai A. K., Sharmila S., Abhilash S., Chattopadhyay R., Borah N., Krishna R. P. M., Joseph S., Roxy M., De S., Pattnaik S. and Pillai P. (2013) Simulation and extended range prediction of monsoon intraseasonal oscillations in NCEP CFS/GFS version 2 framework. *Current Science,* 104:1394-1408.

Saji N. H., Goswami B. N., Vinayachandran P. N. and Yamagata T. (1999) *A dipole mode in the tropical Indian ocean. Nature,* 401:360–363.

Shankar D, Shetye S. R. and Joseph P. V. (2007) Link between convection and meridional gradient of sea surface temperature in the Bay of Bengal. *Journal of Earth System Science,* 116: 385–406.

Sharmila S., Joseph S., Chattopadhyay R., Sahai A. K. and Goswami B. N. (2015) Asymmetry in space–time characteristics of Indian summer monsoon intraseasonal oscillations during extreme years: Role of seasonal mean state. *International Journal of Climatology,* 35:1948–1963. doi:10.1002/joc.4100

Shukla J. and Paolino D. A. (1983) The Southern Oscillation and long range forecasting of the summer monsoon rainfall over India. *Monthly Weather Review,* 111:1830-1837.

Sikka D. R. (1980) Some aspects of the large-scale fluctuations of summer monsoon rainfall over India in relation to fluctuations in the planetary and regional scale circulation parameters. *Proceedings of Indian Academy of Sciences Earth Planetary Sciences,* 89:179 – 195.

Sikka D. R. and Gadgil S. (1980) On the maximum cloud zone and the ITCZ over India longitude during the southwest monsoon. *Monthly Weather Review,* 108:1840–1853.

Sreejith O. P., Swapna P., Pai D. S. and Rajeevan M. (2015) An Indian Ocean precursor for Indian Summer Monsoon Rainfall variability. *Geophysical Research Letters,* DOI: 10.1002/2015GL065950.

Sreenivas P., Gnanaseelan C., Kakatkar R., Pavan Kumar N., Chowdary J. S., Parekh A. and Singh P. (2015) Implementation and Validation of Global Ocean Data Assimilation System at IITM. *IITM Research Report,* SR-19.

Suhas E., Neena J. M. and Goswami B. N. (2013) An Indian monsoon intraseasonal oscillations (MISO) index for real time monitoring and forecast verification. *Climate Dynamics,* 40:2605-2616. doi:10.1007/s00382-012-1462-5.

Vimont D. J., Wallace J. M. and Battisti D. S. (2003) The Seasonal Footprinting Mechanism in the Pacific: Implications for ENSO. *Journal of Climate,* 16:2668–2675.

Vinay Kumar and Krishnan R. (2005) On the association between the Indian summer monsoon and the tropical cyclone activity over the Northwest Pacific. *Current Science* 88:602–612.

Walker G.T. (1910) On the Meteorological evidence for supposed changes of climate in India. *Memoirs India Meteorological Department,* 21:1-21.

Walker G.T. (1914) The liability todrought in India as compared with that in other countries. *Memoirs India Meteorological Department,* 21:1-9.

Walker G.T. (1914) Correlations in seasonal variations of weather, VIII: A preliminary study of world weather. *India Meteorological Department,* 24:75-131.

Webster P. J., Magana V. O., Palmer T. N., Shukla J., Tomas R. A., Yanai M. and Yasunari T. (1998) Monsoons: Processes, predictability, and the prospects for prediction *Journal of Geophysical Research,* 103:14451-14510.

Wheeler M. C. and Hendon H. H. (2004) An All-Season Real-Time Multivariate MJO Index: Development of an Index for Monitoring and Prediction. *Monthly Weather Review,* 132:1917–1932.

WintonM.(2000)AReformulatedThree-LayerSeaIceModel,J*ournalofAtmosphericandOceanicTechnology,*17:525–531.

Yu L. and Rienecker M. M. (1998) Evidence of an extratropical atmospheric influence during the onset of the 1997–98 El Niño.*Geophysical Research Letters,* 25:3537-3540. doi: 10.1029/98GL02628

A typical cloud picture during 2015 southwest monsoon

Courtesy: Bhupendra Bahadur Singh